Probing the active site of monoamine oxidase A with inhibitor ligands

By

Robert Maurice George Hynson

UNIVERSITY OF ST. ANDREWS
ST. ANDREWS

A thesis presented for the degree of Doctor of Philosophy at the University of St. Andrews, March 2004

DECLARATION

I, Robert Maurice George Hynson, hereby certify that this thesis, which is approximately 30000 words in length, has been written by me, that it is the record of my work carried out by me and that it has not been submitted in any previous application for a higher degree.

Date 28.04.04 Signature of candidate .....

I was admitted as a research student in September 2000 and as a candidate for the degree of Doctor of Philosophy in September 2000; the higher study for which this record was carried out in the University of St. Andrews between 2000 and 2004.

Date 28.04.04 Signature of candidate .....

I hereby certify that the candidate has fulfilled the conditions of the Resolution and Regulations appropriate for the degree of Doctor of Philosophy in the University of St. Andrews and that the candidate is qualified to submit this thesis in application for that degree.

Date 28/4/04 Signature of supervisor .

In submitting this thesis to the University of St. Andrews I understand that I am giving permission for it to be made available for use in accordance with the regulations of the University Library for the time being in force, subject to any copyright vested in the work not being affected thereby. I also understand that the title and abstract will be published, and that a copy of the work may be made and supplied to any *bona fide* library or research worker.

Date 28.04.04 Signature of candidate . .....

ACKNOWLEDGEMENTS

Firstly I would like to thank my supervisor Dr Rona Ramsay for her continued support and encouragement through all aspects of my three years in St Andrews while doing my PhD. I would also like to thank the members of the Ramsay group, especially Joan Riddell for her tireless help during MAO A purifications.

I would also like to thank many of the people I have had the privilege to work with during my PhD, namely, Dr Johan Wouters, Dr Alexei Medvedev, Dr Douglas Philp, Dr Simon Daff, Dr Tobias Ost, Dr Jaswir Basran and Professor Nigel Scrutton.

Finally a big thank you to all my friends and family for their support and encouragement over the past three years.

ABSTRACT

Monoamine oxidases (MAO) A and B are flavoenzymes important in the regulation of biogenic amines, such as, serotonin, dopamine and adrenaline. Inhibitors of MAO A are of particular pharmacological interest as they act as antidepressants. Evidence is presented here for how the antidepressant MAO A inhibitor pirlindole interacts with the active site of MAO A. Pirlindole binds between two tyrosines with its N3 facing N5 of the flavin. Substituents on C8 of pirlindole increase inhibition up to a point; cyclohexyl is the largest substituent tolerated while larger substituents are detrimental to inhibition. N3 substituents are not tolerated and lead to poorer inhibition. The dehydro derivatives of pirlindole always give better inhibition, perhaps because of their flatter shape.

Pirlindole induces distinct spectral changes to the flavin in MAO A upon binding. Reduction of MAO A when complexed with a pirlindole with no N3 substituent produces a stable semiquinone. In the presence of a pirlindole with a N3 substituent, semiquinone stabilization is never seen, and the reduction goes to completion. This indicates that the N3 of pirlindole is interacting with N5 of the flavin to stabilize the semiquinone. MAO A inhibitors were thought to stack with the flavin in the active site, an energetically favorable interaction in solution, but this does not happen in MAO A.

Circular dichroism spectroscopy shows that the small inhibitor, amphetamine, perturbs only tyrosines upon binding, whereas the larger inhibitor pirlindole perturbs tyrosine, phenylalanine and tryptophan upon binding. Reduction induces large changes in the aromatics in MAO A. Reduction to the semiquinone increases the phenylalanine and

tryptophan spectral regions the most, whereas for full reduction tyrosine, tryptophan and phenylalanine are all increased greatly. Substrate reduction induces a larger change in the flavin than dithionite reduction. Reduction by clorgyline (an irreversible suicide inhibitor) induces a very large increase in the phenylalanine region, and also a large decrease at 330 nm thought to be due to the formation of an N5 adduct.

ABBREVIATIONS

Abs	Absorbance
Ala	Alanine
AD	Alhzeimer's disease
AMP	Adenosine monophosphate
Arg	Arginine
Asn	Asparagine
BCA	Bicinchoninic acid
BSA	Bovine serum albumen
Cys	Cysteine
DEAE	Diethylaminoethyl
DMSO	Dimethylsulfoxide
DTT	Dithiothreitol
EDTA	Ethylenediaminetetracetic acid
EPR	Electron paramagnetic resonance
FAD	Flavin adenine dinucleotide
FMN	Flavin mononucleotide
FT-IR	Fourier transform infra red spectroscopy
Glu	Glutamic acid
Gln	Glutamine
Gly	Glycine
GOR	Garnier-Osguthorpe-Robson
HSS	High speed supernatant
HSP	High speed pellet
Ile	Isoleucine
KPi	Potassium phosphate buffer
LSS	Low speed supernatant
Leu	Leucine
Lys	Lysine
MAO	Monoamine oxidase
MAOi	Monoamine oxidase inhibitor
MPTP	1-Methyl-4-phenyl-1,2,3,6-tetrahydropyridine
MPP^+	1-Methyl-4-phenylpyridinium

N-CαMBA	*N*-Cyclopropyl-α-methylbenzylamine
PAO	Polyamine oxidase
1-PCPA	1-Phenylcyclopropylamine
2-PCPA	2-Phenylcyclopropylamine
PD	Parkinson's disease
Phe	Phenylalanine
PLA	Phospholipase A
PLC	Phospholipase C
PLP	Phospholipase pellet
PLS	Phospholipase supernatant
PMSF	Phenylmethylsulfonyl fluoride
RHFC	Restricted Hartree fock calculation
Ser	Serine
TMADH	Trimethylamine dehydrogenase
Trp	Tryptophan
TXP	Triton X-100 pellet
TXS	Triton X-100 supernatant
Tyr	Tyrosine

INDEX

1. Introduction

The aim of this project is to probe the active site of monoamine oxidase A (MAO A) using a set of pirlindole inhibitors. The interactions of these conformationally constrained inhibitors with the active site should give us information about the active site of MAO A. The affinity of ligands of different dimensions will reveal the relative size and shape of the active site. One very important aspect of the project is to examine how these inhibitors interact with the flavin adenine dinucleotide (FAD) in the active site and, in particular, how the inhibitors alter the redox properties of the FAD in the enzyme. From this study and other more statistically based studies like it, it is anticipated that a rational approach to inhibitor design will be made possible for this pharmacologically important enzyme, a key target for antidepressant therapy. In this introduction there will be a brief description of the properties of flavins and flavoproteins to familiarize the reader with the importance of the flavin cofactor in MAO, then the background for MAO, and, lastly an outline of how the aims of this project will be achieved.

1.1. Flavins and flavoproteins

Flavoproteins have the unique feature of being able to catalyze a large number of diverse biochemical reactions. They are involved in a number of electron transfer reactions including activation of oxygen for oxidation and hydroxylation reactions, dehydrogenation, light emission and DNA repair (1). From the vast majority of these diverse enzymes studied, some common features exist, the main one being that at some point during the reaction, electrons will be transferred to the flavin. The chemistry of

these reactions occurs at the N5 and C4 atoms of the isoalloxazine ring system of the flavin.

The structure of the isoalloxazine ring is shown in Fig. 1.1.1. Reduction of the flavin can occur via two one-electron reduction steps, or one two-electron step. For FAD in solution, reduction occurs as a two electron transfer with a mid-point potential of around –200 mV (2). Flavoproteins have the ability to stabilize the one electron reduced semiquinone form of the flavin through specific protein-flavin interactions. The semiquinone may be in either a red anionic or blue neutral form. Proteins can also modulate the redox potentials of FAD in a range from –400 mV to +60 mV (3). The isoalloxazine ring of the flavin is electron-deficient with the negative charge localized around the two carbonyls of the pyrimidine ring. The degree to which this negative charge is stabilized is important in determining the redox potentials of the flavin. In nearly all flavoproteins for which the 3D structure is known, there is always a positive entity hydrogen bonded to the N1-C2=O2 locus. This could be a full charge as in a Lys or Arg side chain, or partially charged such as an N terminal of an α helix or a cluster of peptide nitrogens. The positive charge is important in stabilizing the anionic form of the fully reduced flavin and increasing the mid point potential of the flavin. Mutational studies on dihydroorotate dehydrogenase (4) and trimethylamine dehydrogenase (5), have shown that by replacing the positively charged residue close to the N1-C2=O2 locus with a neutral side chain, an inactive enzyme results. The presence of negative or hydrophobic residues in this region lowers the potential, highlighting the importance of the positive charge.

A second recurrent feature in the protein-isoalloxazine interactions concerns hydrogen bonding to N5. In most flavoproteins, the N5 is hydrogen bonded to a hydrogen bond donor, typically a backbone or side chain nitrogen. This hydrogen bond is stereospecific, always located on the opposite side of the isoalloxazine ring from substrate binding (3). The proximity of this hydrogen bond to N5 is generally expected to increase oxidative power. Interestingly, vanillyl-alcohol oxidase (6) and glycolate oxidase (7) both lack the N5 hydrogen bond and exhibit very high redox potentials of >25 mV.

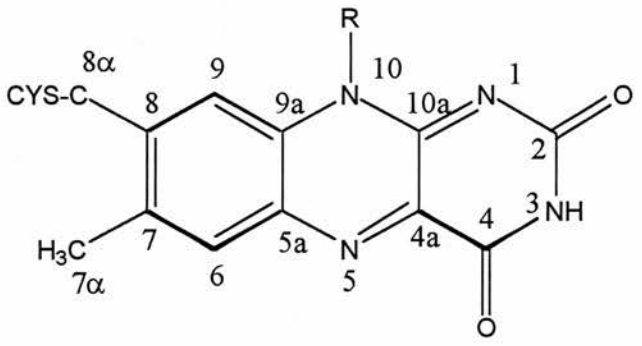

Fig. 1.1.1. Structure of the isoalloxazine ring. In FAD, R is the adenine dinucleotide group that anchors the flavin in the protein structure. The thioether bond between C8 and Cys as found in MAO is indicated.

1.2. Monoamine oxidase

Monoamine oxidase [MAO, EC 1. 4. 3. 4; amine:oxygen oxidoreductase (deaminating, flavin-containing)] is a flavoprotein located on the outer mitochondrial membrane of all cells, catalyzing the oxidative deamination of primary, secondary and tertiary amines to their corresponding imines, (Scheme 1). Its roles include the regulation of biogenic amines in the brain and peripheral tissues, and the biodegradation of aromatic monoamines including the neurotransmitters, serotonin, adrenaline and dopamine (8). MAO plays a central role in some psychological and neurological disorders and also acts as a scavenger for exogenous amines such as tyramine and tryptamine, which cause blood pressure problems if they enter the bloodstream. It also catalyses the biotransformation of MPTP into MPP^+, the neurotoxin that induces Parkinson's Disease. MAO plays a protective role in energy production, oxidising dopamine, an inhibitor of complex I in the electron transport chain, which could disrupt ATP production (9).

There are two forms of MAO, A and B, which are characterized by overlapping but distinct substrate and inhibitor specificities. MAO A preferentially oxidizes serotonin and is inhibited by clorgyline (10) while MAO B preferentially oxidizes 2-phenylethylamine and is inhibited by deprenyl (11). Both MAO A and B metabolise benzylamine and dopamine, and are irreversibly inhibited by pargyline. Throughout the body, the A form predominates in catecholamine neurons whereas the B form predominates in astrocytes, serotonergic neurons and radial glia (12). Until the two enzymes were cloned and the primary sequences determined, it was thought that they might be the same protein with

two active sites. From the primary sequence it has been determined that they are indeed two distinct proteins with molecular weights of 59,700 daltons for MAO A and 58,800 daltons for MAO B (13). The two isoforms are distributed in differing amounts around the body. In mammals, both the A and B forms are present in most tissues. In humans, the placenta expresses predominantly MAO A (14) whereas blood platelets express exclusively MAO B (15). Both MAO A and B contain two subunits, each containing a covalently bound flavin adenine dinucleotide (FAD) (14,16). The FAD is covalently bound to a cysteine in the enzyme through a thioether bond at the 8 position of the isoalloxazine ring (17,18). This covalent bond is thought to increase oxidative power. This cysteine is not essential for activity. Mutational studies have shown that when Cys-398 in MAO A is mutated to alanine, various different flavins, including riboflavin, were reconstituted into the enzyme and catalytic activity retained (19).

MAO is implicated in various psychological and neurological disorders. For example depression is associated with low serotonin levels in the brain. Levels of serotonin, a neurotransmitter selectively oxidized by MAO A, can be elevated by administration of a MAO A selective inhibitor such as clorgyline. Therefore, MAOIs can be used to treat depression by increasing serotonin in the brain. Patients with Parkinson's disease (PD) generally have lowered dopamine levels, as well as having the increased hydrogen peroxide levels that are associated with the development of PD. MAO B specific inhibitors such as deprenyl can be used as an adjunct in its treatment along with L-DOPA therapy (although deprenyl also has other modes of action).

Oxidation of amine substrates by MAO is coupled to the reduction of FAD, the cofactor in MAO. The product of the reaction is the imine which is non enzymatically hydrolyzed to the corresponding aldehyde and ammonia. FAD is then re-oxidized by molecular oxygen with the production of H_2O_2.

Scheme 1

$R\text{-}CH_2\text{-}NH_2 + E\text{-}FAD \rightarrow RCH{=}NH + E\text{-}FADH_2$

$R\text{-}CH{=}NH + H_2O \rightarrow R\text{-}CHO + NH_3$

$E\text{-}FADH_2 + O_2 \rightarrow E\text{-}FAD + H_2O_2$

The re-oxidation by O_2 of the reduced flavin in MAO occurs quite slowly ($1s^{-1}$), but occurs far more rapidly in the presence of substrates (20), so the oxidative pathway can be written as,

$S\text{-}E\text{-}FADH_2 + O_2 \rightarrow S\text{-}E\text{-}FAD + H_2O_2$

The stimulation of re-oxidation by substrate is substrate specific. Steady state kinetics on MAO B demonstrated that with phenylethylamine, re-oxidation occurs via a binary complex (reduced flavin and oxygen), whereas with benzylamine a ternary complex predominates (reduced flavin, substrate and oxygen) (20).

1.3. Substrates

MAO A and B have overlapping but distinct substrate specificities. MAO A preferentially oxidizes serotonin whereas MAO B preferentially oxidizes β-phenylethylamine (Table 1.3.1). MAO A and B both metabolise a number of biogenic amines including; N-methyl-2-hydroxy-2-(3,4-dihydroxyphenyl)-ethylamine (dopamine), 2-hydroxy-2-(3,4-dihydroxyphenyl)-ethylamine (noradrenaline or epinephrine), and 2-phenylethylamine (21). MAO can also metabolise other exogenous amines, such as benzylamine, kynuramine, tyramine, tryptamine, MPTP, and octapamine.

The asymmetry round the α-carbon in the substrate is important. There is a distinct preference for two hydrogens on the α-carbon of primary amines and indeed α-methylated monoamines have been shown to inhibit MAO, with selectivity towards the A form of the enzyme. α-Methylation of 2-phenylethylamine, a good B substrate, produces amphetamine, a reversible MAO A inhibitor with the S isomer having greater affinity than the R isomer. Removal of an α-hydrogen by MAO is stereospecific and involves the abstraction of the pro-R-hydrogen. This pro-R-hydrogen corresponds to the hydrogen present in R-amphetamine. When the methyl group occupies the position of the non-abstracted hydrogen (S-isomer), the inhibitor has greater affinity for the active site (22,23). However, secondary amines and tertiary amines, such as MPTP, are still substrates (24,25).

Table 1.3.1. Kinetic constants for several MAO substrates determined for purified human liver MAO A and beef liver MAO B from steady state kinetics.

Substrate	MAO A			MAO B			MAO B/ MAO A
	k_{cat} (s^{-1})	K_M (mM)	k_{cat}/K_M ($mM^{-1}.s^{-1}$)	k_{cat} (s^{-1})	K_M (mM)	k_{cat}/K_M ($mM^{-1}.s^{-1}$)	
Kynuramine	2.65	0.15	17.7	2.75	0.084	32.7	1.85
Benzylamine	0.02	0.9	0.022	10	0.36	27.8	1264
β-Phenylethylamine	0.75	0.5	1.5	3.62	0.067	54	36
Tryptamine	2.65	0.03	88.3	0.67	0.13	5.15	0.058
serotonin	2.8	0.4	7	0.077	0.28	0.28	0.04
5-Methoxytryptamine	1.81	1.84	9.8	0.3	0.4	0.75	0.08
MPTP	0.2	0.09	2.2	3.3	0.3	11	5

Data taken from (20).

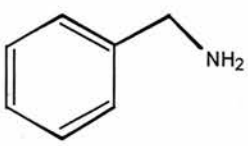

Benzylamine

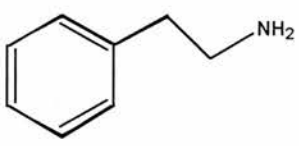

Phenylethylamine

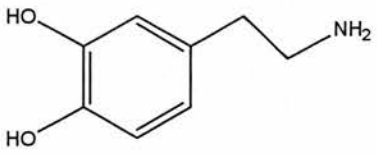

Dopamine

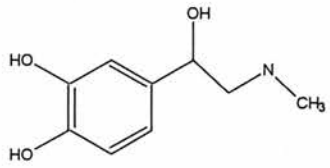

Epinephrine

Serotonin

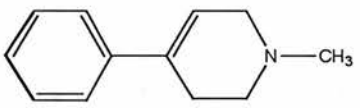

MPTP

Fig. 1.1.3.1. Structures of some MAO substrates.

MAO substrates do not show absolute specificity for one isoenzyme. The isoenzymes have different but overlapping specificities (26). Table 1.3.1 shows that by comparing the specificity constant (k_{cat}/K_M) for MAO A and MAO B, that MAO A preferentially oxidizes kynuramine and serotonin, while MAO B preferentially oxidizes benzylamine and phenylethylamine, with all the other amines showing varying specificities for both isoenzymes (20).

From Table 1.3.1 some general conclusions can be made about the structure of substrates and their specificity for either MAO A or B. Substrates that bear no polar group other than the amine, such as benzylamine, pentylamine and phenethylamine are

considered preferentially B substrates. Substrates with a hydroxy group remote from the nitrogen, such as tyramine and serotonin, are more selective for MAO A. The introduction of an OH group in the β position of phenethylamine gives (±)β-phenylethanolamine, which is more selective for MAO B than phenethylamine. However, it has been established, that R (–) phenylethanolamine is preferentially oxidized by MAO A whereas S (+) phenylethanolamine is preferentially oxidized by MAO B (27).

MAO catalyses the bioactivation of N-methyl-4-phenyl-1,2,3,6-tetrahydropyridine (MPTP) to $MPDP^+$ and then, more slowly, to MPP^+. MPP^+ is accumulated in mitochondria and inhibits NADH-dehydrogenase (9). The loss of ATP production results in cell death causing brain lesions leading to symptoms of Parkinson's disease. Studies on analogues of MPTP have revealed structural data about the selectivity of MAO A and B substrates (28). Bulky lipophilic analogues are preferentially oxidized by MAO A, while smaller analogues are preferentially oxidized by MAO B. Molecular flexibility within the molecule enhances reactivity with MAO B but not with MAO A. From the studies on MPTP, it was concluded that substrate selectivity in MAO is a complex interplay between molecular size and flexibility (28).

1.4. Structure

1.4.1. Primary structure

The amino acid sequences have been determined for human liver and placental MAO A, bovine adrenal MAO A, rat liver MAO A, human liver, platelet and frontal cortex MAO B and rat liver MAO B, using cDNA clones. These sequences show remarkable similarity, with 85% sequence identity between different sources of either MAO A or MAO B (13). Sequence identity between MAO A and MAO B is 73%. MAO A and B both consist of a dimer of monomers containing 527 and 520 residues with monomer molecular weight of 59,700 and 58,800, respectively (13).

MAO A and B both contain the pentapeptide sequence Ser-Gly-Gly-Cys-Tyr in which the FAD cofactor is covalently bound to the cysteine via a thioether bond to the 8-methyl of the isoalloxazine ring. This cysteine is residue 406 in MAO A and 397 in MAO B (17,18). Studies on pure MAO using quantitative amino acid analysis and flavin titration with dithionite show a ratio of one FAD per 63 kDa (MAO A) and 57 kDa (MAO B) for the human enzyme, hence MAO contain one FAD per monomer subunit (14).

From the primary amino acid sequence four regions have been determined in MAO. Firstly, in the N-terminal domain, there is an adenine (AMP) binding site (residues 15-45) which shares high sequence identity with other flavoproteins. It includes the sequence (GXGXXG) which is important in the formation of the Rossman nucleotide binding domain. Secondly, there is a highly conserved region (residues 389-460 MAO A) which contains the cysteine involved in covalent attachment of the flavin. This region shares

94% sequence identity between human liver MAO A and B and is the FAD binding domain. A third unknown domain is thought to be responsible for substrate binding and catalysis (29,30). Finally the C-terminal consists of a hydrophobic region, residues 504-521 in MAO A, which is flanked by positive residues thought to be responsible for anchoring the enzyme to the mitochondrial membrane.

Human liver MAO A and B are derived from separate genes located on the X chromosome, in the p arm, region 11.23-11.4 (31). Both MAO A and B genes have an identical intron exon organization consisting of fifteen exons, suggesting they originated from duplication of one common ancestral gene.

Site directed mutagenesis has proven a useful tool to probe for essential amino acid residues. The functional importance of cysteines in both forms of MAO has long been known (32). There are nine cysteines (Cys) in MAO, one of which is involved in the covalent attachment of the flavin. Shih and co-workers performed a mutational study in which each cysteine was mutated, in turn, to a serine and the enzyme expressed in COS cells. Substituting cysteines 374 or 406 in MAO A and substituting cysteines 156, 365 or 397 in MAO B with serines resulted in complete loss of activity. The enzyme mutated at Cys-406 in MAO A and Cys-397 in MAO B, the cysteines responsible for the covalent flavin attachment, were shown to both be inactive when mutated to serines. This was thought to be due to the enzyme losing its ability to bind FAD. However, Edmondson's work, cloning the MAO into yeast, showed that various FAD analogues can be incorporated into the enzyme in the absence of the Cys-397 in MAO B, and the enzyme

regains activity (33). The loss of activity of MAO A Cys-374-Ser and MAO B Cys-156-Ser and MAO B Cys-365-Ser suggested that these residues are important for catalytic activity either by being involved in the catalytic cycle in the enzyme, or for maintaining the correct tertiary structure for catalysis to take place. However, MAO A Cys-374-Ala and MAO B Cys-365-Ala were both fully active when expressed in yeast in this lab (34).

Site directed mutagenesis was also used to determine the role of residues Glu-34, Arg-42 and Tyr-44 in MAO B (35,36). Mutations of Glu-34 to Asp, Gln or Ala resulted in a dramatic decrease in activity compared to the wild type MAO B. Glu-34 is important for catalytical activity and is located in the domain responsible for AMP binding. From the crystal structure, it is seen that the ribose ring of the FAD adenosine moiety is specifically hydrogen-bonded to the carboxyate group of Glu-34. The Glu-34 interaction is found in the dinucleotide binding motifs in FAD-dependent enzymes and mutation of this residue to Ala, Asp, or Gln results in over a 90% loss in catalytic activity of the mutant MAO B. The only electrostatic interaction seen between the protein and the flavin is between the anionic pyrophosphate of the FAD and the positively charged guanidino group of Arg-42. This interaction was predicted by mutagenesis experiments in which the Arg-42-Ala mutant was found not to incorporate FAD into MAO B. The Arg-42-Lys mutant did partially incorporate FAD which demonstrates the requirement for a specific electrostatic interaction at the pyrophosphate linkage (37). Tyr-44 was mutated to Phe, Ser and Ala. Substitution to Phe had no effect on either MAO B activity or FAD incorporation, while substitutions with non-aromatic residues resulted in dramatic

decrease in both activity and FAD incorporation. The aromatic residue at position 44 is required for FAD binding, and with it, catalytic activity in MAO B.

Another tyrosine residue important for activity in MAO A is Tyr-444 (38). The corresponding conserved residue in MAO B along with Tyr-407 lie in the active site producing an aromatic cage above the *re* side of the isoalloxazine ring of the flavin. Mutating Tyr-444 to phenylalanine resulted in an enzyme that is greater than 100-fold slower than the wild type at oxidizing serotonin, while retaining 25% benzylamine oxidizing activity. The role of these aromatic residues in forming an aromatic cage is unknown. An aromatic cage is also seen in polyamine oxidase (PAO) (39) and trimethylamine dehydrogenase (40), so this feature maybe related to amine oxidation. It is postulated to align the nitrogen of the substrate adjacent to the flavin.

1.4.2. Secondary structure

The secondary structural contents of both MAO A and B were determined using Fourier transform infra-red FT-IR spectroscopy (41). The statistical method of GOR (Garnier-Osguthorpe-Robson, statistical method of secondary structure assignment) was used to assign the secondary structure with the primary sequence in order to deduce the folding in both MAO A and B. Comparison of the results of both enzymes show that there are differences in the region of residues 100-200 in the aligned sequences. This region could be responsible for differing 3D folds of the two enzymes and the differing substrate and inhibitor specificities.

1.4.3. Tertiary structure

The crystal structure of MAO B was solved to 3 Å in 2002 (42) and more recently to 1.8 Å (43). Structural determination of both MAO A and B has been hampered by the hydrophobic nature of the enzymes and a need to keep them in detergents to prevent aggregation after extraction from the mitochondrial membrane. Theoretical models have been produced for both MAO A and B based on the polyamine oxidase (PAO) structure (39) but these models did not resolve the active sites well enough to give detailed information about the substrate binding sites (30).

The structure of MAO B is compact with an overall fold most similar to L- amino acid oxidase and PAO. The structure shows that the enzyme is a homodimer as previously established (42,44,45), with extensive monomer-monomer interactions. About 15% of the surface of each monomer is buried upon dimer formation.

The C-terminal helix from residues 489-515 is flanked by positively charged residues and is involved in anchoring the enzyme to the outer mitochondrial membrane. Not all of the C-terminal is seen in the structure, probably due to the flexibility of the end of the C-terminal. Additionally to this C-terminal helix, residues 481-488 form an extended polypeptide with their hydrophobic side chains pointing towards the membrane, further anchoring the enzyme to the membrane.

The first structure revealed the inactivator, pargyline, covalently bound to N5 of the isoalloxazine ring of the flavin. The area in which the pargyline is bound defines the

substrate binding site. This cavity has a volume of 410 $Å^3$ and is lined by aromatic and aliphatic residues, creating an environment hydrophobic in nature. Preceding the active site is a second, entrance cavity, 290 $Å^3$ in volume, lying between the active site and the surface of the enzyme. This cavity is shielded from the surface by a loop (residues 99-112) which is proposed to act as a gating switch. Tyr-326, Ile-199, Leu-171 and Phe-169 separate the two cavities. For a substrate to reach the flavin, it must enter the entrance cavity after opening by movement of the loop, then these four residues must open up to allow the substrate to move from the entrance cavity to the active site. The purpose of the loop and the entrance cavity is not known, but it might explain some of the properties of MAO.

MAO B mainly acts on small amines such as dopamine, while MAO A mainly acts on much bulkier amines such as serotonin. The differences between the MAO A and B sequences along the substrate cavity include Leu-171 (MAO B)/ Ile-180 (MAO A), Cys-172/Asn-181, Ile-199/ Phe-208 and Tyr-326/Ile-335. Three of these residues separate the entrance and active site cavities; the side chains of these residues affect not only the steric accommodation of the substrate but also the separation of these two cavities. By altering these residues, the two cavities may fuse together to form one long cavity that may accommodate larger substrates and inhibitors, as observed in MAO A. Mutation of these cavity-separating residues have altered the substrate and inhibitor specificities to resemble MAO A (46).

The original structure was published with the irreversible inhibitor pargyline covalently bound to the flavin in the active site. From this structure, benzylamine was modeled into the active site, and from this model, substrate binding was proposed to occur between Tyr-398 and Tyr-435 with the amine recognition site between the two hydroxy groups of these tyrosines. The more recently solved structure of MAO B with the competitive inhibitor isatin bound shows that isatin binds between the two tyrosines with its nitrogen facing the N5 of the flavin in a similar orientation to that predicted when benzylamine was docked (42).

The active site of MAO B shows no active site base, ruling out H^+ abstraction by an active site residue (47). This gives further evidence that the non-protonated amine binds to the enzyme as proposed on the basis of binding of non-protonated amines, determined by pH studies (48). It also has no conserved cysteine, in contrast to evidence for active site cysteines from spectral and redox changes after cysteine modification, and modification of cysteines by the reactive product of cyclopropylamine oxidation.

1.5. Redox properties

A recurring feature of flavoproteins is the hydrogen bonding interactions that occur between the flavin and the protein. Hydrogen bonds to the isoalloxazine ring in MAO B include N3·····Tyr-60 oxygen 2.8 Å, C4=O·····Tyr-60 N 2.75 Å, C2=O·····Met-436 N 2.75 Å, and N5·····H_2O, 2.91 Å. All flavoenzymes involved in oxidation have a hydrogen bond donor to N5 on the opposite side of the isoalloxazine ring to the substrate within 3.44 Å of N5. In MAO B, this hydrogen bond is to a water molecule 2.91 Å from N5 which is also hydrogen bonded to the α-amino group of Lys-296. This latter hydrogen bond, involving a water molecule and the Lys residue, is also found in several other flavoprotein oxidases including polyamine oxidase (49).

Both MAO A and B can be reduced chemically by dithionite via two steps, the first generating the anionic semiquinone indicated by an increase in absorbance at 412 nm and a decrease in absorbance at 456 nm in the UV-vis spectrum, and the second producing the hydroquinone shown by bleaching of the flavin spectrum (Fig. 1.5.1). The mid-point potential for free FAD in solution is –210 mV, the mid point potential for an amine in solution is +1 V, and that of oxygen for O_2/H_2O_2 is +295 mV. This leaves a puzzling conundrum of how MAO manages to overcome the energy barrier of transferring two electrons from the amine to the flavin. The enzyme itself must be able to increase the potential of the flavin so that it is closer to that of the amine, or it must be able to lower the potential of the amine closer to the value of the flavin. The potential of an amine can be lowered if measured in a hydrophobic solvent. It is well known that MAO A and B both oxidize and are inhibited by hydrophobic substrates and inhibitors respectively.

With the advent of the 3D structure of MAO B it has now been confirmed that the active site is lined by many hydrophobic residues (45). The mid point potentials for the oxidised/semiquinone and semiquinone/reduced couples are –159 ±4 mV and –262 ± 3 mV for MAO A and –167 ± 4 mV and –275 ± 3 mV for MAO B (50), indicating that the binding of FAD to MAO has changed the redox properties of the flavin. In MAO, FAD can be reduced in two steps through a stabilised semiquinone unlike free flavin. The midpoint potentials for the overall reduction (FAD_{ox}/FAD_{red}) calculated from the two phases for the unliganded enzyme is –210 mV for MAO A and –221 mV for MAO B, similar to free flavin. In the reduction of MAO by substrate, no semiquinone is ever seen, and the mid-point potential is positively shifted by up to 500 mV depending on the substrate used (50). This increases the potential to around +250 mV and therefore closer to the potential of the amine. Inhibitors, on the other hand, do not change the potential of the first electron, but they do prevent full reduction occurring, stabilizing the semiquinone.

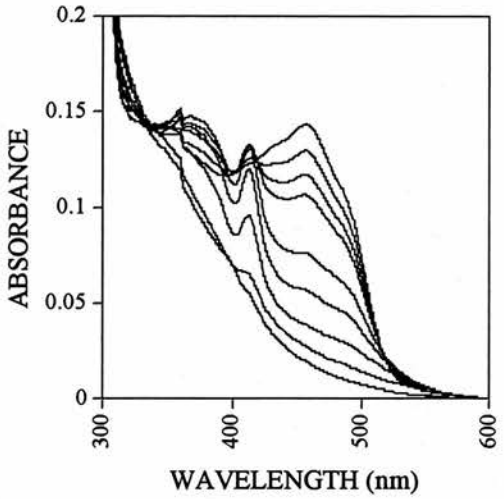

Fig. 1.5.1. Titration of MAO A with dithionite. Dithionite (1 mg/ml) was added to an anaerobic sample of MAO A (9.4μM), plus methyl viologen (1μM), each spectrum was recorded 15 minutes after addition of dithionite.

1.6. Monoamine oxidase in health

One of the main pharmalogical aims in MAO A research is to develop potent, reversible MAO A-selective inhibitors for the treatment of depression. MAO A and B play a key role in many other diseases including Parkinson's Disease (PD), Alzheimer's Disease (AD), social phobias and schizophrenia. However, MAO A and B in gut and blood protect against vascular effects of ingested amines, so recent pharmacological interest has also arisen in preventing inadvertent inhibition of MAO by other drugs (51).

Patients with PD generally have lowered dopamine levels. MAO B specific inhibitors such as *l*-deprenyl can be used in its treatment in combination with L-DOPA therapy in order to delay the progression of its symptoms by increasing dopamine levels (52). MPTP, which was an impurity in a synthetic heroin mimic, is metabolized by MAO to MPP^+, a neurotoxin which kills nigrostriatal neurons, causing Parkinson's disease (53). MAOIs such as deprenyl, administered to mice before MPTP show a neuroprotective property, as they reduce the levels of MPP^+ produced when MPTP is administered, lowering the incidence of cell death in the substantia nigra in this model of PD (54). The discovery that the oxidation of MPTP to MPP^+ with the consequent neuronal damage, similar to that seen in PD, has led to a useful animal model for PD, and it is anticipated that studies on MPTP-induced PD in mice will help determine the causes of PD in humans.

Alzheimer's disease is a neurodegenerative disorder with progressive decline in cognitive function found mainly in the elderly. Treatment involves administration of

acetyl-cholinesterase inhibitors. MAO B levels can increase by up to 3-fold in the frontal cortex of patients which results in increased production of hydroxy radicals which are correlated with the development of characteristic amyloid β-peptide plaques. Administration of the MAO B selective inhibitor *l*-deprenyl may help prolong the life of patients with AD through lowering hydroxyl radicals (55). Several other actions of deprenyl are thought to occur in neuroprotection unrelated to its MAO B inhibitory activity. Recent studies show that deprenyl prevents oxidative DNA damage of neurons by a mechanism independent of MAO-B inhibition (56). In retinal cells, deprenyl blocks apoptosis induced by hypoxia and growth factor withdrawal and regulates the expression of apoptosis-related genes (57). The most recent strategy for the treatment of AD is to combine the propargyl moiety of deprenyl with the carbamate moiety of cholinesterase inhibitor to produce a dual inhibitor, TV-3326 (58).

Cigarette smoke has been reported to inhibit MAO A and B. This may be one reason why smoking is more prevalent in individuals with depression and why smoking cessation is less successful in depressive patients. Smokers and former smokers have reduced MAO A and B activities in the brain compared to non-smokers. By virtue of the neuroprotective properties of MAOIs, there is a reduced incidence of Parkinson's disease in smokers (59).

1.7. Cheese effect

One of the major problems with the first generation of antidepressants was termed the cheese effect. As the name suggests people taking MAOIs as antidepressants suffered side effects when they ate cheese. The cheese effect is associated with the presence of tyramine and other sympathomimetic amines in cheese. If tyramine is ingested and the patient is taking an irreversible unselective MAOI, the tyramine cannot be metabolized due to the inhibition of MAO. Consequently, tyramine can gain access to the blood system. As tyramine is a good substrate for the noradrenergic uptake system, it will be concentrated in noradrenergic nerves. This causes release of stored noradrenaline, resulting in the constriction of the vascular epithelium and this increases systolic blood pressure. The exogenous amines compete for the reuptake system, so the hypertensive effect is prolonged. Since less noradrenaline is taken back into the terminals, the storage vesicles are depleted of noradrenaline and orthostatic hypotension can occur.

The first generation of MAOIs were unselective and irreversible forming a covalent adduct to the N5 of the flavin in both MAO A and MAO B. This rendered the enzyme incapable of metabolizing tyramine and therefore the cheese effect is seen. Due to the irreversible nature of these inhibitors, it was necessary to wait until new enzyme was synthesized by the body before the tyramine could be metabolised, which could be a matter of days or weeks (21).

The second generation of MAOIs were selective for either MAO A or B but still irreversible. Due to the selectivity of these inhibitors, when one form of the enzyme is

inhibited the other uninhibited form should be free to metabolise any tyramine present. The intestinal wall normally disposes of >80% of an oral tyramine load (60). In studies on rat intestines, MAO A, which represented 70% of MAO present in the rats intestine, was responsible for most of the tyramine metabolism (61). When a MAO A selective inhibitor was administered, metabolism of tyramine was reduced to 27% of the control, while administration of a MAO B selective inhibitor did not affect metabolism of tyramine, showing that MAO A is the key to metabolism of ingested tyramine. The irreversible MAO B selective inhibitors administered to patients had reduced risk of the cheese effect (e.g. deprenyl), whereas MAO A selective inhibitors retained their dangerous side effects (e.g. clorgyline).

The third generation of MAOIs were both selective and reversible. The reversible nature of these inhibitors meant the tyramine ingested could compete kinetically with the inhibitor and therefore could be metabolized. These inhibitors show only mild signs of the cheese effect and can therefore be administrated without dietary restrictions, for example, moclobamide (51).

1.8. Kinetic and chemical mechanism

Steady state and stopped-flow kinetic data have been used to investigate the kinetic mechanism of MAO A and B. The mechanism has been probed to determine the intermediates in the reaction pathway, the rate limiting steps in the reaction, and how these rate constants have implications for metabolic control. The main focus of studying

and understanding the mechanism of MAO is for the rational design of inhibitors for this pharmalogically important enzyme.

Steady state kinetics suggested that oxidation of some substrates by MAO B followed a binary mechanism (e.g. phenylethylamine) whereas with others (e.g. benzylamine) a ternary complex mechanism was followed (62). Stopped-flow experiments confirmed these results. It provided further evidence that ternary complexes form not only between reduced enzyme and oxygen, but also between reduced enzyme substrate and oxygen (63). These studies also showed that the re-oxidation of the ternary complex was much faster than that of the binary complex. Closer examination of the rate constants and dissociation constants suggested that the mode of re-oxidation is not exclusive, and proceeds by way of competition between the alternative pathways, as a result of different rates of re-oxidation of the reduced enzyme and the reduced enzyme-substrate complex and their respective dissociation constants (Fig. 1.8.1). The same is true for MAO A (64), where kynuramine stimulates the rate of re-oxidation in the ternary complex, as does benzylamine with MAO B. Inhibitors also bind to reduced enzyme, but inhibit re-oxidation of the flavin by oxygen (65).

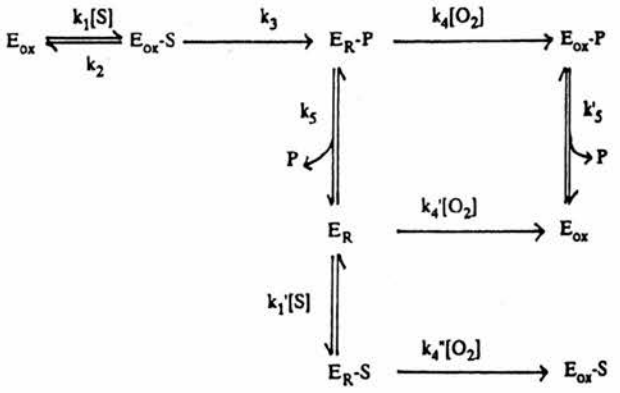

Fig. 1.8.1. Alternate pathways of re-oxidation of reduced MAO via binary or ternary complexes (20).

Competition between the slow and fast pathways of oxidation in MAO has several physiological implications (66). At low amine concentrations, regeneration of oxidized MAO A will be slow because the binary complex predominates, whereas if there is a surge of amine, such as after a meal or synaptic transmission, then the re-oxidation by the ternary complex will predominate, and a higher turnover capacity is available. In the steady state for MAO A, the reduction of flavin by substrate is rate-limiting and the K_M for oxygen is very low (6 μM for MAO A from placenta) (64,67) ensuring that MAO A is insensitive to minor O_2 variations at normal expected levels. In contrast, re-oxidation is rate limiting for MAO B which has a much higher K_M for oxygen (230 μM), close to that of air saturated buffer at 30°C. The K_M for oxygen in MAO B varies with substrate (68), so that at low O_2 concentrations MAO B activity will be much decreased. The pattern of amine oxidation could alter dramatically as the oxygen level in a particular region fluctuates.

Unlike the kinetic mechanism, the chemical mechanism is still poorly understood. The reaction catalyzed by MAO has two halves, a reductive half reaction where the amine substrate is oxidized to an imine by the flavin, which is in turn reduced to the two electron reduced hydroquinone. In the second half of the reaction the flavin is re-oxidized by molecular oxygen back to the fully oxidized form ready to start the process again. The imine product is hydrolyzed by H_2O to the corresponding aldehyde, but whether this happens in the active site or once the imine has left the active site has not been established. Steady state kinetics of product inhibition of MAO B suggest that hydrolysis of the imine product occurs before dissociation of the imine from the enzyme occurs (69). In contrast, stopped-flow kinetic studies on a group of para-substituted benzylamine analogues suggests that a kinetically stable reduced enzyme-imine complex is formed that reacts with O_2 at rates consistent with catalysis. If so, imine hydrolysis would occur after release from the enzyme (70).

The reaction catalyzed by MAO is that of an oxidative deamination with transfer of two electrons from substrate to FAD, a process which could occur by deprotonation (carbanion), hydride transfer, polar nucleophilic addition, or electron transfer (radical cation).

The deprotonation mechanism has been dismissed due to the high pK_a of the methylene protons of the substrate (71). Although other enzymes have mechanisms that can lower the pK_a of the critical hydrogens, there is no apparent way in which MAO can do this.

One approach in determining whether a carbanion intermediate is involved in the mechanism is the use of a substrate with a leaving group vicinal to the anticipated carbanion center. Experiments demonstrating β-elimination of a halide ion from substrate analogues in enzyme catalyzed reactions by transcarboxylases, propionyl-CoA carboxylase (72), succinate dehydrogenase (73), D- and L-amino acid oxidases (74) and butyryl-CoA dehydrogenase (75) have been taken as evidence for a carbanion intermediate in these reactions. In plasma amine oxidase, 2-Cl-2-phenylethylamine has been used to determine whether a carbanion is generated by direct abstraction of the α-hydrogen from the substrate leading to Cl^- elimination. This can be postulated to involve a carbanion intermediate resonance stabilized by Schiff's base formation with the pyroquinoline co-factor of plasma amine oxidase. Steady state kinetics have shown that no β-elimination of Cl^- occurs, and the normal reaction product 2-Cl-phenylacetaldehyde is formed, therefore ruling out the possibility of a carbanion intermediate mechanism in MAO (47). Weyler noted, however, that the dihedral angles of the amine constrained within the enzyme active site may have been such that the antiperiplanar orientation preferred for elimination is not achieved.

The observation that MAO activity increased with increased pH prompted Smith *et al* (76) to propose that MAO catalysis proceeds via a hydride transfer mechanism. This mechanism involves the rate limiting $H^{\cdot}$ abstraction from the α-carbon of the amine substrate leading to the α-amyl radical. Rapid electron transfer then occurs, resulting in the protonated imine and the flavin hydroquinone. Electronegativity considerations and the fact that the hydride transfer mechanism is such a high energy process suggests that it

is unlikely to occur in MAO. Hydride transfer would involve the removal of electrons from elements with electronegativities similar or greater than hydrogen and localization of these electrons on hydrogen. MAO catalyses the ring opening reactions (giving subsequent enzyme inactivation) for a variety of cyclopropylamines (77) and cyclobutylamines (78). In some of these compounds, there is no α-hydrogen present to be abstracted. These results cannot be rationalized in terms of the hydride transfer mechanism.

The polar nucleophilic mechanism originally proposed by Hamilton is proposed to occur via nucleophilic attack at the flavin C-4α position by the deprotonated amine. Proton abstraction then occurs from the alpha carbon of the amine-flavin C4a adduct facilitated by an active site base in the active site. Formation of the protonated imine results from elimination from the reduced flavin. Support for this mechanism comes from evidence of oxidative deamination of benzylamine by N(3)-methyllumiflavin. Primary, secondary and tertiary amines also form stable adducts with N(5)-ethyl-N(3)methyllumiflavin perchlorate, which can then undergo base catalyzed elimination to the corresponding imine and reduced flavin. One drawback with this mechanism is that no active site base is seen in the active site of the crystal structure of MAO B.

A modification of Hamilton's mechanism (79), proposed by Edmondson and co-workers, suggested that C-H bond cleavage occurs via a direct hydrogen atom transfer from the α carbon to a protein based radical in the active site with subsequent electron transfer to the flavin. EPR spectra of resting bovine MAO B indicated an organic radical

species present (80), this species could be sufficiently reactive to remove a hydrogen from the amine substrate. However, the idea of a resting radical residue within the active site of the enzyme is now less likely because the highly purified recombinant human liver MAO B from *Pichia pastoris* and recombinant human liver MAO A from *Saccharomyces cerevisiae* showed no detectable EPR signals in their resting states (81,82). The radical in bovine MAO B must have been an artifact of purification.

QSAR studies on a series of closely related substrates are useful mechanistic tools for the study of enzyme-catalysed reactions. Examples of this approach for enzymes similar to MAO include the quinoproteins, plasma amine oxidase, methylamine dehydrogenase and aromatic amine dehydrogenase, and also the flavoproteins, D-amino acid oxidase and lactate dehyrogenase. Edmondson and co-workers have used this approach to investigate the polar nucleophilic mechanism for MAO. Correlations from a number of different para-substituted benzylamine substrates strongly support the mechanism of a C-H bond cleavage, ruling out any mechanism involving hydride transfer. Steady state kinetics and rates of flavin reduction both show a positive correlation with the electronic parameter σ, indicating that electron withdrawing substituents significantly enhance a C-H bond cleavage (83). The increase in reaction rate is facilitated with delocalisation of electron density into the benzyl ring, suggesting negative charge develops at the α carbon in the transition state consistent with the proton abstraction mechanism for C-H bond cleavage. The aminium cation mechanism and the polar nucleophilic mechanisms both involve proton abstraction steps, and both mechanisms could be supported by the positive correlation of the σ parameter. It is however difficult to discriminate between the two

mechanisms due to the inability to detect any C-4α-flavin adducts or any radical species, possibly because very low concentrations of these species are present in the reaction cycle.

The fourth class of mechanism proposed for MAO is the radical mechanism. The radical mechanism for MAO originated in the early 1960s (84). Many radical mechanisms have been proposed for flavoenzymes over the years. One model of radical mechanism based on the work of Bruice (85) and Massey and Ghisla (86), is initiated by carbanion formation followed by two single electron transfers to the flavin. MAO catalysed carbanion formation does not appear favorable, so this process does not seem likely.

Non-enzymatic amine oxidation can occur with chemical oxidizing agents, electrochemically, and photochemically. All of these processes occur by way of electron transfer mechanisms. It therefore seemed reasonable that enzymatic oxidation of amines by MAO could proceed via an electron transfer mechanism. One electron transfer from the amine group to the flavin gives the amine radical and flavosemiquinone; loss of a proton will then give the carbon radical. The pKa of an α-proton of an amine is too high for an enzyme to be capable of removing it. However, the pKa of an α-proton of an amine radical cation is only about 10, and with the pH optimum of the enzyme being 9, this proton could easily be removed by the enzyme. The radical generated can be oxidized further either by a second electron transfer (Fig. 1.8.2. pathway a,), or by radical

combination with an active site radical, either the flavin radical or an active site amino acid radical, followed by β-elimination to the immonium product (Fig. 1.8.2. pathway b).

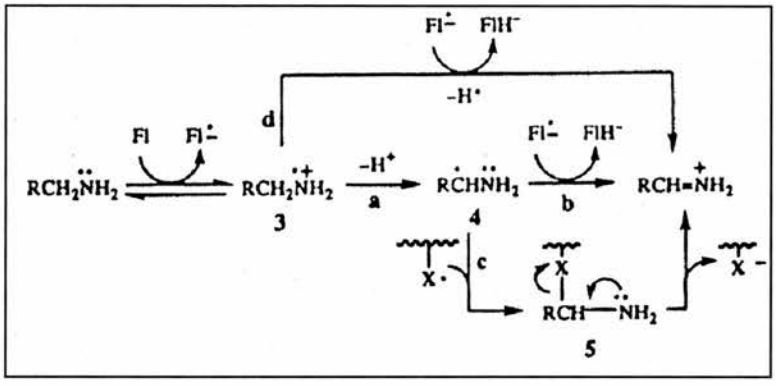

Fig. 1.8.2. One electron transfer mechanism in MAO catalysis (87).

One aspect of the electron transfer mechanism that needs to be clarified is the thermodynamics of electron transfer. Krantz and co-workers suggested that the first electron transfer was reversible and therefore not rate determining. This would rationalize the kinetic isotope effect observed for the oxidation of [α,α-$^2H_2$] substrates (88). Depending on the relative rates of k_{-1} (the reverse rate of initial electron transfer) and k_2 (proton abstraction) for each substrate, the kinetic isotope effect could range from 1-7. Considering the thermodynamics of the uncatalysed reaction, the reversibility of this first step seems reasonable.

The oxidative potential of free flavin is –0.2 V and the oxidative potential for a primary amine is > +1 V. The first electron transfer would therefore be endothermic by 1.25 V and the reversible reaction exothermic by the same amount. This seems a large energy barrier to overcome for the first electron transfer to be reversible. However, the oxidative potential of a primary amine may be lowered by 0.5 V by changing the molar ratio of the

organic solvent to water mixture (89). The active site of MAO B is indeed very hydrophobic and could thus lower the oxidative potential of the amine. Distortion of the oxidized flavin (normally planar) to a bent structure would lower the LUMO energy of the flavin making the acceptance of the initial electron a lower energy event. The flavin in MAO B has been shown to be bent along its N5-N10 axis by about 30° forcing it into the shape of reduced flavin and making it a much stronger oxidant (45).

There has been no direct evidence for the production of a radical in MAO during substrate catalysis. EPR (90) and stopped-flow spectrophotometry (68) have been used to identify radicals during substrate catalysis of benzylamine and phenylethylamine, but no radicals were ever observed. This does not necessarily mean they do not exist. The failure to detect a radical during substrate catalysis may be due to the formation of a radical ion pair between the flavin and the substrate during the reaction, or, because of the rapid reversibility of the initial electron transfer, there is too small a concentration of radical to be observed either using EPR or stopped flow spectrophotometry.

1.9. Inhibitors of MAO

1.9.1. Irreversible inhibitors

MAO A and B are irreversibly inhibited by mechanism-based inhibitors. These include acetylenic amines, allenic amines, substituted hydrazines and cyclopropylamines. The inhibitors all form similar adducts but the selectivity for either MAO A or B varies with inhibitor structure. The two well-characterized and important classes of irreversible inhibitors are the acetylenic amines and cyclopropylamines, which will be concentrated on here. The main sites of nucleophilic attack in the active site of MAO are N5 and C4 of FAD.

1.9.1.1 Acetylenic amines

Acetylenic inhibitors of MAO A and B include deprenyl (MAO B), clorgyline (MAO A) and pargyline (MAO A and B). These inhibitors reduce the flavin and form a covalent adduct with N5 of the flavin. The chemical evidence for this has now been confirmed by X-ray crystallography, where pargyline is shown to be covalently bound to N5 of the reduced flavin in MAO B (42).

These inhibitors were some of the first inhibitors of MAO to be used clinically after the hydrazine inhibitors (91); in fact deprenyl is still being investigated as an adjunct for the treatment of Parkinson's disease. The main problem with these inhibitors is the irreversible nature of their inhibition, so that their effect lasts up to several days until enough MAO is resynthesised. The half-life of MAO ranges between 3 days for rat liver,

to 30 days for rat brain or heart (92). If MAO is completely inhibited, then ingested exogenous amines, such as tyramine from cheese, can pass through the intestine (the site that MAO normally degrades exogenous amines) and can enter the bloodstream. Here it can be taken up by adrenergic nerve terminals, act to release and replace the normal neurotransmitter stores, thereby compromising synaptic nerve transmission (93). The common side effect is hypotensive crisis seen in patients on irreversible MAO inhibitors with a high content of cheese and red wine in their diet. This is known as the cheese effect due to cheese being the main source of tyramine in the diet.

1.9.1.2 Cyclopropylamines

There is a high level of interest in cyclopropylamine inhibitors of MAO due to the pharmacological importance of *trans*-2-phenylcyclopropylamine (2-PCPA) more commonly known as tranylcypromine. The mechanism of their inhibition involves one electron transfer to the flavin followed by hemolytic cleavage of the cyclopropyl ring with the formation of an adduct, which was thought to occur with an amino acid residue in the active site, or the flavin. There are reports that this adduct is formed with a cysteine residue, but this awaits conformation (94). The crystal structure of MAO B with 2-PCPA shows the adduct is formed through the C-4α of the flavin. Previous reports have suggested that this inhibitor forms only one adduct in MAO B, not to N5 of the flavin, but to an amino acid residue in the active site, proposed to be a cysteine. In the crystal structure there is only one adduct, to C-4α of the flavin, and no additional electron density was seen around any cysteines in the structure (43).

Inactivation of MAO B by 1-PCPA is thought to occur via two pathways, the first adduct is with C-4α of the flavin. The second adduct was thought to be a cysteine residue in the active site (95). The mechanism proposed for 1-PCPA involves one electron transfer from 1-PCPA to the flavin followed by hemolytic cyclopropyl ring opening to a common radical intermediate (96), this is then trapped by either the flavin radical or the $S^{\bullet}$ radical of the cysteine. There is direct evidence for the flavin adduct from electrospray ionization mass spectrometry (97), but no direct evidence for the attachment to a cysteine residue.

Another class of cyclopropylamines was also shown to inactivate MAO B. N-Cyclopropyl-α-methylbenzylamine (N-CαMBA) was shown to inactivate MAO B without attachment to the flavin; the attachment was postulated to occur with an active site residue (98). This adduct was stabilized by chemical reduction with sodium borohydride to avoid degradation. After digestion with Lys-C endopeptidase and HPLC separation of the peptides, Cys-365 was proposed to be the site of adduct attachment in MAO B (99). The recent crystal structure of MAO B has shown that Cys-365 is not in the active site but on the surface of the enzyme near the entrance of the active site.

1.9.2. Reversible inhibitors

The first MAO inhibitor to be used as an antidepressant was discovered during screening for antituberculosis drugs. The discovery that inhibition of MAO led to an elevation in mood resulted in an appreciation of the role of MAO in the brain (51).

The early irreversible inhibitors led to undesirable vascular effects caused by an inability to metabolise dietary amines such as tyramine, demonstrating that MAO plays an important role in scavenging for exogenous amines. Since the vascular side-effects with irreversible inhibitors (commonly known as the cheese effect) were identified, design of MAO inhibitors has focused on the development of inhibitors reversible in nature and selective for either MAO A or B.

The properties required for efficacy of reversible inhibitors are not fully understood and many studies have been undertaken to understand the mode of action of these inhibitors in order to develop safer, more potent antidepressants. Table 1.9.2.1. lists a number of reversible MAO inhibitors, from which it is clear that a wide number of different structures inhibit MAO. From the many studies on the different classes of inhibitors, a general pharmacopheric model for MAO inhibition is now recognized. Firstly, a molecule needs to have an aromatic ring with a nitrogen, or sometimes sulphur or oxygen within one bond of the ring, and secondly, the molecule needs to be lipophilic in nature. MAO A is capable of binding positively charged molecules such as MPP^+ whereas MAO B binds them poorly (Table 1.9.2.1.)

Scheme 2

$$E + I \underset{k_{-1}}{\overset{k_1}{\rightleftharpoons}} (E*I) \underset{k_{-2}}{\overset{k_2}{\rightleftharpoons}} (E*I^*)$$

Reversible MAOIs include competitive inhibitors and time dependent tight binding inhibitors. Scheme 2, above, shows the difference between a reversible and a time dependent inhibitor. Reversible inhibitors bind to the enzyme in a freely reversible manner (E*I). Tight binding inhibitors bind firstly to the enzyme in a freely reversible manner (E*I), then over time the enzyme undergoes a time-dependent structural change causing a tighter enzyme-inhibitor interaction (E*I*). In both cases the inhibition is reversible.

The first proposed model for reversible MAO inhibitors came from Codoñer (100). The observation that in solution β-carbolines change the spectrum of riboflavin was consistent with a stacking interaction. Experiments were undertaken at different temperatures to determine the equilibrium constants of the molecular complexes formed between riboflavin and β-carbolines, and from these results thermodynamic parameters were calculated. On this basis, a stacking interaction was proposed to occur between riboflavin and β-carbolines in solution. Studies on pure MAO observing the changes in the FAD spectrum upon addition of inhibitors also showed spectral changes, inferring that a similar stacking interaction could also occur between inhibitor and FAD in the enzyme (101,102).

Reversible inhibitors selective for MAO A include β-carbolines, pirlindole, amiflavin, amphetamine, toloxatone, cimoxatone and befloxatone. Inhibitors selective for MAO B include some tricyclics, caroxazone and 7-ether substituted coumarins. α-Methylation of phenylethylamine to amphetamine converts a good B substrate into an A selective inhibitor, with the S isomer being more selective for MAO A. This highlights the importance of the α asymmetric center in MAO substrates and inhibitors.

Table 1.9.2.1. Inhibition data for a selection of reversible MAO A and B inhibitors.

Inhibitor	Source of MAO	MAO A K_i μM	MAO B K_i μM	MAO A selectivity
S(+)Amphetamine [23]	Rat liver	20	770	39
R(-)Amphetamine [23]	Rat liver	70	600	8.6
S(+)Amiflavin [23]	Human brain	0.4	210	525
R(-)Amiflavin [23]	Human brain	0.9	25	28
Harmine [23]	Human liver	0.005	7000	1400000
(±)Toloxatone [23]	Rat brain	1.8	44	24
(±)Cimoxatone [23]	Rat brain	0.004	0.08	20
Pirlindole [103]	Human liver A Rat brain B	0.264	52	197
Tetrindole [103]	Human liver	0.05	130	2600
Coumarin–7-ether substituent [104]	Rat brain	>10	0.0009	<0.00009
Coumarin-7-sulphonic acid ester [104]	Rat brain	0.008	5	625
Oxazolidinone [105]	Rat brain	20	0.008	0.0004
Indole derivative [106,107]	Rat brain	8	8000	1000
MPTP [108]	Purified enzyme	18	100	6
MPDP [108]	Purified enzyme	2.4	200	83
MPP^+ [108]	Purified enzyme	3	230	77

1.9.2.1. Oxazolidinones

Oxazolidinone derivatives were among the first series of compounds to be extensively studied as inhibitors of MAO A and B after the two forms were identified. They can be either reversible or irreversible for MAO A and or B. Cimoxatone and toloxatone were two of the first reversible inhibitors developed as effective antidepressants with K_i values of 0.03 μM and 1.8 μM respectively. Toloxatone underwent clinical trials and was the first reversible selective MAO A inhibitor used as an antidepressant in clinical practice. Further studies following on from the development of toloxatone led to the discovery of befloxatone which is a selective reversible inhibitor of MAO A with a K_i of 2 nM. The inhibition is time dependent and fully reversible. The lack of any amine entity in either toloxatone or befloxatone explains their reversible nature. Indeed the related compounds, 5-(aminomethyl)-3-aryl-oxazolidinones give irreversible inhibition. It is clear that the amine confers the irreversible nature of these inhibitors (29). Another class of inhibitors derived from oxazolidonones or tetrazoles are aryl diazoheterocycles (29), the development of which has led to some very potent selective MAO B inhibitors.

Several features have emerged from these studies that are relevant to enzyme inhibitor interactions of selective MAO B inhibitors. As for MAO B substrates, lipophilicity is important for MAO B inhibitors. The presence of a benzoxy group in the para position of the aryl oxadiazolones and aryl oxazolidonones is essential for activity; electron donating or withdrawing groups in this terminal phenyl ring reduces activity. The role of the heterocycle is not well understood, a five membered ring gives greater affinity than a six membered ring. As seen for substrates of MAO B, the length of the lateral chain of the

aryl diazo derivatives should not be longer than two carbon atoms. This indicates that groups on the lateral chain could interact with the same binding site as that of the amine of the substrate, explaining the competitive nature of these compounds.

With the increased understanding of the inhibition of MAO, it has become apparent that a vast array of compounds inhibit MAO. Some of these compounds are antibiotics based on the oxazolidinone structure; some of these compounds show signs of the cheese effect, as seen in many earlier MAO inhibitors. There is ongoing work to try to reduce the cheese effect in these compounds while retaining their antibiotic activity (51).

1.9.2.2. Indole derivatives

Indole derivatives have been mentioned previously as substrates, such as serotonin and tryptamine. Endogenous MAO inhibitors such as the β-carbolines have been found to selectively inhibit MAO A with potency in the nM region. Harmine in particular has a K_i value for MAO A of 5 nM and an IC_{50} of 7000 μM for MAO B. Studies on purified enzyme showed that the inhibitors interact with the covalently bound FAD to induce distinct spectral changes, the magnitude of which correlates with inhibitory efficacy (109).

Indole and isatin (2,3-dioxindole) analogues have been used to study the active site dimensions of MAO A and B (107,110). QSAR analysis revealed that the active site of MAO A and B have different dimensions: 13 Å (length) x 7 Å (height) x 4 Å (width) and

8.5 Å (length) x 5.1 Å (height) x 1.8 Å (width) respectively. The ability of MAO A to accommodate larger molecules is illustrated by the indole compound in Fig. 1.9.2.2.1 which is selective for MAO A, with IC50 values of 6 μM and 8000 μM for MAO A and B respectively.

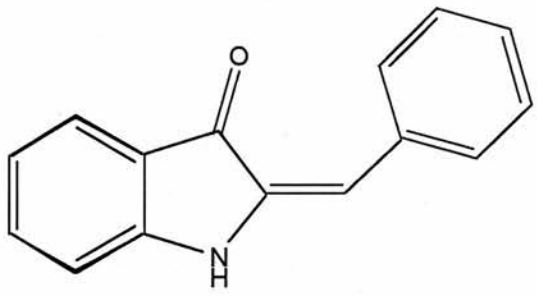

Fig. 1.9.2.2.1. Indole derivative

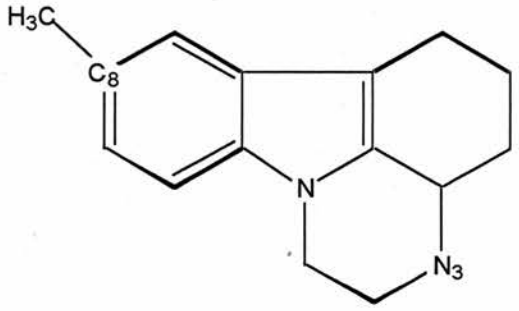

Fig. 1.9.2.2.2. Pirlindole

1.9.2.3. Pirlindole

Another indole series of inhibitors used to probe the dimensions of the active site of MAO was based on pirlindole (2,3,3a,4,5,6-hexahydro-8-methyl-1H-pyrazino[3,2,1-j,k]carbazole hydrochloride) and tetrindole (2,3,3a,4,5,6-hexahydro-8-cyclohexyl-1H-pyrazino[3,2,1-j,k]carbazole hydrochloride). Pirlindole is an antidepressant developed in Russia (111). Its nucleus, shown in Fig. 1.9.2.2.2, has been lengthened at both ends (C8 and N3) to probe the dimensions of the active site of MAO A. Further analysis of the inhibition by pirlindoles has developed a mould of the active site by overlaying the more potent inhibitors on top of the core nucleus of pirlindole, giving a three dimensional mould of the active site.

A study on a series of pirlindole analogues varying the C8 substituent determined the 3D size limitations for inhibitors of MAO A. The dimensions determined from this study were: 14 Å (length) x 7 Å (height) x 4.5 Å (width) shown in Fig. 1.9.2.3.1 (112,113). This model was determined with conformationally constrained analogues; analogues larger in any of the dimensions than the box were poor inhibitors of MAO A. However, flexible analogues that were larger than the box could be tolerated. This size, determined kinetically, was confirmed by the crystal structure (114).

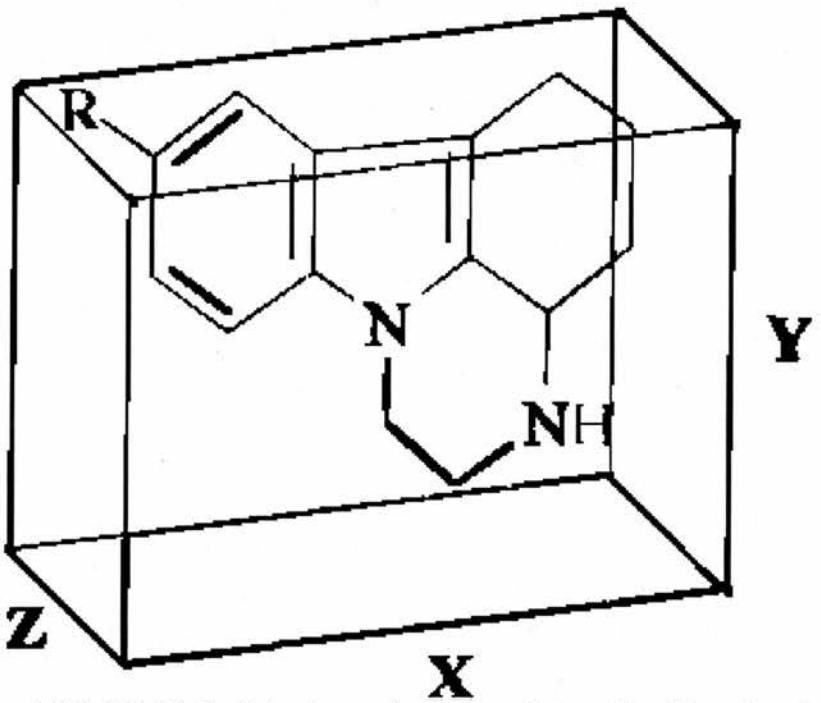

Fig. 1.9.2.3.1. Pirlindole shown in its box determined by structure kinetic analysis.

Compounds with various different electronic C8 substituents were also tested for inhibitory activity. With the requirement for an aromatic ring in the inhibitor structure for good inhibition, it was thought that electron withdrawing or donating groups attached to

this ring would effect inhibition. The kinetic results showed no correlation between K_i and the Hansch constant (π) which is a description of electron donating or withdrawing power (101). The hydrophilic nature of the electron donating or withdrawing substituents may have had unfavorable interactions with the active site of the enzyme, an area where hydrophobic substituents are favorable. The active site of MAO B is lined with many hydrophobic residues; the unfavorable interactions may have masked the true results of these substituents.

Another study on a larger series of pirlindole analogues was undertaken to further charaterise the dimensions of the active site of MAO A. The biologically active conformations of inhibitors that fitted the previously determined box were aligned, to reveal the shape and size of the active site cavity accommodating these compounds (115).

Studies to predict whether pirlindole, like other inhibitors, could stack with the flavin were undertaken in a theoretical study. Calculation of the energy of one of the frontier orbitals implicated in the charge transfer interaction, the highest occupied molecular orbital occupied (HOMO) by electrons of those pirlindoles tested, showed a good correlation between the HOMO energy and MAO A inhibition. These results showed that the higher HOMO energy, the weaker the energy necessary for the electron transfer involved in charge transfer interactions between the inhibitor and the flavin. Additional information was also gained from analyzing the molecular electrostatic potential maps (MEP) maps. The orientation deduced from the MEP maps allowed maximal overlay of the HOMO of the inhibitor and LUMO of the flavin. These results were in agreement

with previous studies performed on reversible inhibitors of MAO A including, toloxatone, befloxatone, brofaromine, harmine, R40519, and moclobemide (116), which have all shown that those compounds could interact with the flavin in MAO A by charge transfer interactions (Frederik Ooms, personal communication).

1.9.2.4. Other tricyclics

There have been a number of other tricyclic compounds studied for their MAO inhibitory properties. Various 6:5:6 and 6:6:6 tricyclics both linear and non-linear systems have been shown to be potent reversible MAO A and B inhibitors. MAO A selective inhibition is seen in aromatic 6:5:6 and 6:6:6 linear tricyclics when the central ring of the tricyclic system has a large L group and a small S group, Fig. 1.9.2.4.1 (117).

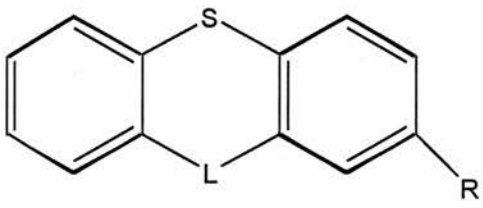

Fig. 1.9.2.4.1. Structure of a tricyclic inhibitor.

1.9.2.5. Coumarins

Coumarin analogues are selective for either MAO A or B depending on the substitution of the core structure. Position 7 is the key site for varying the activity and selectivity of

these inhibitors, shown in Fig. 1.9.2.6.1. Ether substituents yield B-selective inhibitors while sulphonic acid esters yield A-selective inhibitors (118).

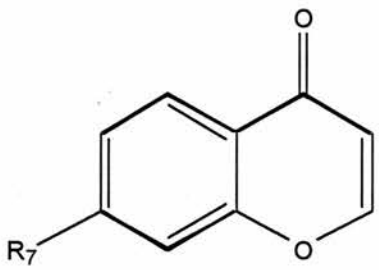

Fig. 1.9.2.5.1. Structure of coumarin.

1.9.2.6. The inhibitor pharmacophore

A wide variety of compounds inhibit both MAO A and B. The compounds described in this section vary in size and shape, from small simple molecules such as isatin, 7 Å in length, to large molecules such as the oxazolidinones up to 30 Å in length. Studies of their efficacy as inhibitors have highlighted several important features for the inhibition of MAO. The molecule needs to be hydrophobic with an aromatic ring with a nitrogen, oxygen or sulphur within 2 bonds of the ring. For rigid molecules to inhibit MAO A they must not exceed the dimensions 14 Å (length) x 7 Å (height) x 4.5 Å (width), whereas for MAO B they must not exceed 8.5 Å (length) x 5.1 Å (height) x 1.8 Å (width). Longer molecules may be tolerated if they are flexible, as seen for many of the oxazolidinone compounds, which in some cases are very long. From the crystal structure of MAO B with isatin bound, it has been shown that the nitrogen in isatin binds close to N5 of the flavin (43), highlighting the importance for a nitrogen in the inhibitor structure. It has yet to be confirmed whether oxygen or sulphur can bind in the same region, close to the flavin in the way the nitrogen in isatin does.

1.10 Aims of the project

Understanding the mechanism of the inhibition of MAO A is of key importance in the rational design of new potent, selective inhibitors with a safer profile. This information will lead to a better treatment of depression and an improved quality of life for these patients.

When this project started, little was known about how reversible inhibitors of MAO A interacted with the active site. It had been proposed that a stacking interaction could occur between the inhibitor and the flavin, and several models of the active site were proposed on the basis of QSAR studies, but experimental evidence could not confirm their existence.

The aim of this project was to determine the mode of interaction of the reversible MAO A inhibitor pirlindole with the active site of MAO A. Procedures involved in doing this include:

- Determination of the kinetic constants involved in inhibition.

- A study of the spectral changes induced by inhibitor binding to MAO A and how this effects the redox properties of the flavin.

- A theoretical study to determine whether it is possible for these inhibitors to stack with the flavin and to determine from other data if there is any direct evidence for this.

- Circular dichroism will be used to investigate how inhibitor binding and reduction of the flavin by dithionite, substrate or irreversible inhibitor affect the structure of the enzyme.

2. Methods and Materials

2.1. *Saccharomyces cerevisiae* growth

Human liver monoamine oxidase A (MAO A) was expressed in the vector pGPD (G)-2 (Amgen, Thousand Oaks, CA91320) in *Saccharomyces cerevisiae* RH218 (ATCC 44076) and MAO A expression induced by galactose (119). A single colony of MAO A expressing *Saccharomyces cerevisiae* was taken to inoculate a 5 ml culture medium containing yeast minimal media (YMM) which consists of 0.50% casamino acids (CAA), 0.67% yeast nitrogen base (YNB), and 2% (w/v) glucose and incubated in a thermostat-regulated shaking incubator at 30°C and 200 rpm agitation for 24 hours. Inoculum (1 ml) was aseptically transferred to two fresh 5 ml tubes of the same sterile medium and grown for 24 hours. Each 5 ml inoculum was used to inoculate two batches of 50 ml medium and left to grow for 24 hours. Each of these was then used to inoculate two batches of 500 ml medium and left to grow for a further 24 hours. Using sterile technique, the two 500 ml cultures were poured into a fermentor (New Brunswick Scientific) with the same medium (8.5 L volume) and left to grow at 30°C, stirring at 200 rpm with aeration at 2 L per minute. Samples (1 ml) were taken every hour when convenient and the absorbance read at 600 nm to produce a growth curve as shown in Fig. 2.1.1. Once the absorbance reached 18-20 or started to plateau, induction of MAO A was started by adding 500 ml sterile 50% (w/v) galactose and growth was continued until it reached a plateau after a further 24-30 hours. Minimal growth is seen on galactose. After the 24-30 hours, the yeast was harvested by centrifugation at 1500 g for 30 minutes and then stored at -70°C.

Typical yields from a 10 L fermentor are 150-170 grams of yeast with a yield of 1 U/g which is low compared with the published figure of 2 U/g (119).

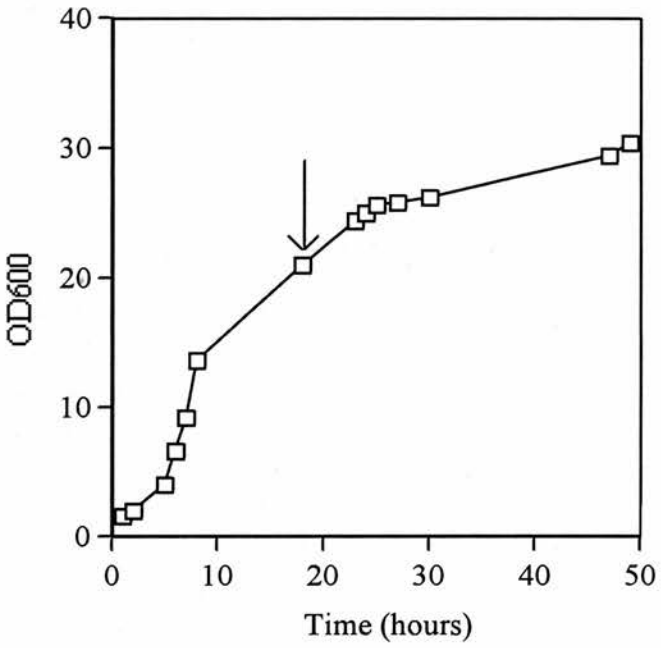

Fig. 2.1.1. Fermentation of *Saccharomyces cerevisiae* expressing MAO A. The fermentation was performed at 30°C with air supply of 2 L/min and agitation of 200 rpm. Galactose was added to 2% final concentration when OD_{600} reached 20, indicated by the arrow, and cells were harvested 24-30 hours after galactose induction.

2.2. MAO A purification

Human liver MAO A was expressed in *Saccharomyces cerevisiae* and purified according to the method established by Weyler and Salach (120). Cells were thawed and washed by suspending the cells in a volume of wash buffer (0.1 M Tris-HCl, pH 7.5) four times the cells dry weight and centrifuging at 1500 g for 20 minutes, 4°C, discarding the supernatant. The pellet was resuspended in one times the cell dry weight of cell breakage buffer (0.1 M Tris-HCl, 1 mM EDTA, 3 mM DTT, 0.5 mM PMSF pH 7.5, at 4°C). Aliquots of 30 ml were added to an equal volume of zircon silicon beads (710-1180 microns) (Sigma) in a metal cylinder, pre-chilled in an ice-salt mix. Cells were broken with five cycles of 1 min of breakage in a Braun cell mill, chilling for 1 min between runs. This cell suspension was then centrifuged at 900 g for 20 minutes, at 4°C, and the pellet discarded.

The supernatant from the low speed spin (LSS) was ultracentrifuged at 130,000 g (Beckman 50.1 Ti rotor) at 4°C for 35 minutes, the supernatant (HSS) was discarded and the pellets resuspended in extraction buffer (0.1 M triethanolamine, pH 7.2, Sigma). The protein concentration of the resuspended pellets was determined using the BCA method (Pierce) and diluted to 25 mg/ml. To this membrane suspension, $CaCl_2$ was added to a final concentration of 25 mM, as were 1 mg phospholipase C (Sigma) and 670 units phospholipase A (prepared from *Naja Naja kaouthia* venom) per 500 mg protein. The pH was adjusted and maintained at 7.2 with 2 M NH_4OH and the temperature was maintained at 30°C with continuous stirring for 1 hour. This suspension was centrifuged for 30 minutes at 48,000 g, 4°C. The supernatant (PLS) was discarded and the pellets

(PLP) resuspended in extraction buffer. The PLP suspension was measured for protein using the BCA method (Pierce) and adjusted to 15 mg/ml. TritonX-100 was added to 0.5% (v/v) final concentration and the mixture homogenised and maintained at 30°C for 30 minutes with continuous stirring. The material was centrifuged at 48,000 g for 30 minutes, 4°C. The pellets (TXP) were discarded and the yellow supernatant (TXS) loaded at 1 ml/min onto a DEAE Sepharose CL-6B fast flow (Sigma) column (100 x 2 cm), pre-equilibrated with degassed buffer A (20 mM KPi, pH 7.0, 20% glycerol, 0.5% Triton-X 100, 3 mM DTT). Once the sample was loaded onto the main column it was washed with 300 ml buffer A, and then eluted with a linear gradient of buffer B (20 mM KPi, pH 7.0, 20% glycerol, 0.8% n-octyl-β-D-glucopyranoside, 3 mM DTT, 0.5 mM PMSF, 0.5 mM D-amphetamine) and buffer C (200 mM KPi, pH 7.0, 20% glycerol, 0.8% n-octyl-β-D-glucopyranoside, 3 mM DTT, 0.5 mM PMSF, 0.5 mM D-amphetamine). The first third of the gradient was discarded, the final two thirds were collected in 10 ml fractions and assayed for activity and absorbance at 280 nm and 456 nm. Fractions were pooled into main, lead, and end fractions and concentrated in Amicon concentrators with YM10 membranes (Millipore) to approximately 2 ml. A spectrum (300-600 nm) was taken of each final concentrated sample. Spectra were also taken after additions of kynuramine and dithionite; the percentage of active enzyme in the sample was determined by dividing the absorbance change upon addition of kynuramine by the total absorbance change after dithionite addition and multiplying by 100. The final product was stored at -20°C in a solution of 50 mM potassium phosphate, pH 7.0, containing 0.8% n-octyl-β-D-glucopyranoside, 3 mM dithiothreitol, 0.5 mM D-amphetamine, and addition of glycerol to a final concentration of 50%. In some purifications where the Triton extract was turbid,

a preliminary DEAE column (7x20 cm) was used to clarify the sample before loading on to the main column. The enzyme was bound to the column at 20 mM KPi and then washed with 50 mM KPi before being eluted with 200 mM KPi. The sample was then diluted to 20 mM KPi before being applied to the main column.

MAO A activity was assayed spectrophotometrically at 314 nm in a 1 ml cuvette containing assay buffer (50 mM KPi, pH 7.2, 0.05% Triton X-100) and 1 mM kynuramine at 30°C. Protein quantity was determined using either the Biuret or the BCA method during purification and the Peterson-Lowry method after purification. Before use, glycerol and amphetamine are minimized by dilution in 50 mM KPi, pH 7.2 and 0.05% Triton X-100 buffer for enzyme assays (at least 100 fold) or removed completely by dialysis or G50 Sepharose chromatography for spectral work.

Table 2.2.1 summarises yield and purification during a typical purification starting with 150 g *Saccharomyces cerevisiae* from a 10 L fermentation. A typical purity for a purification is 90% for the main fraction based on an SDS-PAGE gell. Recombinant human liver MAO A was expressed and purified as described under 2.1 and 2.2. The enzyme was purified in 49.8% yield, higher than the literature values for *Pichia pastoris* and human placenta (35%) (120,121) but slightly lower than the published yield for *Saccharomyces cerevisiae* (60-80%) (119). The specific activity for the final enzyme is 1.75 (U/mg protein), comparable to the values for MAO A purified from *Pichia pastoris* (1.76 U/mg protein) (121) and human placenta (1.7 U/mg protein) (120) using the same purification procedure. For each step of the purification the specific activity increases, as

would be expected during a purification. The enzyme activity drops through the purification except for the phospholipase step. This has been seen in several purifications in this laboratory and is probably due to inaccurate activity measurements during earlier stages of the purification resulting from the turbidity of these samples.

Table 2.2.1. Purification of MAO A

Step	Solution	Volume (ml)	Activity Total U	Protein (mg/ml)	Specific activity (U/mg_{prot})	Step Activity Yield (%)
Cell breakage	LSS	1100	140	18.73	0.0068	100
Membranes						
-supernatant	HSS	950	10.3	15	0.00069	7.4
-pellet	HSP	145	129.9	40.1	0.022	92.8
Phospholipase	PLS	225	12.3	13.33	0.0041	8.79
digestion	PLP	75	154	35.6	0.058	110
Triton	TXS	165	154	7.1	0.132	110
extraction	TXP	88	3.2	18.1	0.002	2.3
Chromatography	Lead	2.5	8	5.78	0.56	5.7
	Main	5.5	61.7	6.4	1.75	44.1
Total at end			69.7			49.8

Fig. 2.2.1 shows the elution profile of the DEAE sepharose column used in the final step of purification of MAO A. MAO A elutes in the final third of the potassium phosphate gradient. The ratio of A456/A280 and the activity profiles mirror each other indicating that the increase in A456 is due to flavin in MAO A.

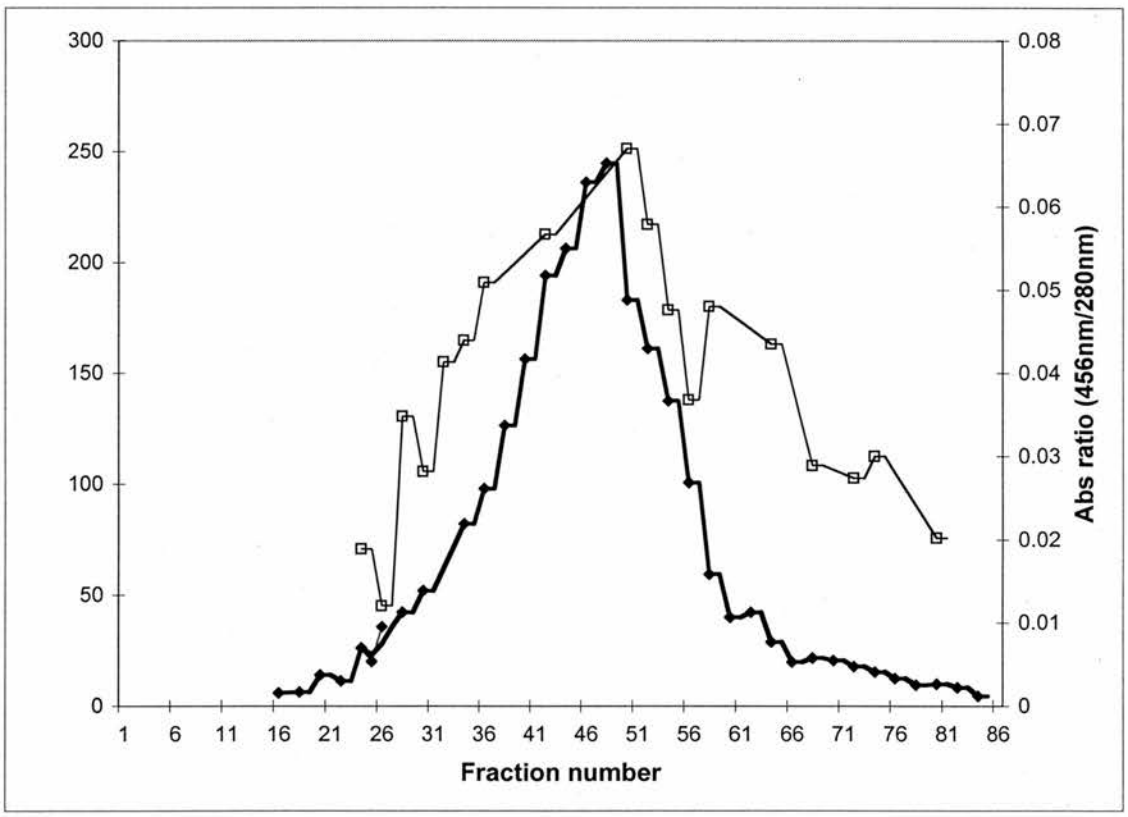

Fig. 2.2.1. Chromatogram of MAO A purification. MAO A was eluted from a DEAE sepharose column using a linear gradient of 20 mM to 200 mM potassium phosphate pH 7.0 (chapter 2.2). The first third of the gradient is discarded; 10 ml fractions were collected for the remainder of the gradient. The lines show the activity of MAO A using 1 mM kynuramine and 100 μL of each fraction (♦) and the ratio of absorbance at 456 nm/280 nm (□). The main sample corresponds to the pooled fractions 36-58. The lead/end sample corresponds to the pooled fractions 20-35 and 59-80.

To determine the FAD concentration and the proportion of functional enzyme in the preparation of MAO A, the reduction of flavin upon anaerobic addition of substrate to anaerobic fully oxidized enzyme was first determined by changes in the flavin spectrum. Addition of a few crystals of dithionite reduces the enzyme fully. The difference in the reduction by substrate and dithionite is used to calculate the percentage of active enzyme. Fig. 2.2.2 shows the spectra of fully oxidized, substrate reduced and dithionite reduced MAO A. Spectra B and C were taken in the presence of substrate which absorbs strongly in the region below 440 nm. The percentage activity was determined to be 90%. The average percentage activity over seven preps was 94.3%.

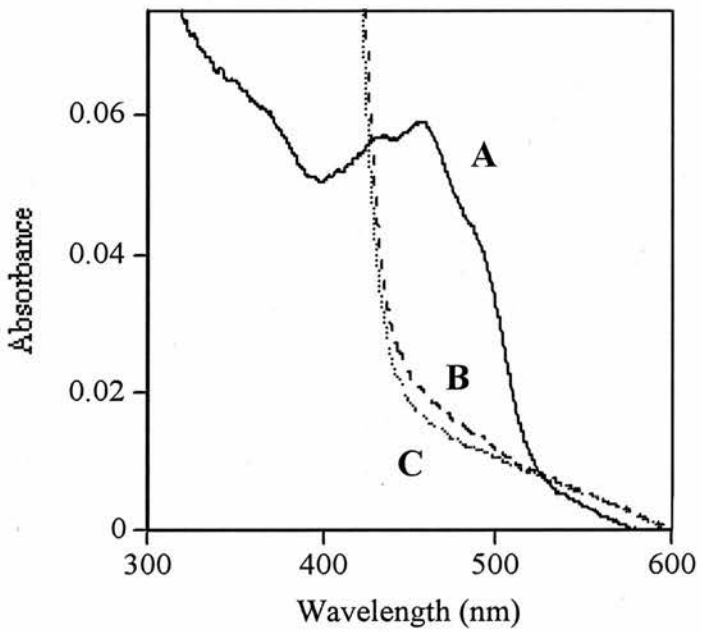

Fig. 2.2.2. Reduction of MAO A by substrate followed by dithionite. Anaerobic oxidized MAO A (A) was reduced by excess kynuramine (B) and the remaining enzyme reduced by dithioninte (C) The concentration of FAD present was calculated using the extinction coefficient of 10,800 M^{-1} cm^{-1} determined by Weyler and Salach (120).

2.3. Steady state kinetics

Steady state kinetics were determined in 50 mM KPi, pH 7.2 and 0.05 % Triton X-100 (assay buffer) at 30°C using a Shimadzu UV-2101PC spectrophotometer equipped with a thermostatically controlled 6 cell changer and computerized data collector. Initial rates of enzyme-catalysed oxidation of kynuramine were measured at 314 nm (ε□12300 M^{-1} cm^{-1}) by the formation of and spontaneous cyclisation of the product to 4-hydroxyquinoline which absorbs at 314 nm (122).

2.3.1. K_M and V_{max} determination

All kinetic constants were determined at 30°C at fixed concentration (air saturation 0.238 mM) of the second substrate, oxygen. Assay buffer was pipetted into 6 quartz cuvettes and substrate added from a 50 mM solution of kynuramine to give a final concentration in 1 ml of 0.1, 0.2, 0.3, 0.5, 0.7, 0.9 mM. The cuvettes were placed in the 6 cell changer and left to equilibrate to 30°C. Enzyme was added using a Rainin 250 μL electronic digital pipette and mixed to start the reaction. The K_M and V_{max} values were determined by the Shimadzu kinetics software which fits the data directly to the Michaelis-Menten equation. The results were displayed as a Hanes plot.

2.3.2. K_i determination

Inhibitor constants (K_i values) were determined by assaying the enzyme catalysed reaction under the same conditions as for K_M and V_{max}. The substrate concentrations were fixed at 0.1, 0.2, 0.3, 0.5, 0.7, 0.9 mM and the inhibitor concentration was varied (a different concentration for each set). The K_M and $K_{M(app)}$ were obtained from the Shimadzu kinetics program. The $K_{M(app)}$ values were plotted against inhibitor concentration where the intercept on the *x* axis corresponds to the K_i. At least 4 different inhibitor concentrations were used for each K_i determination (see Fig. 3.1.1.1). For K_i values determined after 5 minutes, the enzyme and inhibitor were pre-incubated at 30°C for 5 minutes in the cuvette and the reaction started by the addition of substrate. For the time course, enzyme and inhibitor (at a concentration giving approximately 50% inhibition at 0.3 mM kynuramine) were pre-incubated together for up to 5 minutes and the reaction started by the addition of 0.3 mM kynuramine. For K_i determinations where the K_i value was less than 10 nM (the concentration of the enzyme in the assay) the enzyme concentration was lowered to below the K_i value. All inhibitors were freely soluble in, and dissolved in DMSO.

2.4. Stopped flow spectrophotometry

Enzyme was prepared in 50 mM HEPES pH 7.5 by running the enzyme through a G50 Sepharose spin column to remove glycerol, DTT and amphetamine. Enzyme was then centrifuged at 15,500 g for 10 minutes at 4°C to remove any aggregated enzyme. The volume of the enzyme was measured and a spectrum taken. The enzyme was then transferred to a nitrogen box and reduced using dithionite (1 mg/ml)

Reduced enzyme pre-mixed with either inhibitor or kynuramine was shot against air-saturated buffer and the rate of re-oxidation measured at 456 nm over a period of up to 10 seconds, using an Applied Photosystem three sringe stopped flow spectrophtometer.

2.5. Spectral studies

2.5.1. Inhibitor titrations of MAO A

Before titration experiments, the small molecules added to preserve the enzyme in storage (DTT, D-amphetamine and glycerol) were removed by gel filtration. G50 Sepharose was poured into each of two spin columns in 50 mM KPi, pH 7.2, 0.05% Brij (MAO spectral buffer), centrifuged at 430 g for 2 minutes and the flow-through discarded. A maximum of 100 µl of enzyme was loaded onto each spin column and spun at 430 g for 1 minute and the enzyme recovered. The enzyme was then centrifuged in a microfuge tube at 15,500 g at 4°C for 10 minutes to remove any aggregated enzyme and the volume measured. It was then transferred to the 3-arm cuvette and made anaerobic. All the arms of the cuvette were sealed with silicon greased glass connectors and the

cuvette attached to the gas train. Argon was cycled through the cuvette by, in turn, sucking air out and allowing argon to enter the cuvette. This was repeated 10 times and then left to equilibrate with argon for 10 minutes. The syringe was washed with water and then filled with anaerobic inhibitor before transferring it to the side arm of the cuvette letting argon flow through to stop any air entering. The argon flow is stopped, the cuvette sealed and transferred to the spectrophotometer. A baseline from 300-600 nm was previously recorded with MAO spectral buffer using the same cuvette. A spectrum (300-600 nm) is run of the original enzyme and after every addition of inhibitor until no further change occurs. A final addition of inhibitor, to give a final concentration of 100-fold K_i is done to ensure saturation of the active site by inhibitor. Difference spectra are calculated by subtracting the spectrum of enzyme alone from each spectrum in turn.

2.5.2. Dithionite titrations

Dithionite (1 mg/ml) previously standardized with riboflavin (100 μM) was titrated into the MAO A-inhibitor solution using an automatic syringe, aliquoting 2 μl at a time under anaerobic conditions. Spectra were taken 15 minutes after each addition and mixing. To facilitate the redox equilibrium, a catalytic amount (1 μM) of methyl viologen was added.

2.6. Redox potential determination

MAO A was prepared in 500 mM KCl, 100 mM HEPES, 0.2% Brij, pH 7.5 by running the enzyme through G50 Sepharose spin columns to remove glycerol, DTT and amphetamine. Enzyme was centrifuged for 10 minutes at 4°C at 15,500 g, the volume measured and a spectrum taken. The enzyme was concentrated to 0.5 ml and a concentration of 200 μM. This was made anaerobic by cycling argon and transferred to a nitrogen box where the enzyme is transferred to a poteniometric cell and several mediators added (Benzyl viologen 1 μM, methyl viologen 2 μM, HNQ 1 μM and FMN 2 μM) to aid equilibrium. A potential of 0 mV relative to the standard hydrogen electrode was applied and a spectrum taken. Successive potentials were applied to the enzyme solution from 0 to –300 mV in 15 mV steps allowing 15 minutes for equilibration of electrons between mediators and enzyme and a spectrum taken after 15 minutes. This process was reversed for the oxidation of the enzyme with 15 mV steps equilibrated for 15 minutes and a spectrum taken after 15 minutes. This work was done using equipment in the lab of Dr S. Daff, University of Edinburgh.

2.7. Molecular modeling

2.7.1. HOMO/LUMO and molecular electrostatic potential calculations

Structures of inhibitors were drawn on Chemdraw, files transferred to Gausian 96, 3D energies minimized and the files saved as Cartesian co-ordinate files. These files act as input files for the gausian 98 Restricted Hartree-Fock calculations (rhfc) to calculate electrostatic potentials and E_{HOMO}/E_{LUMO} topologies. The files resulting from these calculations are then converted from ecp51 files to plt files using the conversion program gcube2plt so they can be viewed in gOpenMol (http://www.csc.fl/~laaksone/gopenmol/) (123). The molecular XYZ co-ordinates used for gOpenMol are given in an fchk file and allow the 3D structure of the molecule to be viewed in gOpenMol. The plt files are used to view the results of the g98 rhfc for either electrostatic potentials or E_{HOMO}/E_{LUMO} calculations. The co-ordinates of these results can be aligned on the 3D structures of the compounds. The initial parts of this work were performed in the lab of Dr Johan Wouters, Facultés Universitaires Nore-Dame de la Paix, Namur Belgium.

2.7.2. Charge matching calculations

Frontier orbital and molecular electrostatic potential (MEP) calculations were made at the Restricted Hartree-Fock (RHF) level of electronic theory using Gaussian 94 package on an IBM SP2 computer system. Calculations have been performed using the 3-21G basis set in LCAO expansion of the molecular orbitals. The atom-centered charges were determined for lumiflavin and thirteen β-carbolines. Atom centred charges derived from

electrostatic potential calculations using the AM1 semi-empirical method were used to match the π-surfaces. These electronic structure calculations for a series of harmine derivatives were performed on a Silicon graphics O2 workstation using SPARTAN (version S.1.3, Wavefunction Inc., Irvine CA, USA, 1999). The charges for the atoms predicted to lie close together in the stacking model shown in Fig. 3.4.4.2 and 3.4.4.3 were used to calculate a net score for the electrostatic attraction of each pair of atoms. A negative value would indicate an unfavourable pairing, whereas a positive value is favourable. The net values were plotted against the logarithm of the experimentally determined K_i values from the literature (124).

2.8. Circular dichroism spectroscopy

Before spectra were taken the small molecules added to preserve the enzyme in storage (DTT, D-amphetamine, glycerol) were removed by G50 Sepharose filtration. Samples were prepared in 50 mM KPi, pH 7.5, containing 0.05% Brij-35 and made anaerobic by cycling argon. At the BBSRC-supported circular dichroism facility at the University of Glasgow (Professor Nicholas C. Price), CD spectra were recorded at 20°C using either a JASCO J-600 or a JASCO J-810 spectropolarimeter. Spectra were recorded in anaerobic quartz cells of 0.5 cm pathlength (Starna). Appropriate blanks were subtracted from each spectrum. In each case 2 scans were averaged, with a scan rate of 20 nm/min and a time constant of 2 seconds.

3. RESULTS

3.1.1. Kinetics

Previous studies on pirlindole analogues showed the maximal size for a good inhibitor of MAO A was 14 Å (length) x 7 Å (height) x 4.5 Å (width) (101). Further analogues were synthesized by Professor V.S. Velezheva, Institute of Organoelement Compounds, Russian Academy of Sciences, Moscow, to develop a three dimensional mould of the active site. The kinetic study reported here was undertaken to look at the effect of both C8, C10 and N3 substituents as well as de-saturation of the indole ring. The substituents add length or width, and de-saturation makes the molecule more planar. Fig. 3.1.1.1. shows a graph of how the K_i was determined for compound **2**.

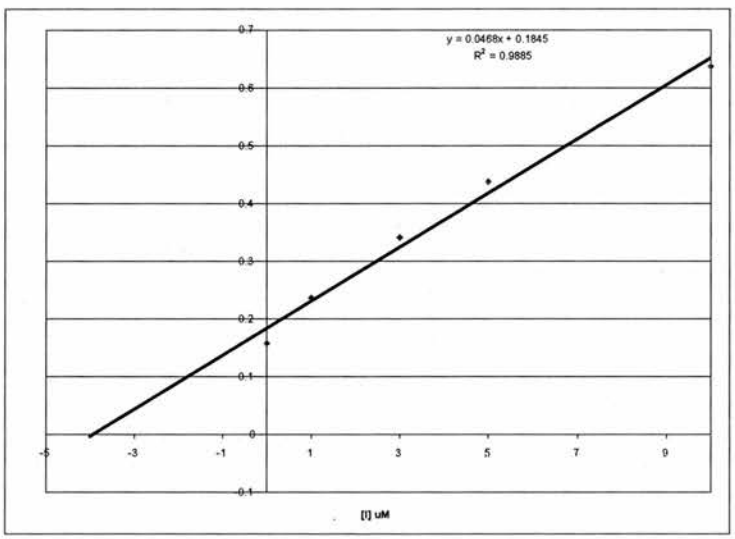

Fig. 3.1.1.1. Plot of $K_{M\,(app)}$ versus inhibitor concentration for inhibitor 2 to determine K_i. The inhibitor concentrations were, 0, 1, 3, 5 and 10 μM and the K_i was 3.94 μM.

Table 3.1.1.1 shows the initial K_i values (without preincubation). Increasing the size by adding a C8 substituent, from **1** (no substituent) to **6** (CH_3, methyl) to **11** (C_6H_{11}, cyclohexyl) increased inhibition. However introduction of the largest rigid substituent, ($C_{10}H_{15}$ admantyl) to give **25**, decreased inhibition. The cyclohexyl derivative **11** is probably at the optimal size for inhibition and any further increase in size will be sterically hindered. Analogues with smaller substituents (**1** and **6**) will have less interactions with the protein. However, **17** (C_6H_5-$(CH_2)_2$) with the largest overall length at 15 Å in length had a K_i of 0.41 μM, 10-fold lower than **1** and 2-fold lower than **25**. The flexibility of this longer substituent allows the inhibitor to fit in the active site.

Increasing the size of the N3 substituent increased inhibition for the series with no C8 substituent. However, increasing the size of the N3 substituent decreased inhibition for the methyl and the cyclohexyl series. The decrease in inhibition in the cyclohexyl series was more dramatic for IC_{50} values than for K_i values for the methyl series (Table 3.1.1.1). The cyclohexyl series were not available for full analysis in St Andrews so were only tested for IC_{50} values by A. Medvedev (Moscow). The parent compound, pirlindole **6**, was 20-fold more potent than its N3-methyl keto derivative **3** whereas tetrindole **11** was 500-fold more potent than its N3-methyl keto derivative.

Interestingly, although a methyl group at C8 conferred a 20-fold lower K_i (**6** vs. **1**), a methyl group at C10 did not change the K_i value (**1** vs **18**). The derivative with a methyl group at C10 **18** was 20 times less potent than the derivative with a methyl at C8 **6** .The

C10 methyl group when combined with the C8 methyl group (**6** vs. **19**) had a significant effect, compound **19** is one of the most potent inhibitors in this study.

K_i values and hydrophobicity (C log P) were examined to compare the hydrophobicity of the two regions occupied by substituents at C8 and N3. The hydrophobicity of the whole molecule, indicated by the C log P value could not account for the relative efficacy of the small sample of compounds with C log P values. For example, inhibitor **25** has the highest C log P value of 5.75, but is one of the poorer inhibitors tested compared with the other compounds tested with known C log P values. Also, inhibitor **1** has a higher C log P value than inhibitor **8** (2.77 and 2.59 respectively) but is a poorer inhibitor.

For the substituent at C8, using the Hansch constant (π) as a measure of hydrophobicity of the subsituents rather than the whole molecule (125), the K_i values indicated the expected trend of better inhibition with increased hydrophobicity, up to a point. Thus for the C8 substituents, H, CH_3 and C_6H_{11}, the π values are 0, 0.5 and 2.08 respectively, and the K_i values decrease from 5.2 to 0.26 to 0.05 μM. However, for this size of substituents it can be said that increasing the size of substituent and increased hydrophobicity go hand in hand, and that hydrophobicity may be one feature that favors binding, but is not the determining factor. For the admantyl $C_{10}H_{15}$ derivative, the π value is higher still at 2.4, but the K_i increases higher than the methyl or cyclohexyl derivatives. For the substituent at N3 there is no trend with either series. Either admantyl (**10** with a higher π of 2.4) or formyl (**7** with a lower π of –0.65), increased the K_i compared to **6** with a π of 0 for the H atom.

Introducing conjugation at N3 did not affect the 3D size of the compounds, but in all cases the dehydro derivative was more potent than the saturated derivative (Table 3.1.1.1, **6** vs. **21**, **22** vs. **18**, **11** vs. **23**). In previous studies, electron donating or accepting groups at C8 impaired inhibition of MAO A, but all compounds were saturated at N3. Here, compound **26** with the strongly electron withdrawing Br at C8 is also a dehydro derivative with a double bond at N3. This compound was found to have a K_i of <3 nM, lower than can be accurately determined in the spectrophotometric steady state assay.

After a 5-minute pre-incubation of enzyme and inhibitor, the K_i values were approximately 6-fold lower than without pre-incubation. However, the difference between the K_i values remained the same, indicating that the increased affinity due to pre-incubation is independent of the structure of the ligand. A plot of % activity versus time is shown in Fig. 3.1.1.2 for inhibitor **1**. The profiles for the other inhibitors were similar to inhibitor **1**, with maximal inhibition occurring at 5 minutes.

Fig. 3.1.1.3 shows the Lineweaver-Burk plots for compounds **2** and **11**. The K_i for inhibitor **2** is an initial K_i where enzyme was added last to initiate the reaction. For compound **11** the K_i is determined after enzyme and inhibitor were preincubated for 5 minutes and substrate added last to initiate the reaction. For inhibitor **2**, the 5 lines intercept just to the left of the *y*-axis (competitive inhibition), whereas for inhibitor **11** the intercept lies further to the left, nearly at the *x*-axis (mixed inhibition) For all inhibitors studied, the inhibition is reversible (A Medvedev, personal communication).

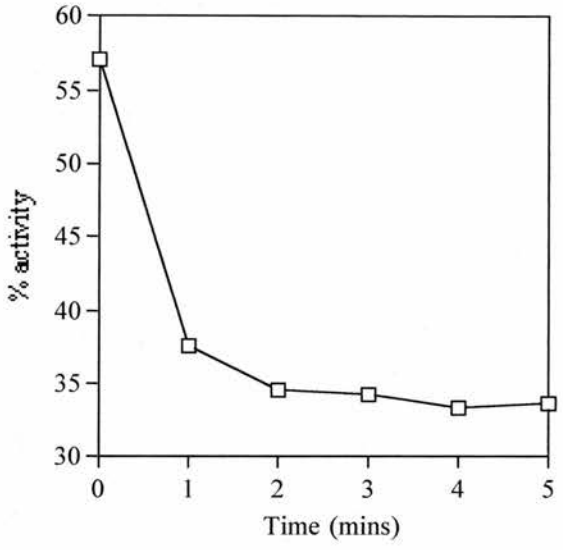

Fig. 3.1.1.2 Time course for inhibitor 1. Enzyme and inhibitor (4 μM) were pre-incubated in the cuvette for 1,2,3,4 or 5 minutes and the reaction started by the addition

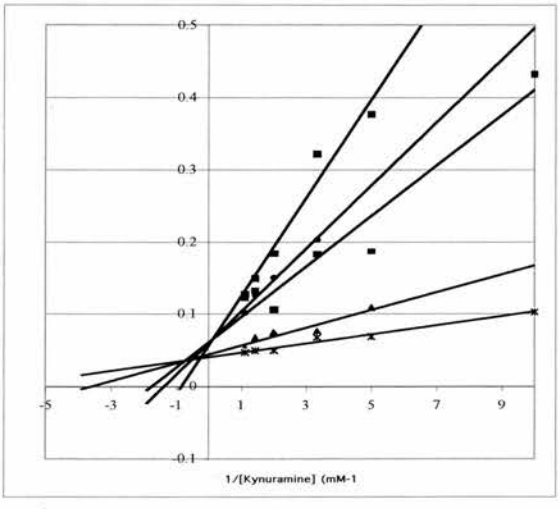

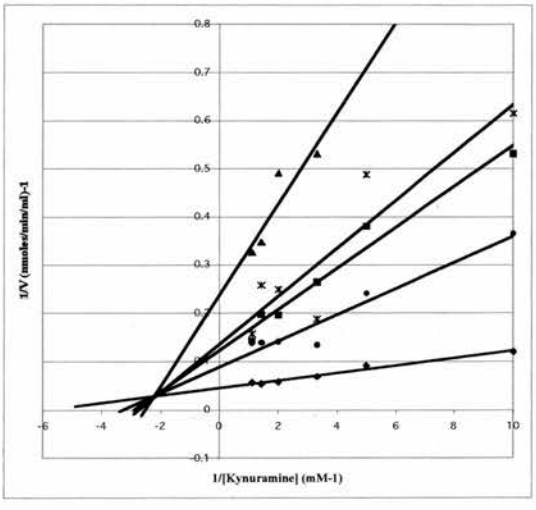

of 0.3 mM kynuramine.

Fig. 3.1.1.3. Lineweaver Burk plots for compound 2 (left) initial K_i and 11 (right) 5 minute K_i. The inhibitor concentrations for **2** were 0 (✳), 3 (▲), 5 (■), 10 (●), and 20 (■) μM. The inhibitor concentrations for **11** were 0 (◆), 0.001 (●), 0.005(■), 0.007 (✳), and 0.01 (▲)μM. These plots are based on single replicates.

Table 3.1.1.1. Effect of substituents at either end of the rigid pirlindole ring system on the inhibitory potency against rat liver mitochondria MAO A.

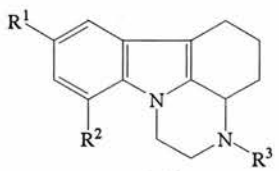

1-19

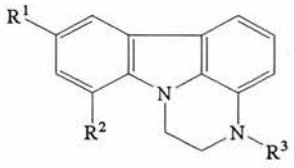

20

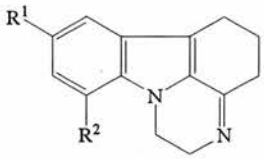

21-24

No	Substituents			Dimensions of ligand (angstroms)			MAO A K_i (μM)	C Log P	Hansch constant (π)	
	R^1	R^2	R^3	X	Y	Z			R^1	R^3
1	H	H	H	8.63	6.71	2.86	5.156	2.77	0	0
2	H	H	CHO	9.42	6.93	3.09	3.94		0	-0.65
3	H	H	$COCH_3$	11.18	6.88	3.14	4.376		0	-0.55
4	H	H	COC_6H_5	12.82	7.99	4.18	2.92		0	2.08
5	H	H	$COC_{10}H_{15}$	13.55	8.04	5.32	+		0	2.4
6	CH_3	H	H	9.87	6.86	2.87	0.264	3.27	0.56	0
7	CH_3	H	CHO	10.43	6.91	3.22	0.67	2.82	0.56	-0.65
8	CH_3	H	$COCH_3$	11.50	6.97	3.61	1.63	2.59	0.56	-0.55
10	CH_3	H	$COC_{10}H_{15}$	14.48	7.97	5.43	4.00		0.56	2.4
11	C_6H_{11}	H	H	13.07	6.95	3.50	0.05	4.92	2.8	0
17	$C_6H_5(CH_2)_2$	H	H	15.01	6.96	2.83	0.411			
18	H	CH_3	H	8.96	6.83	2.83	5.33			
19	CH_3	CH_3	H	9.83	6.78	2.84	0.0157			
20	CH_3	H	H	8.66	6.70	2.67	68.1			
21	CH_3	H	-	9.75	6.74	2.87	0.0147			
22	H	CH_3	-	8.97	6.76	2.85	1.656			
23	C_6H_{11}	H	-	12.59	6.94	3.42	0.0094			
24	$C_6H_5(CH)_2$	H	-	14.90	7.50	2.90	0.0166			
25	$C_{10}H_{15}$	H	H	12.99	7.2	4.45	1.174	5.75		
26	Br	H	-	9.34	6.81	2.86	<3 nM			

ClogP values from (126). Hansch constants are from (125).

3.1.2. Stopped-flow spectrophotometry

Tables 3.1.2.1 and 3.1.2.2 show the rates and amplitudes for the re-oxidation of MAO A by air saturated buffer premixed with varying concentrations of either the substrate kynuramine, or inhibitor 7. Fig. 3.1.2.1 shows 3 representative traces of MAO A re-oxidation alone (Buff), premixed with 20 μM kynuramine (Kyn) and premixed with 100 μM inhibitor 7 (I). From these three traces it is clear that substrate increases the rate of re-oxidation, whereas inhibitor decreases this rate.

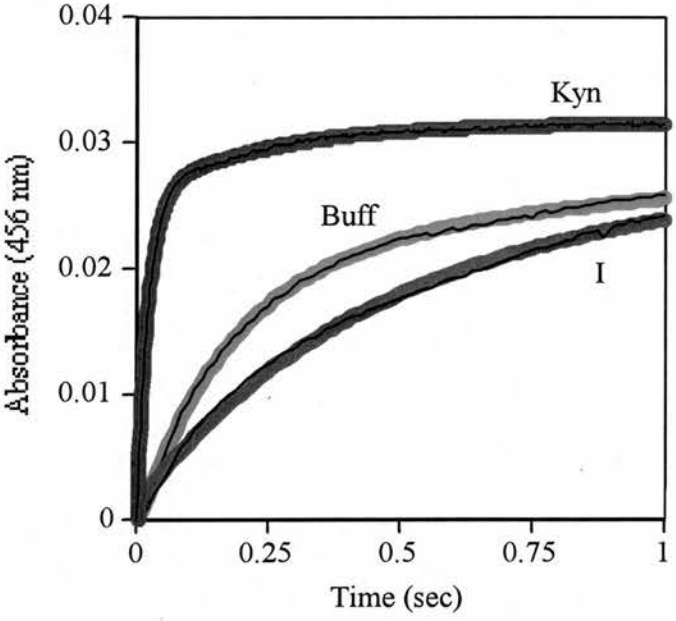

Fig. 3.1.2.1. Anaerobic oxidative half reaction observed by stopped flow spectrophotometry on mixing 6 μM MAO A with air-saturated buffer (Buff, red), 6 μM MAO A premixed with 20 μM kynuramine (Kyn, green), and 6 μM MAO A premixed with 100 μM inhibitor 7 (I, blue), (150 x K_i). Flavin oxidation was measured at 456 nm. The colors represent over 1000 overlapping points and the black line is the biphasic fit.

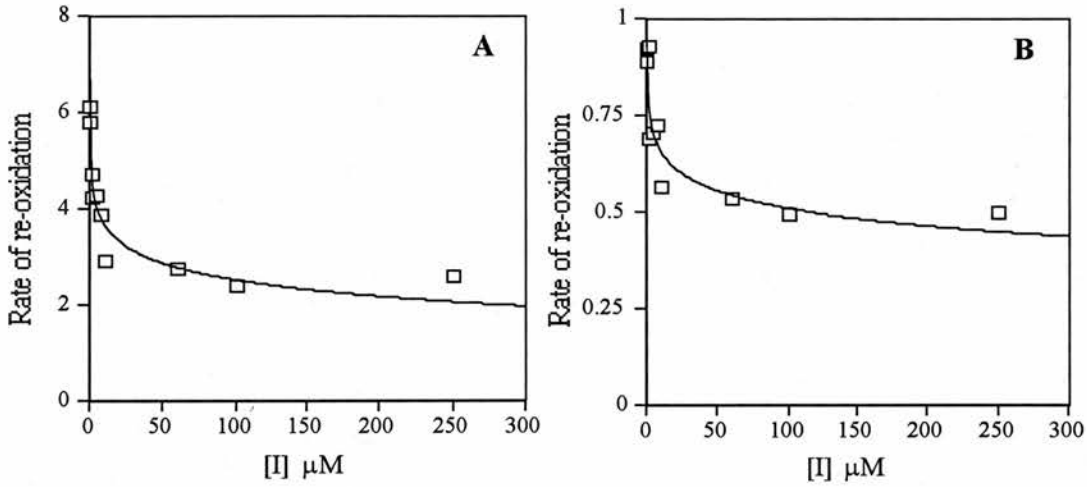

Fig. 3.1.2.2. Rates of re-oxidation (s^{-1}) of MAO A (6 μM) versus inhibitor concentration for inhibitor 7. (A) Fast phase of re-oxidation. (B) Slow phase of re-oxidation.

Previous studies of this kind have shown that the competitive inhibitor, D-amphetamine, and the product inhibitor, MPP^+, both completely inhibit re-oxidation (65,127). Fig. 3.1.2.2 show the rates of re-oxidation plotted against inhibitor concentration for both phases of re-oxidation. It is clear to see that the rates for both the slow and fast phases have the same dependence on inhibitor concentration, and that the inhibition of re-oxidation levels off at about 50% of the original value. It should be noted that the buffer syringe did not contain the ligand, so dissociation of the inhibitor may contribute to the biphasic pattern not previously observed.

Substrates increase the rate of re-oxidation (127). This is structure dependent with kynuramine increasing the rate 125-fold, whereas benzylamine only increases the re-oxidation rate 25-fold (20). In this study, the kynuramine concentration was varied

between 3 μM and 1000 μM (final concentration). The stimulation of re-oxidation is concentration dependent and biphasic, Fig 3.1.2.3. However, there was no kynuramine in the buffer used to re-oxidise MAO A, so the slow phase may represent a combination of the off rate for kynuramine and re-oxidation of enzyme alone.

The amplitude of change of the two phases is different between enzyme pre-mixed with substrate and enzyme pre-mixed with inhibitor. For enzyme pre-mixed with inhibitor the rapid phase represents about 70% of the change, the slow phase consisting of the final 30%. This is consistent through the range of concentrations used. However, for substrate, the amplitudes of each phase differ with changes in concentration. The higher the substrate concentration, the smaller the amplitude for the slow phase of re-oxidation. The samples with 3 μM and 6 μM kynuramine give approximately equal changes in amplitude for the two phases, with amplitude changes for the second phase of 55.2% and 49.5% respectively, whereas for 20 μM and 1000 μM the majority of the change is seen in the first phase. This is consistent with the slow phase being re-oxidation of unliganded enzyme. The low saturation point (about 6 μM) suggests a low K_D value but the data points were too few for an accurate calculation.

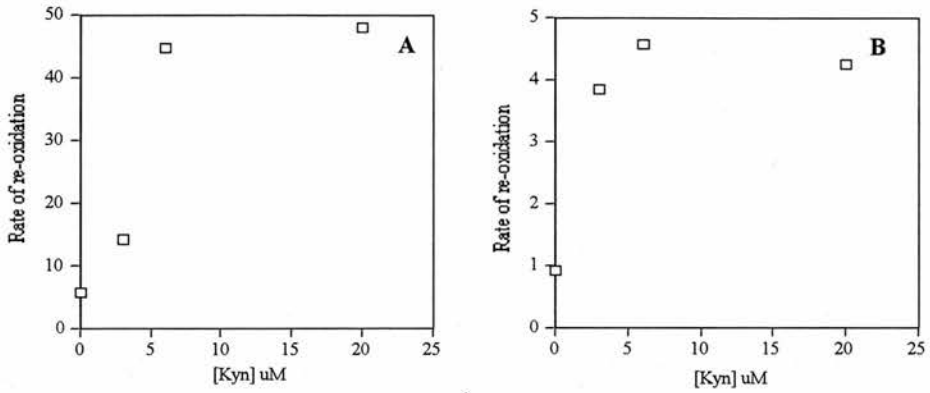

Fig. 3.1.2.3. Rates of re-oxidation (s^{-1}) versus substrate concentration for the substrate kynuramine, based on a four trace average. (A) Fast phase of re-oxidation. (B) Slow phase of re-oxidation.

[I 7] μM	k_1 (s^{-1})	k_2 (s^{-1})	Amp 1	Amp 2
0	5.81	0.927	0.0265	0.0114
0.25	6.12	0.89	0.0221	0.0102
1	4.72	0.934	0.0203	0.0157
2	4.26	0.693	0.0218	0.0092
4	4.3	0.707	0.0242	0.01
7	3.89	0.729	0.02242	0.0101
10	2.921	0.566	0.0226	0.0096
60	2.799	0.539	0.0255	0.0101
100	2.43	0.499	0.02115	0.0089
250	2.63	0.503	0.0239	0.0108

Table 3.1.2.1. Kinetic parameters for MAO A from stopped flow oxidative half reaction in the presence of varying amounts of inhibitor 7 premixed with MAO A (6 μM).

[kyn] μM	k_1 (s^{-1})	k_2 (s^{-1})	Amp 1	Amp 2
0	5.81	0.927	0.0265	0.0114
3	14.25	3.86	0.0081	0.01
6	44.85	4.584	0.0152	0.0149
20	48.08	4.26	0.0294	0.0057
1000	52.2	2.1	0.025	0.0027

Table 3.1.2.2. Kinetic parameters for MAO A from stopped flow oxidative half reaction in the presence of varying amounts of kynuramine premixed with MAO A (6 μM).

3.2 Spectral studies

This section will present the results of spectral studies of inhibitor titrations and dithionite reduction of the enzyme-inhibitor complexes of MAO A. The spectrum of the flavin is a powerful tool for exploring the interactions of ligands with the flavin as well as how these interactions effect the redox properties of the flavin. The two types of spectra shown here will be the spectral changes observed upon inhibitor binding to the enzyme, and spectral changes upon reduction by dithionite of the enzyme saturated with inhibitor. Ten inhibitors were investigated: eight pirlindole derivatives with various groups substituted on C8 and N3, and also with the introduction of a double bond at N3; the classic competitive inhibitor, D-amphetamine; and the stable product inhibitor, MPP^+.

Fig. 3.2.1.1 shows the spectra of MAO A, MAO A-I **4** complex and the difference spectra between these. The difference spectrum is obtained by subtracting the spectrum of the unliganded enzyme from the spectrum of the MAO A-I complex

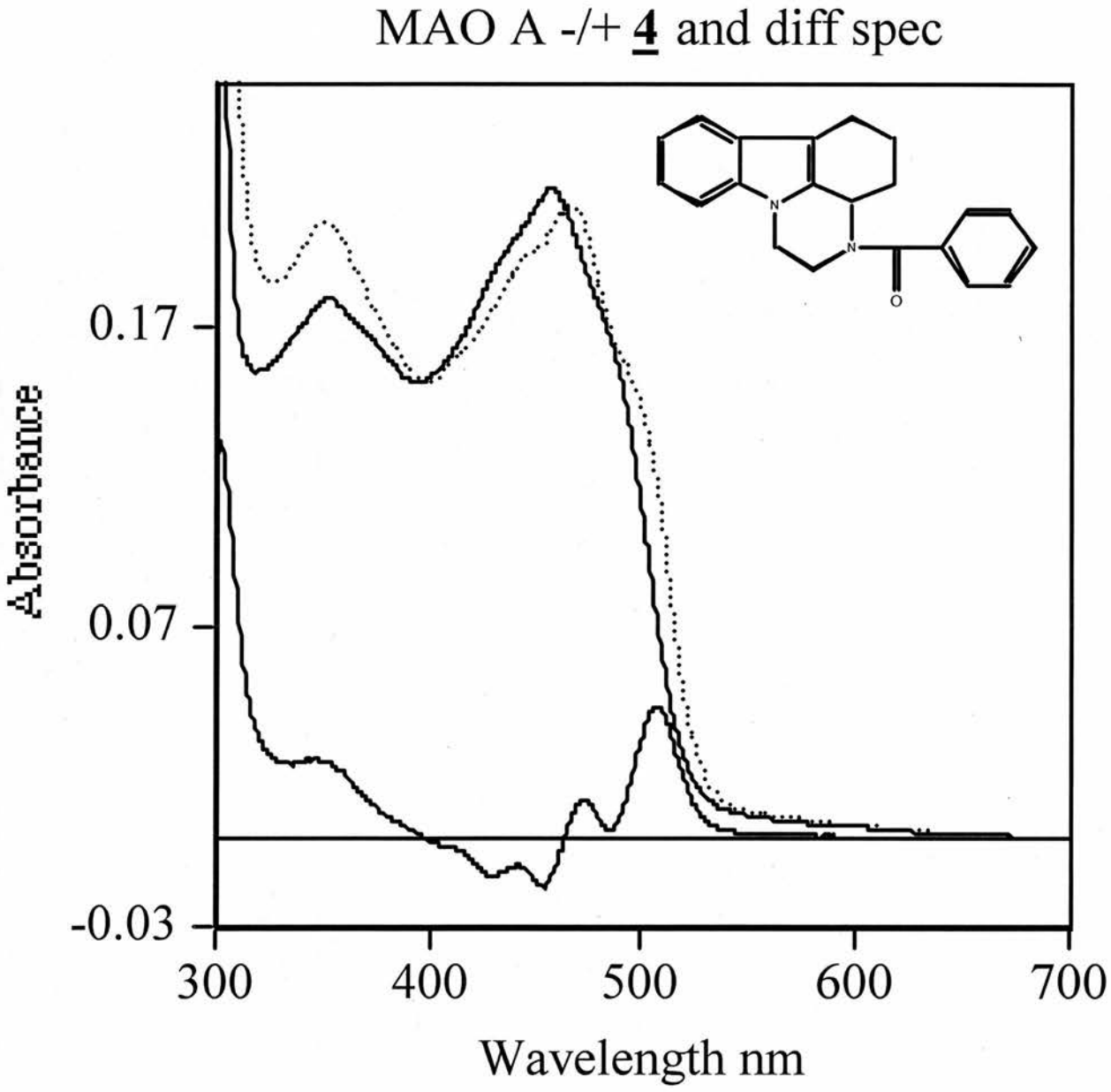

Fig. 3.2.1.1. Inhibitor binding alters the spectrum of MAO A. Spectra of MAO A (solid line), MAO A-inhibitor 4 complex (dotted line), and the difference spectrum of the complex (solid line at origin). The spectrum of the MAO A-inhibitor 4 complex was taken 3 minute after addition of inhibitor 4 (35.9 μM) to anaerobic MAO A (19.9 μM). The original spectrum in the absence of inhibitor was subtracted from that of the enzyme inhibitor complex to obtain the difference spectrum.

3.2.1 Titrations of MAO A with inhibitors

The difference spectrum shown in Fig 3.2.1.1 (solid line at origin) highlights the detail that can be obtained with this technique. The solid line represents the spectrum of MAO A, the dotted line shows the spectrum of the MAO A-I complex. It is clear that there is an overall increase in absorbance between 495 nm and 550 nm, and this is shown more clearly in the difference spectrum where a peak is seen at 510 nm. A second increase in absorbance is seen between 470 nm and 485 nm, with the peak at 475 nm. Between these peaks, at 490 nm, there is little change and a small trough is seen with its minimum just above zero absorbance. From 400 nm to 460 nm there is a decrease in absorbance characterized by a subtle double trough at 420 nm and 440 nm. There is indication of a clear increase centered at 350 nm, the area of the second flavin absorbance peak. However, after this peak there is an overall increase in absorbance mainly due to the spectral interference of the inhibitor masking changes in the flavin spectrum under 400 nm, so in most cases it has only been possible to analyze spectral changes above 400 nm. For all other inhibitors, the difference spectra are presented to look at the influence of inhibitor structure on the flavin spectrum.

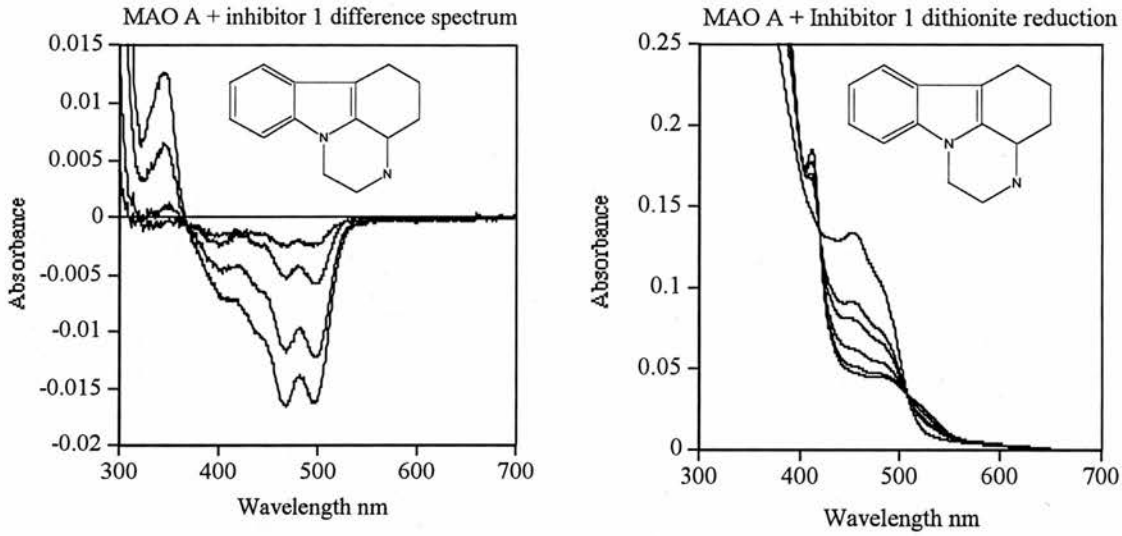

Fig. 3.2.1.2. Spectral changes induced by inhibitor 1 binding to MAO A and subsequent dithionite reduction of the complex. Spectra were recorded 3 min after addition of inhibitor **1** (3.9,15.7,45.8,90.9. μM) to anaerobic MAO A (10.7 μM). The original spectrum in the absence of inhibitor was subtracted from that of the enzyme inhibitor complex to obtain the difference spectra. Right, spectral changes upon reduction of MAO A-I **1** complex (10.7 μM + 602 μM) by dithionite (2,4,6,8,12,16 μL of 1 mg/ml). Spectra were recorded 15 minutes after addition of dithionite.

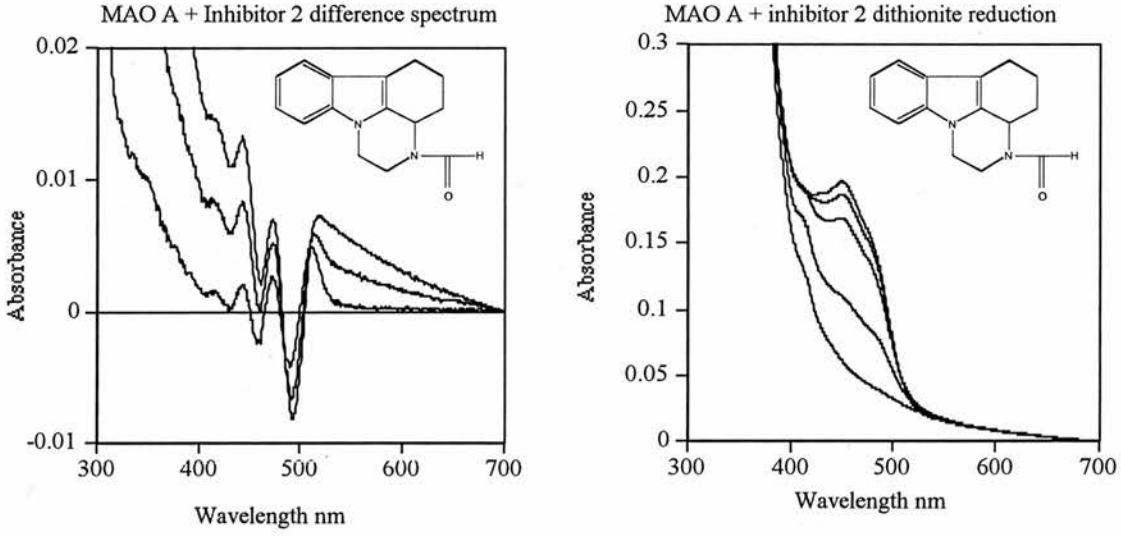

Fig. 3.2.1.3. Spectral changes induced by inhibitor 2 binding to MAO A and subsequent dithionite reduction of the complex. Spectra were recorded 3 minutes after addition of inhibitor **2** (3.98,11.9,23.4. μM) to anaerobic MAO A (12.69 μM). The original spectrum in the absence of inhibitor was subtracted from that of the enzyme inhibitor complex to obtain the difference spectra. Right, spectral changes upon reduction of MAO A-I **2** complex (12.69 μM + 1225 μM) by dithionite (2,4,6,10 μL of 1 mg/ml). Spectra were recorded 15 minutes after addition of dithionite.

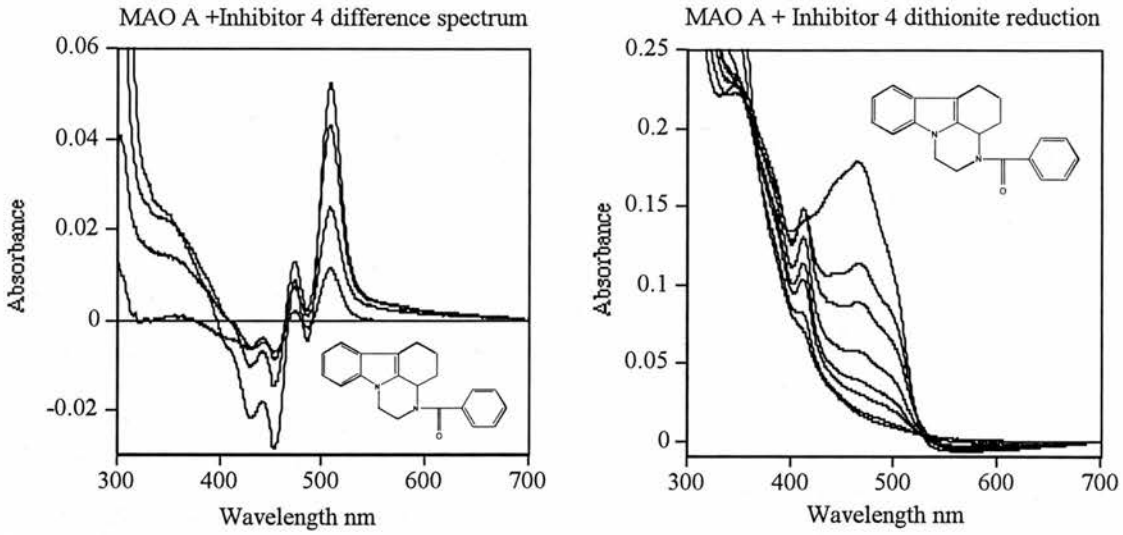

Fig. 3.2.1.4. Spectral changes induced by inhibitor 4 binding to MAO A and subsequent dithionite reduction of the complex. Spectra were recorded 3 minutes after addition of inhibitor 4 (5.3,13.2,31,80.8. μM) to anaerobic MAO A (19.9 μM). The original spectrum in the absence of inhibitor was subtracted from that of the enzyme inhibitor complex to obtain the difference spectra. Right, spectral changes upon reduction of MAO A-I 4 complex (14.81 μM + 336 μM) by dithionite (2,4,8,12,16,20,28 μL of 1 mg/ml). Spectra were recorded 15 minutes after addition of dithionite.

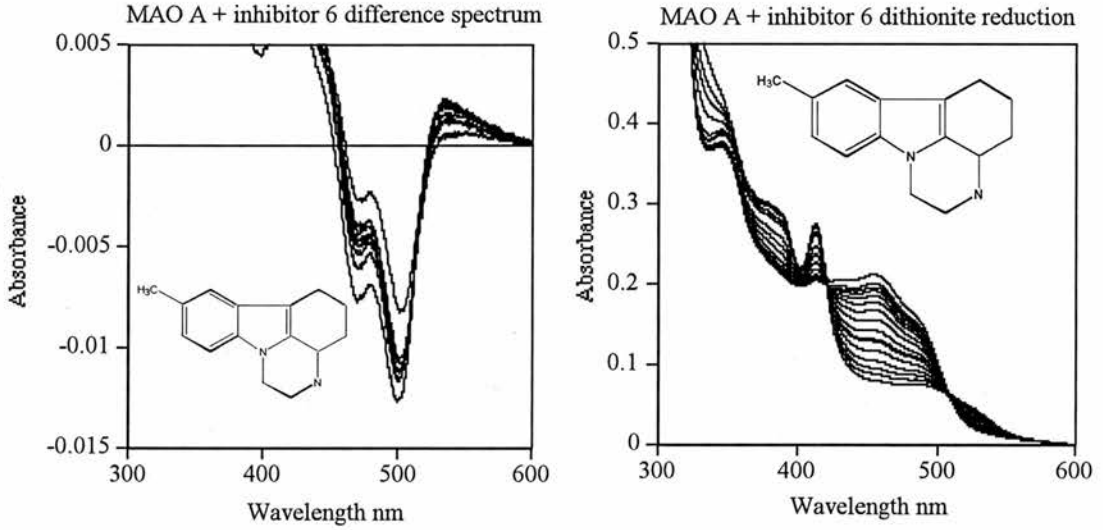

Fig. 3.2.1.5 Spectral changes induced by inhibitor 6 binding to MAO A and subsequent dithionite reduction of the complex. Spectra were recorded 3 minutes after addition of inhibitor 6 (29.5,58.7,87.9,116.8,145.6,174.2,202.6,230.9,286.9 μM) to anaerobic MAO A (12.2 μM). The original spectrum in the absence of inhibitor was subtracted from that of the enzyme inhibitor complex to obtain the difference spectra. Right, spectral changes upon reduction of MAO A-I 6 complex (12.2 μM + 1892 μM) by dithionite (2,4,6,8,10,12,14,16,18,20,22,24,26,28,30,32 μL of 1 mg/ml). Spectra were recorded 15 minutes after addition of dithionite.

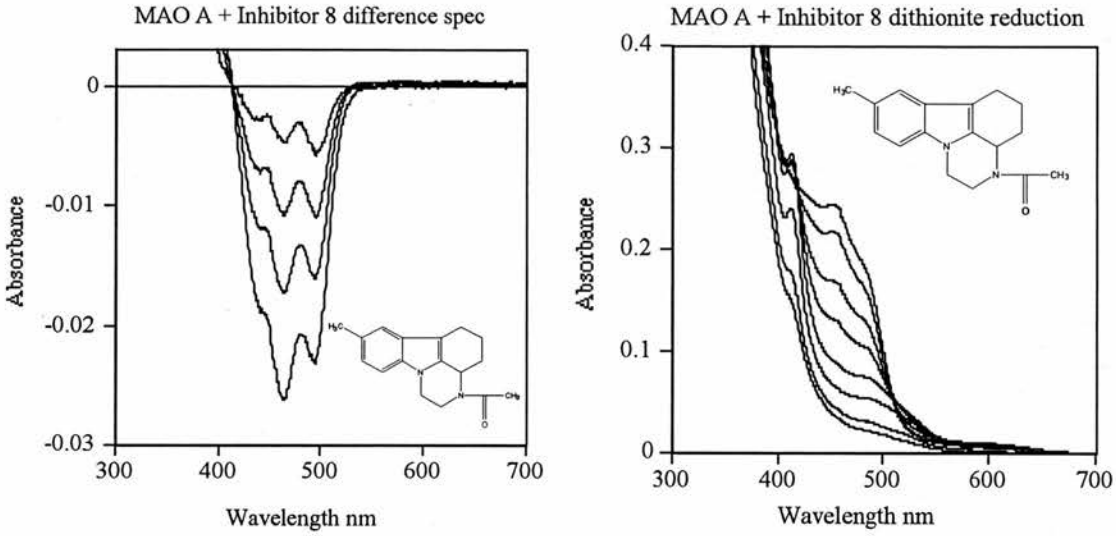

Fig. 3.2.1.6. Spectral changes induced by inhibitor 8 binding to MAO A and subsequent dithionite reduction of the complex. Spectra were recorded 3 minutes after addition of inhibitor 8 (23.4,60.2,103.9,155.4. μM) to anaerobic MAO A (11.2 μM). The original spectrum in the absence of inhibitor was subtracted from that of the enzyme inhibitor complex to obtain the difference spectra. Right, spectral changes upon reduction of MAO A-I 8 complex (18.8 μM + 435 μM) by dithionite (2,4,6,8,10,12,14 μL of 1 mg/ml). Spectra were recorded 15 minutes after addition of dithionite.

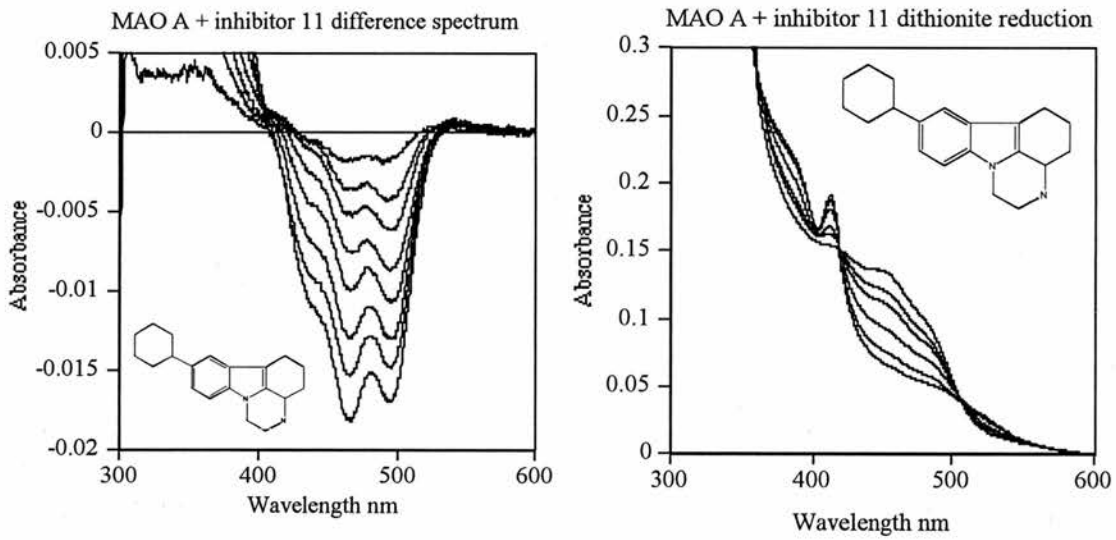

Fig. 3.2.1.7. Spectral changes induced by inhibitor 11 binding to MAO A and subsequent dithionite reduction of the complex. Spectra were recorded 3 minutes after addition of inhibitor 11 (5.98,14.8,29.2,56.7,95.2,119.2,130.7,152.9. μM) to anaerobic MAO A (10.2 μM). The original spectrum in the absence of inhibitor was subtracted from that of the enzyme inhibitor complex to obtain the difference spectra. Right, spectral changes upon reduction of MAO A-I 11 complex (10.2 μM + 180 μM) by dithionite (2,4,6,8,10 μL of 1 mg/ml). Spectra were recorded 15 minutes after addition of dithionite.

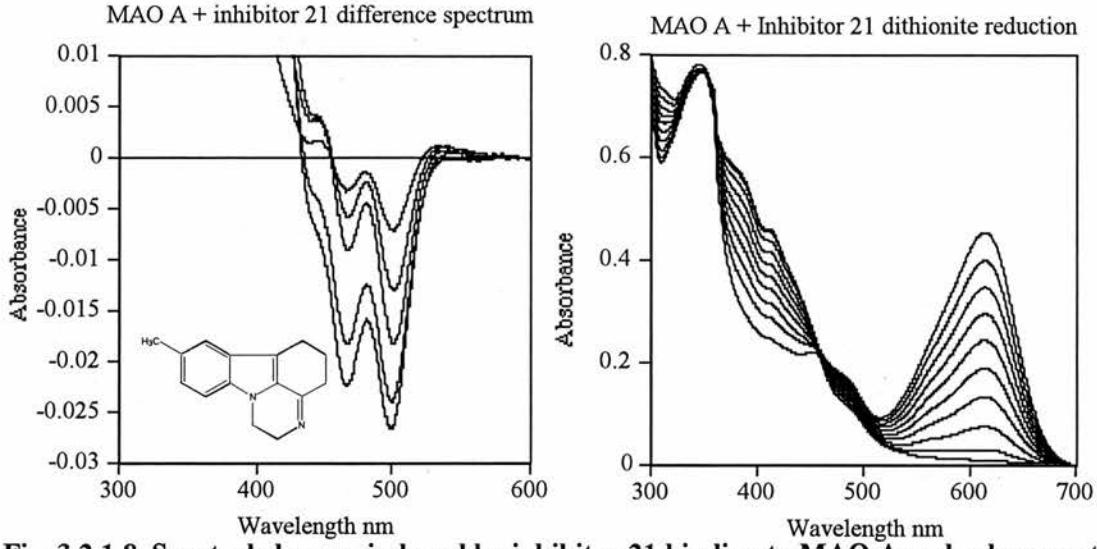

Fig. 3.2.1.8. Spectral changes induced by inhibitor 21 binding to MAO A and subsequent dithionite reduction of the complex. Spectra were recorded 3 minutes after addition of inhibitor **21** (4.95,12.99,32.7,57.5,71.4. μM) to anaerobic MAO A (14.3 μM). The original spectrum in the absence of inhibitor was subtracted from that of the enzyme inhibitor complex to obtain the difference spectra. Right, spectral changes upon reduction of MAO A-I **21** complex (10.5 μM + 15.8 μM) by dithionite (4,10,14,18,22,26,30,34,38 μL of 1 mg/ml). Spectra were recorded 15 minutes after addition of dithionite

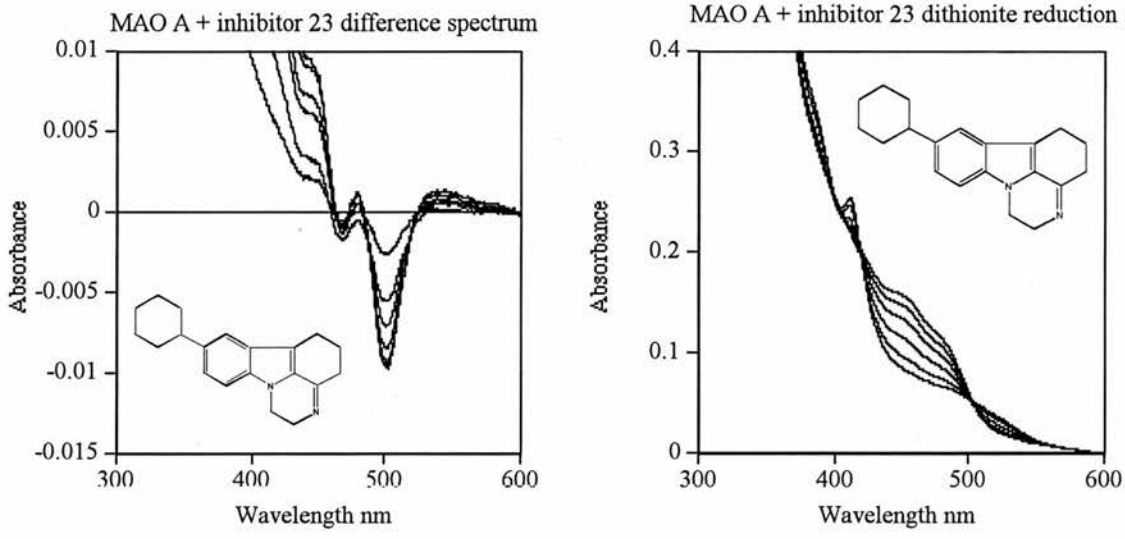

Fig. 3.2.1.9. Spectral changes induced by inhibitor 23 binding to MAO A and subsequent dithionite reduction of the complex. Spectra were recorded 3 minutes after addition of inhibitor **23** (2.53,5.06,7.58,10.08,15.03,17.5. μM) to anaerobic MAO A (11 μM). The original spectrum in the absence of inhibitor was subtracted from that of the enzyme inhibitor complex to obtain the difference spectra. Right, spectral changes upon reduction of MAO A-I **23** complex (11 μM + 113 μM) by dithionite (2,4,6,8,12 μL of 1 mg/ml). Spectra were recorded 15 minutes after addition of dithionite.

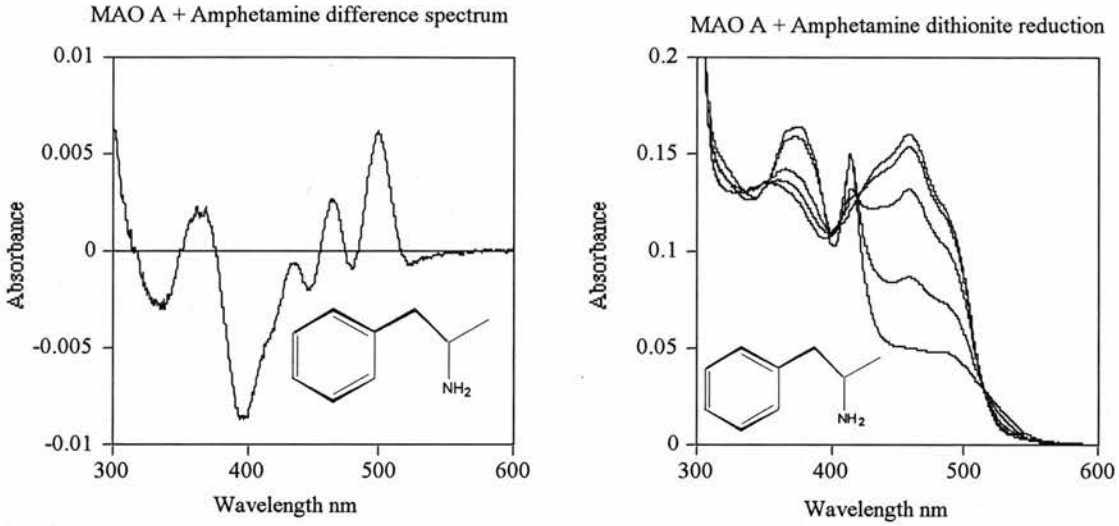

Fig. 3.2.1.10. Spectral changes induced by inhibitor (D-amphetamine) binding to MAO A and subsequent dithionite reduction of the complex. Spectra were recorded 3 minutes after addition of amphetamine (314. μM) to anaerobic MAO A (11.2 μM). The original spectrum in the absence of inhibitor was subtracted from that of the enzyme inhibitor complex to obtain the difference spectra. Right, spectral changes upon reduction of MAO A-amphetamine complex (16.9 μM + 1818 μM) by dithionite (2,4,6,8 μL of 1mg/ml). Spectra were recorded 15 minutes after addition of dithionite.

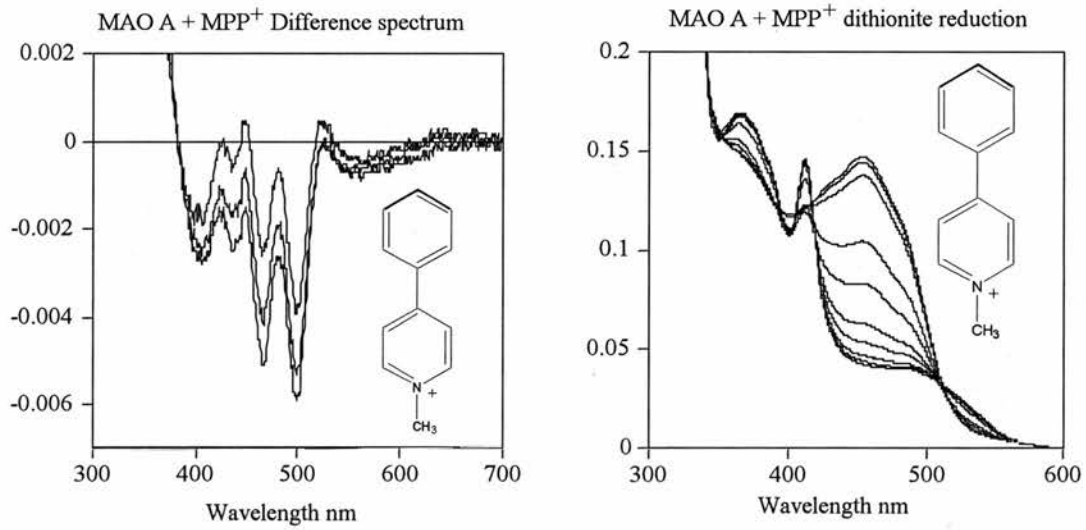

Fig. 3.2.1.11. Spectral changes induced by product (MPP^+) binding to MAO A and subsequent dithionite reduction of the complex. Spectra were recorded 3 minutes after addition of MPP^+ (3.98,7.9,11.9 μM) to anaerobic MAO A (10.82 μM). The original spectrum in the absence of inhibitor was subtracted from that of the enzyme inhibitor complex to obtain the difference spectra. Right, spectral changes upon reduction of MAO A- MPP^+ complex (12.35 μM + 1666 μM) by dithionite (2,4,6,8,10,12,14,18 μL of 1mg/ml). Spectra were recorded 15 minutes after addition of dithionite.

Fig 3.2.1.2 shows the difference spectra obtained during titration of MAO A with inhibitor **1** to form the MAO A-I **1** complex. The spectra show a decrease in absorbance between 400 nm and 510 nm with a double trough at 465 nm and 495 nm. There are no absorbance changes above 510 nm. There is a peak at 350 nm, but below that the spectrum of the inhibitor masks any subtle changes in the flavin spectrum.

Fig 3.2.1.3 shows the difference spectra for the formation of the MAO A-inhibitor **2** complex. The spectra show a small peak at 510 nm, but the clarity of the peak is masked by turbidity seen as a general increase in absorbance from 520 nm to 700 nm. There is a double trough between 400 nm and 500 nm with minima at 465 nm and 495 nm as seen for inhibitor **1**. The two minima are very clearly defined by a peak between them at 470 nm. Below 450 nm, the absorbance of the inhibitor, as well as the turbidity mask changes in the flavin spectrum.

Fig. 3.2.1.4 shows the difference spectra for the formation of the MAO A-inhibitor **4** complex. The spectral differences shown here are different from those with Inhibitor **1** and inhibitor **2**. There is a large peak at 510 nm and a smaller peak at 480 nm. Between these two peaks is a trough at 495 nm, as seen in previous spectra. Below 470 nm there is an overall decrease in absorbance with a double trough at 420 nm and 450 nm. Below 400 nm there is an overall increase in absorbance due to the absorbance of the inhibitor.

Fig. 3.2.1.5 shows the difference spectra for the formation of the MAO A-Inhibitor **6** complex. There is a small increase between 520 nm and 600 nm due to the turbidity of

the enzyme solution. Between 520 nm and 450 nm there is a decrease in absorbance characterized by a double trough with the minimum at 495 nm much lower than the minimum at 465 nm. Below 450 nm there is an increase in absorbance due to the spectral interference of the inhibitor.

Fig. 3.2.1.6 shows the difference spectra for the formation of the MAO A-inhibitor **8** complex. There is no change in absorbance between 520 nm and 700 nm. Between 400 nm and 520 nm there is an overall decrease in absorbance with a double trough at 465 nm and 495 nm, the decrease at 465 nm is slightly lower than that at 495 nm. Below 400 nm there is an overall increase in absorbance due to the absorbance of the inhibitor.

Fig. 3.2.1.7 shows the difference spectra for the MAO A-inhibitor **11** complex. There is no change in absorbance between 530 nm and 600 nm, between 410 nm and 520 nm there is an overall decrease in absorbance characterized with a double trough at 465 nm and 495 nm, the minimum at 465 nm is much lower than that at 495 nm which is very similar to the difference spectrum for inhibitor **8**. Below 420 nm, there is a general increase in absorbance due to the interference of the inhibitor spectrum.

Fig. 3.2.1.8 shows the difference spectrum for the formation of the MAO A-I **21** complex. There is a slight increase in absorbance at 520 nm but this is probably due to turbidity rather than a change in the flavin spectrum. Between 430 nm and 520 nm there is an overall decrease in absorbance characterized by a double trough with minima at 465 nm and 495 nm. The two minima are well resolved and a peak can be seen between them

at 480 nm. Below 430 nm there is an increase in absorbance due to the interference of the inhibitor spectrum.

Fig. 3.2.1.9 shows the difference spectrum for the formation of the MAO A-I **23** complex. There is a slight increase in absorbance at 520 nm but this is probably due to turbidity rather than a change in the flavin spectrum. Between 450 nm and 510 nm there is an overall decrease in absorbance, this is characterised by a double trough with minima at 465 nm and 495 nm. The trough at 495 nm is much lower than the trough at 465 nm, in contrast to inhibitors **8**, **11** and **21**, where the two minima in each difference spectrum are of the same magnitude. The resolution between the two troughs is good and a trough at 470 can be seen. Below 450 nm there is an increase in absorbance due to interference by the inhibitor spectrum.

Fig. 3.2.1.10 shows the difference spectra for the formation of the MAO A-amphetamine complex. The difference spectrum is very clear because there is minimal interference from the inhibitor. There are four main peaks seen in the difference spectra, these are seen at 510 nm, 470 nm, 440 nm and 370 nm. Between these peaks four minima are seen at 480 nm, 445 nm, 400 nm and 330 nm.

Fig. 3.2.1.11 shows the difference spectra for the formation of the MAO A-MPP^+ complex, i.e. the oxidised enzyme-product complex. There is minimal change between 520 nm and 700 nm; between 450 nm and 500 nm there is a decrease in absorbance with two minima at 465 nm and 495 nm These two minima are very sharp and a peak can be

clearly seen between them at 475 nm. Between 400 nm and 450 nm, the absorbance change is very small, but two minima can be seen at 410 nm and 430 nm and two peaks can be seen at 420 nm and 440 nm. Below 400 nm, absorbance is masked due to interference of the inhibitor

Table 3.2.1.1. Molar extinction coefficients at 495 nm (negative) 508 nm (positive) for the ten inhibitors tested for spectral alterations of MAO A.

Inhibitor	C8	N3	ε (M^{-1} cm^{-1})
1	H	H	-3271
2	H	CHO	-630
4	H	$COC_{10}H_{15}$	+2714
6	CH_3	H	-1089
8	CH_3	$COCH_3$	-2054
11	C_6H_5	H	-1988
21	CH_3	-	-587
23	C_6H_{11}	-	-1086
MPP^+		CH_3	-555
D-Amphetamine		$_3HC\text{-}C\text{-}NH_2$	+694

Table 3.2.1.1 shows the molar extinction coefficients near 500 nm for the spectral changes in MAO A upon inhibitor binding. For the inhibitors with positive values the absorbance change is measured at 508 nm whereas for the inhibitors with negative values the absorbance change is measured at 495 nm. Comparing the extinction coefficients for compounds **6**, **11**, **21** and **23**, we see an interesting trend, the coefficients for the cyclohexyl derivatives **11** and **23** are 82% higher than those for the methyl derivatives **6** and **21**, correlating with greater affinity as observed with lower K_i values for the cyclohexyl derivatives. For either the cyclohexyl or methyl derivative, addition of a double bond at N3 resulted in an extinction coefficient that is about 55% of that for the

saturated derivative despite the lower K_i values (Table 2.1.1.1). The remainder of inhibitors studied show little trend between extinction coefficient and structure. The major difference seen for the interaction of these inhibitors with MAO A is the direction of the change in absorbance. Inhibitor **4** and amphetamine both increase the absorbance at 508 nm whereas all the other inhibitors studied give a decrease in absorbance at 495 nm upon inhibitor binding to MAO A.

3.2.2 Dithionite reduction spectra

Fig. 3.2.1.12 shows the spectral changes accompanying reduction of MAO A by dithionite in the absence of ligands. The main features of the spectrum are increases in absorbance at 412 nm and 377 nm during the first stage of reduction. Along with these increases in absorbance, there is a decrease in absorbance centered around 456 nm. The second stage of reduction shows a decrease in absorbance at all wavelengths centered around 456 nm. The two phases of reduction may be seen more clearly in Fig. 3.2.13 (a), which shows a plot of the three wavelengths against volume of dithionite used. The second part of this figure (B) shows a similar plot for the reduction of MAO A complexed with inhibitor **6**, as seen earlier in this chapter (Fig. 3.2.1.5), MAO A complexed with an inhibitor without an N3 substituent will stabilise the semiquinone of the flavin during reduction, and cannot be reduced further.

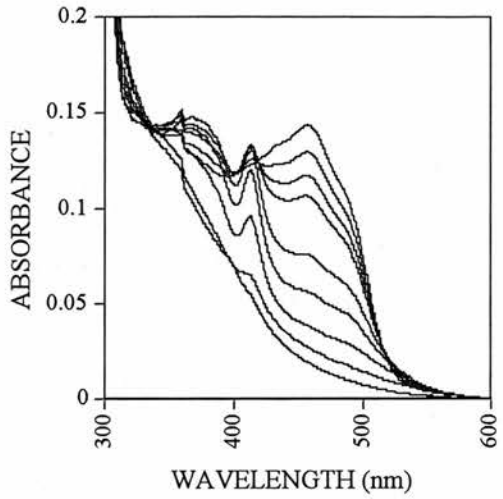

Fig. 3.2.1.12. Titration of MAO A with dithionite. Dithionite (1 mg/ml) was added to an anaerobic sample of MAO A (9.4 μM), each spectrum was recorded 15 minutes after addition of dithionite.

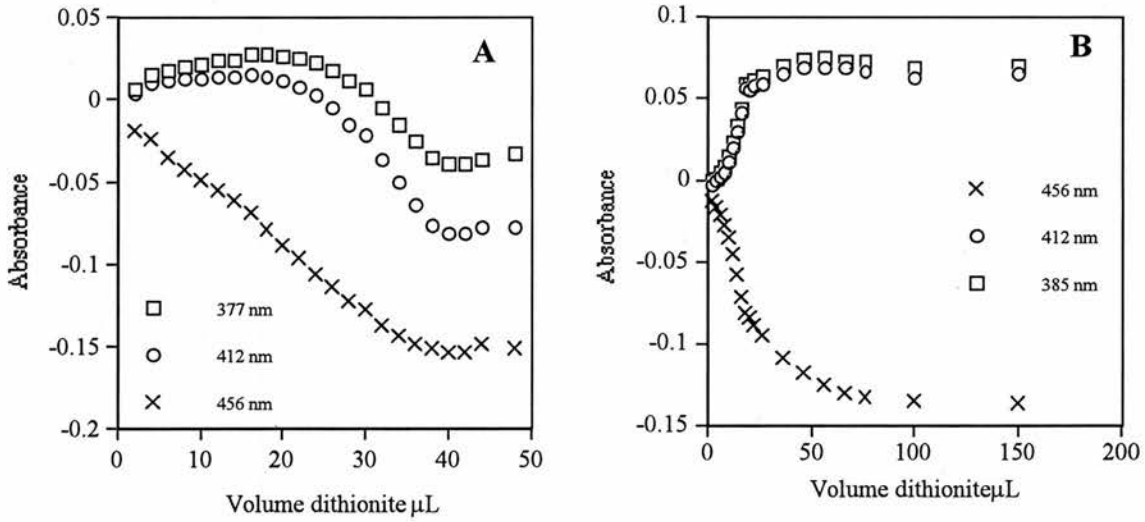

Fig. 3.2.1.13. Plots of difference absorbance during MAO A reduction. A. Plot of 377 nm, 412 nm and 456 nm during dithionite reduction of MAO A (12.2 μM). B. Plot of 385 nm, 412 nm and 456 nm during a dithionite reduction of MAO A (12.2 μM) complexed with I**6** (1892 μM)

The spectra on the right of each of the Figs. 3.2.1.1-3.2.1.11 are the dithionite reductions of the MAO A-inhibitor complex. To ensure saturation of the enzyme with inhibitor, the inhibitor concentration was at least 100 times the K_i. Unliganded MAO A, when reduced by dithionite, is reduced via two steps. The first step involves the formation of about 35% semiquinone characterised by increases in absorbance at 375 nm, 412 nm and 530 nm, and a decrease in absorbance at 456 nm. When the flavin is reduced by a further addition of dithionite the flavin spectrum is bleached with the disappearance of the 375 nm and 412 nm peak and an overall decrease in absorbance between 350 nm and 550 nm.

For the reduction of the MAO A-inhibitor complexes, the inhibitors can be divided into two distinct classes, inhibitors with no substitution on the N3 and inhibitors substituted on N3. The spectra for the unsubstituted inhibitors are shown in Figs. 3.2.1.2, 3.2.1.5, 3.2.1.7, 3.2.1.8, 3.2.1.9, and 3.2.1.10. Three main spectral changes are seen during reduction: firstly, there is a decrease in absorbance between 420 nm and 510 nm centered around 456 nm, characteristic of flavin reduction. Secondly, there is an increase in absorbance at 375 nm and at 412 nm accompanied by an increase in absorbance at 530 nm, indicative of a red anionic semiquinone. With this class of inhibitor, a full yield of semiquinone is seen and no further reduction occurs even with excess dithionite, mediators or overnight incubation. This means that when the inhibitors are bound to MAO A the anionic form of the semiquinone of FAD is strongly stabilized.

The spectra for reduction of MAO A with inhibitor **21** shown in Fig. 3.2.1.8 looks different from the other inhibitors. This titration was undertaken in the presence of the redox dye, indigo trisulphonate, in the hope of determining the mid-point potential of the oxidised/semiquinone couple. With successive additions of dithionite the dye is reduced, indicated by a reduction in absorbance at 610 nm. The isobestic point of this dye is conveniently at 456 nm, the wavelength of maximal change in the spectrum of MAO when it is reduced. Definitive values for the mid-point potential could not be determined due to lack of equilibrium between the dye and the flavin.

The second class of inhibitors consists of those substituted on N3. These inhibitors do not stabilize the semiquinone in the same way the unsubstituted inhibitors do. The spectral changes seen after successive additions of dithionite are shown in Fig. 3.2.1.3, 3.2.1.4 and 3.2.1.6 for three different MAO A-inhibitor complexes. There is a varying amount of semiquinone yield, partly masked by some inhibitor absorbance at 412 nm, where semiquinone is also seen. In these spectra there is a decrease in absorbance at 456 nm indicative of flavin reduction. At the same time there is an increase in absorbance at 530 nm and 412 nm indicating that some semiquinone is being formed. However, as more dithionite is added, the flavin spectrum is bleached and fully reduced flavin is formed. With the N3 substituted inhibitors, stabilisation of the semiquinone does not occur. The mM extinction coefficient for the two semiquinone peaks at 412 nm 380 nm (377 nm for unliganded MAO A and 385 nm for MAO A-**6** complex) are comparable to the values determined in (102). For the unliganded enzyme, the extinction coefficients (mM^{-1} cm^{-1}), were, 1.80 (377 nm) and 0.01 (412 nm), lower than the literature values of

2.74 and 2.11 mM^{-1} cm^{-1}, respectively (102). For the MAO A-**6** complex were 5.787 (385 nm) and 5.34 (412 nm), very similar to the literature values of 5.65 and 5.27 mM^{-1} cm^{-1}, respectively.

3.2.3 Summary of spectral results

The spectral changes induced by inhibitor binding to the enzyme can be split in to two different groups. In the first group, the inhibitors give a simple double-troughed difference spectra with the two minima at 465 nm and 495 nm. The second group of inhibitors induce a more complex spectral change characterized by a peak at 510 nm, as shown clearly for inhibitor **4** in Fig. 3.2.1.4, with other peaks and troughs at lower wavelengths. The relationship between inhibitor structure and the classes in which they lie is not completely clear-cut. For example, inhibitor **4**, with a cyclohexyl substituent on N3, has a spectrum characterised by a peak at 510 nm, whereas inhibitor **8** that has a formyl group on N3, has a spectrum characterized by a double trough at 465 nm and 495 nm. This will be discussed further in the Discussion.

Inhibitor binding also alters the redox properties of the flavin and the effect of inhibitor in the active site of the enzyme on the reduction of the flavin by dithionite is also dependent on structure. When the enzyme-inhibitor complex is reduced by dithionite, inhibitors without a substituent on N3 stabilise the semiquinone and no further reduction is seen. Inhibitors with a substituent on the N3 of the inhibitor do not stabilize the semiquinone, so that a small amount of semiquinone appears but is succeeded by full reduction.

3.3. Redox potentiometry

Fig. 3.3.1 shows the spectral changes observed during reduction of MAO A during the reductive and oxidative half reactions while determining its mid-point potential. Comparing these spectra to the spectra of a dithionite reduction in Fig. 3.2.1.12 there is one obvious difference. The dithionite reduction of MAO A proceeds through a red anionic semiquinone to the fully reduced hydroquinone. During the reductive titration by the potentiometric method to determine the mid-point potential no semiquinone was observed. This was thought to be due to the conditions used in reduction, which involved changing the voltage applied to the enzyme solution in order to supply the electrons to FAD. The experiment was performed in 500 mM KCl which may have contributed to the destabilization of the semiquinone.

Fig. 3.3.2 shows a plot of potential versus absorbance at 453 nm for both the oxidative and reductive phases of MAO A. For a mid-point potential to have any meaning the reductive and oxidative phases should be reversible, in which case the two plots will mirror each other. In the case of MAO A using this method the two phases are not reversible and the oxidative phase is shifted to the right. The mid point potential obtained for the reductive phase was of –220 mV similar to the literature value (128).

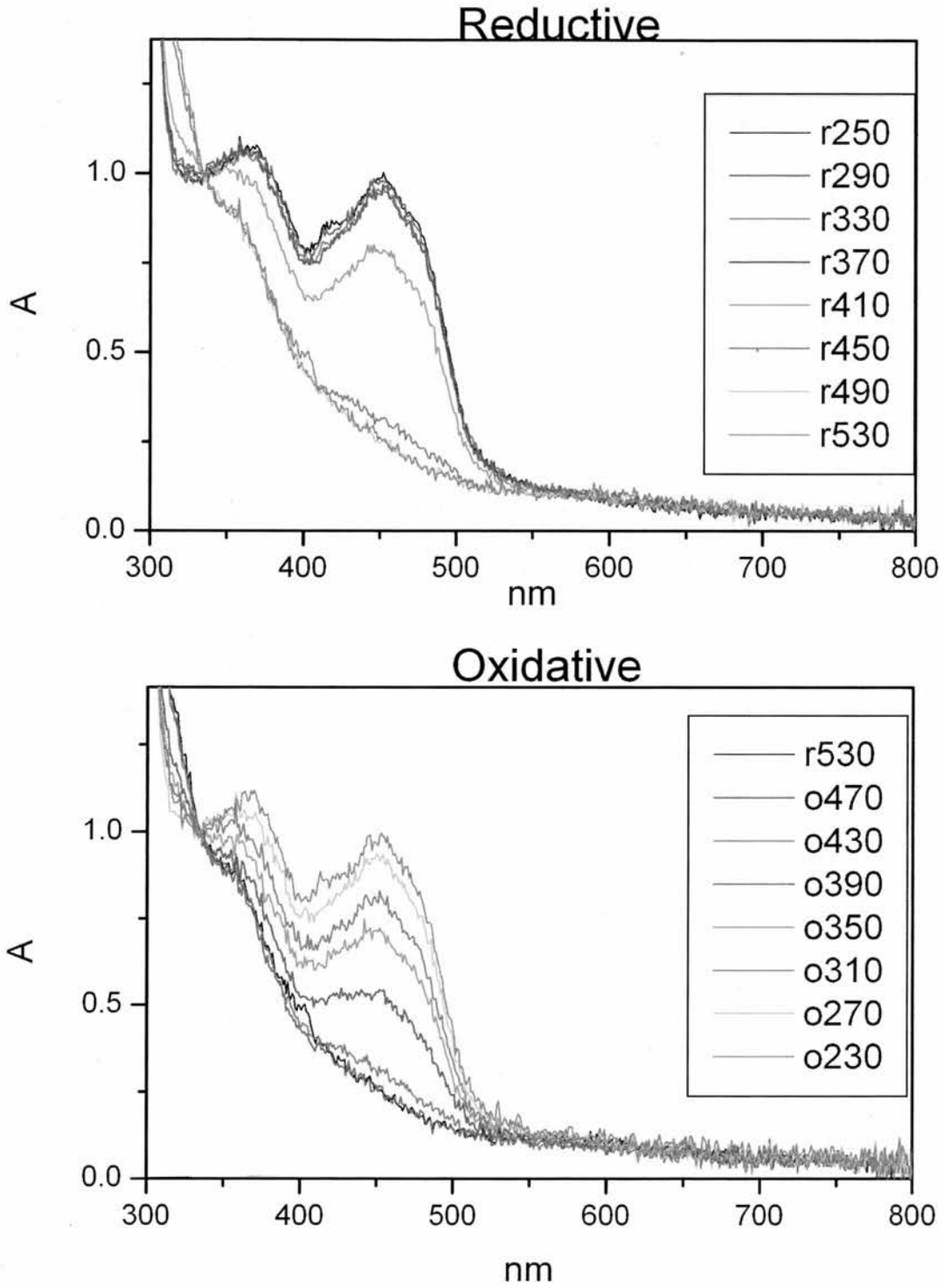

Fig. 3.3.1. Reductive and oxidative phases of a mid-point potential determination.

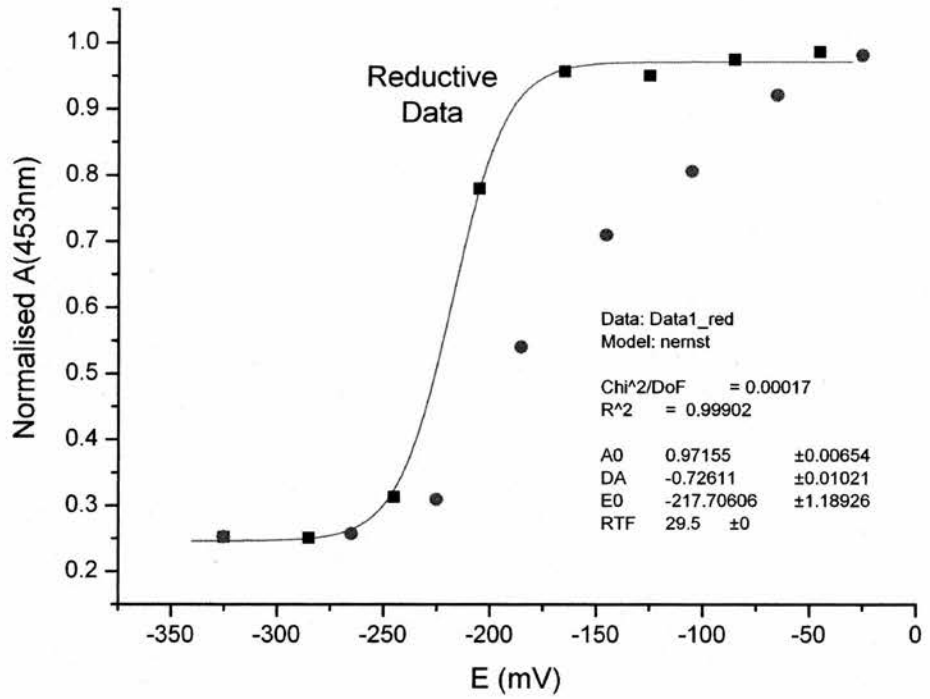

Fig. 3.3.2. Plot of potential verses absorbance (453 nm) for the reductive (black squares) and oxidative (red circles) phases of a potential determination for MAO A in high salt.

3.4. Molecular modelling

Codoñer first suggested that MAO A inhibitors might stack with the flavin in the active site of MAO A based on the observation that β-carbolines alter the spectrum of riboflavin in solution. Interactions between a series of MAO A inhibitors and lumiflavin were modelled based on quantum mechanical calculations. Theoretically, MAO inhibitors such as harmine could stack well with flavin in MAO (116). Perturbation of the MAO spectrum by inhibitor suggested stacking might be relevant in the active site (109). Inhibitors **6**, **11**, **21** and **23** were modelled to determine whether the factors that influence the stabilisation of stacking in the model system, namely, the electrostatic field that plays a role in recognition, and/or molecular orbital topology that contributes to charge transfer, could explain the differences in K_i values and spectral changes observed in MAO A.

3.4.1. Crystal structure of inhibitor 10

Crystals of inhibitor **10** were grown from a 2 mM inhibitor solution in 80:20 ethanol:DMSO. This solution was placed inside a larger sealed container containing diethyl ether so that the vapour from the diethyl ether diffused into the inhibitor solution over a period of days. The inhibitor is insoluble in diethyl ether, and as the concentration of diethyl ether increases, the inhibitor slowly comes out of solution in the form of crystals, suitable for structural analysis by X-ray crystallography.

Fig. 3.4.1.1 shows the crystal structure of inhibitor **10**. It shows clearly that the main structure of the inhibitor is planar, as predicted by the energy-minimised structure. The two rings on the right are both bent down relative to the main planar part of the molecule;

this bend is also seen in the theoretical structure seen in Fig. 3.4.2.1 for the unsubstituted inhibitor **6**. The remaining part of the molecule is the carbonyl admantyl group attached to N3 of the pirlindole molecule. The pirlindole-carbonyl-admantyl groups lie in an antiparallel orientation in the crystal lattice, so as to accommodate the size of the pirlindole and admantyl moieties. This structure is consistent with the energy minimised structure obtained theoretically

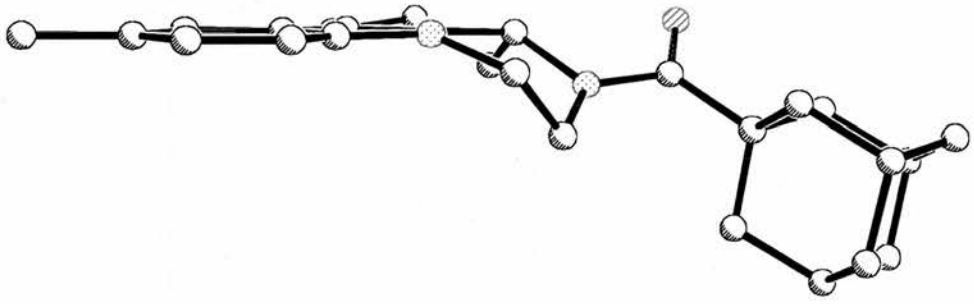

Fig. 3.4.1.1. Crystal structure of inhibitor 10. Crystals were grown in an 80:20 solution of ethanol:DMSO with diethyl ether as the precipitant vapour. Atom colours: White is carbon, blue is nitrogen, and red is oxygen. The crystal structure was solved by Dr A. Slawin, School of Chemistry, University of St Andrews

3.4.2. Molecular orbital topologies and electrostatic field calculations

The frontier orbital topologies for the lowest unoccupied molecular orbitals (LUMO) in lumiflavin and for the highest occupied molecular orbital (HOMO) in inhibitors **6** and **21** are shown in Fig. 3.4.2.1 (top row). The patterns of iso-electron density of the HOMO for the two inhibitors (and also for **11** and **23**, not shown) are very similar. This indicates that the solution model for flavin-inhibitor stacking stabilised by charge transfer will not differentiate these four inhibitors and so cannot explain the different spectral changes induced in MAO A by each of those inhibitors (see chapter 3.2, Figs. 3.2.1.5, 3.2.1.7, 3.2.1.8 and 3.2.1.9). Similarly, the distribution of the molecular electrostatic potential is only slightly affected by the introduction of a double bond (Fig. 3.4.2.1, middle row). Clearly, the molecular orbital calculations cannot distinguish between these two molecules to an extent that would alter the thermodynamic advantage of stacking in the model system.

The bottom row of Fig. 3.2.1.1 shows the difference in shape between the parent compound **6** for which the crystal structure is known (J. Wouters, unpublished), and the analogue with the double bond, **21**. This is the only difference revealed by the theoretical work that might be sufficient to influence the stacking of these similar compounds with lumiflavin. The steric difference offers the possibility of better stacking in the model system between the more planar **21** and the very flat lumiflavin ring (shown in Fig. 3.4.2.1, bottom panel, left), which is consistent with the lower K_i value found with the enzyme (Table 2.1, Ki for **6** is 0.264 μM and for **21** is 0.0147 μM). However, better

stacking would also predict a stronger effect on the flavin spectrum, and this is not found for the enzyme-inhibitor interaction (Table 3.2.1.1) where ε_{500} for **6** is -1089 mM^{-1} cm^{-1} but for **21** is -587 mM^{-1} cm^{-1}).

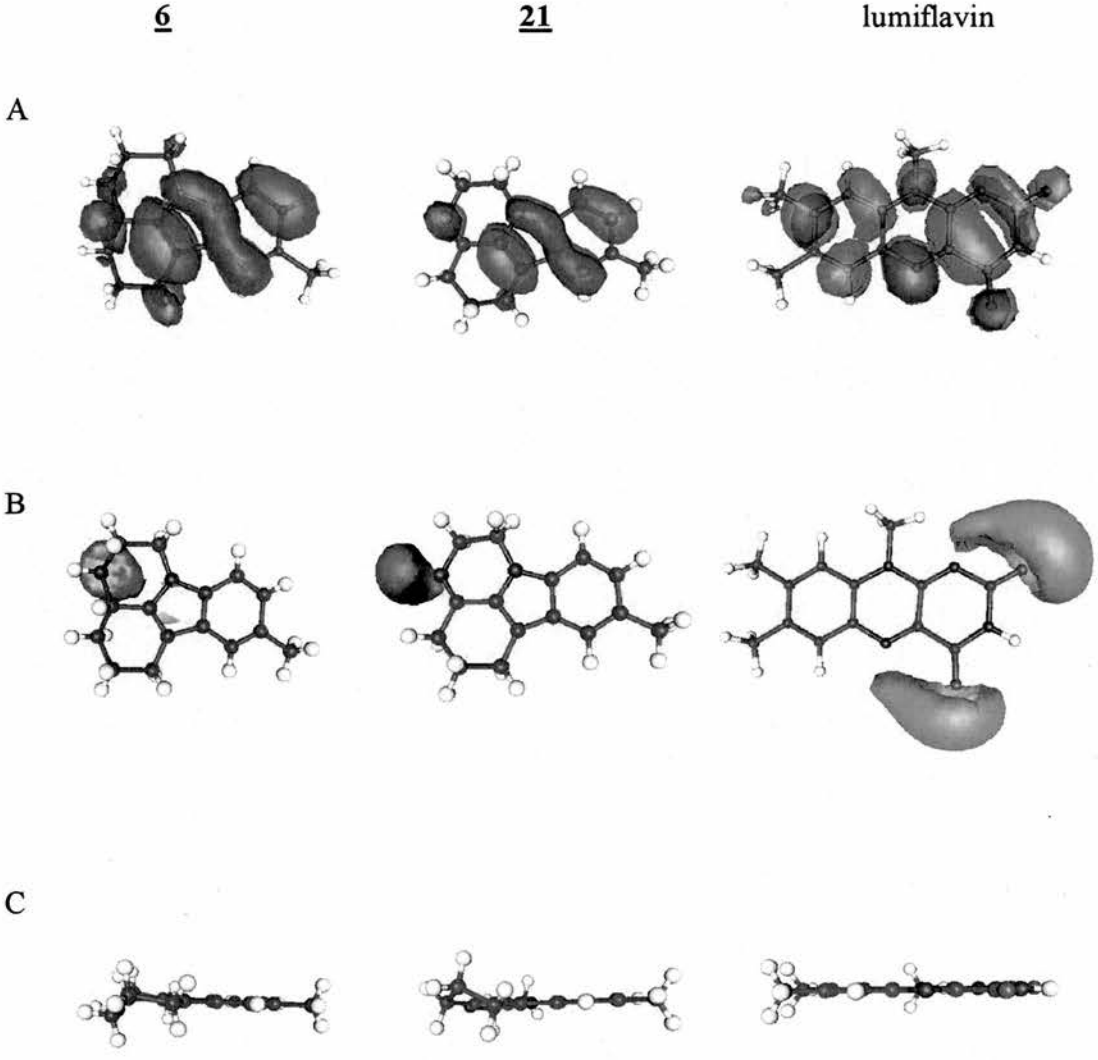

Fig.3.4.2.1. Molecular modelling of the frontier orbital topology, molecular electrostatic potential, and shape of the pirlindole analogs. Top row: frontier orbital topology for the HOMO of inhibitors **6** and **21** and for the LUMO of lumiflavin. Middle row: MEP of the inhibitors **6** and **21**, and of lumiflavin. Bottom row: side view of the energy minimised structures for inhibitors **6** and **21** and for lumiflavin.

3.4.3. Theoretical overlay of pirilindole and lumiflavin

There are two major contributions to the stability of molecular complexes, electrostatic interactions which act over long ranges and charge transfer bonding which acts over short ranges. On this basis a theoretical model can be proposed for the interaction between inhibitor and lumiflavin, as previously performed for a number of inhibitors (116).

The inhibitor is first orientated to the flavin nucleus by the long range electrostatic forces to give it the best complementarity of repulsive and attractive zones. The electrostatic potential map of lumiflavin has two areas of negative charge centred around the two carbonyls on the pyrimidine ring of the flavin, (Fig. 3.4.2.1). The remainder of the molecule contains a positive region spread over both sides of the tricyclic ring. The inhibitor **6** is characterised by a negative charge localised above N3 and a small area of negative charge over both sides of the aryl ring. The inhibitor is oriented with the flavin so that the negative area surrounding N3 is positioned at the opposite end of the carbonyls on the flavin with the negative side facing the flavin. This allows the small negative region above and below the aryl ring of the inhibitor to fit between the two carbonyls of the flavin. The orientation deduced from the potential maps of the inhibitor and flavin also allows good overlap between the LUMO of lumiflavin and the HOMO of the inhibitor (as found for (129)). Charge transfer proposed to occur from experimental measurements (129) do in fact occur between the aryl ring of the inhibitor and the pyrimidine ring of the flavin in this model.

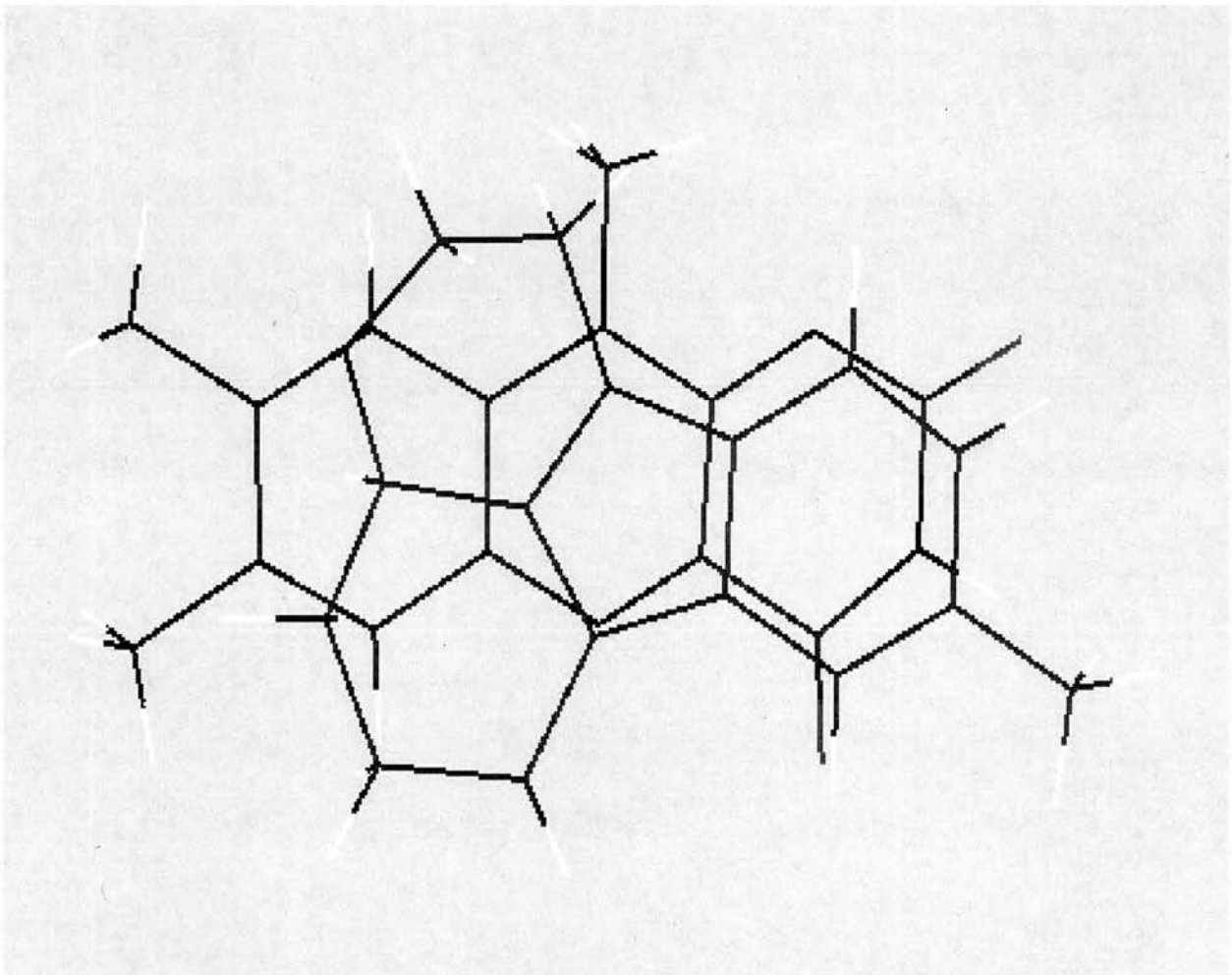

Fig. 3.4.3.1 Predicted overlay for stacking of lumiflavin and inhibitor 6 based on optimal HOMO/LUMO overlap and optimal electrostatic complementarity.

3.4.4. Charge matching of β-carbolines stacking with lumiflavin

The atom-centered charges were determined for lumiflavin and thirteen β-carbolines. The charges for the atoms predicted to lie close together in the stacking model shown in Fig. 3.4.4.4 were used to calculate a net score for the electrostatic attraction of each pair of atoms. A negative value would indicate an unfavourable pairing, and a positive value a favourable one. The net values were plotted against the logarithim of the experimentally determined K_i values from the literature (124). The correlation evident in Fig. 3.4.4.4, correlation coefficient 0.86, indicates that the charge matching in this optimised overlay model (Fig. 3.4.4.4) is a good predictor of inhibitor efficacy.

Two points lying well below the correlation line are for the 6-methoxy derivatives. For these derivatives the methoxy group clashes with the 2-carbonyl group of lumiflavin. The lowest values for charge matching were obtained for analogues lacking any methoxy group, the charges on both C6 and C7 carbons are –0.08. When a methoxy group is attached to C6, the charge of +1.8 clashes with the C2 of lumiflavin that is positive due to the electron withdrawing effect of the oxygen, and, thus, should make 6-methoxy derivatives poor inhibitors. In fact, the Ki values are better than would be predicted, so the 6-methoxy derivatives must adopt an alternative orientation in the active site to give these lower than expected K_i values.

Fig. 3.4.4.1. Structures of β-carbolines used in this study taken from (124)

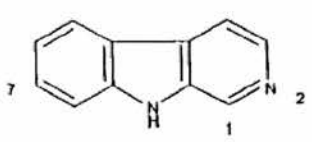

1 Norharman

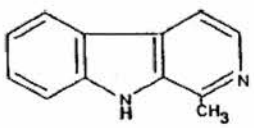

4 Harman

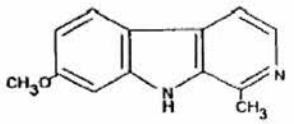

7 Harmine

2 2-Methyl norharman

5 2-Methyl harman

8 2-Methyl harmine

3 2,9-Dimethyl norharman

6 2,9-Dimethyl harman

9 2,9-Dimethyl harmine

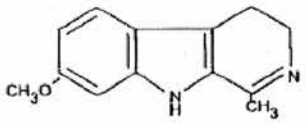

10 Harmaline

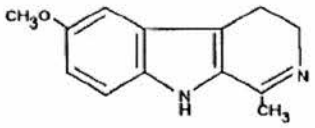

12 6-Methoxy harmalan

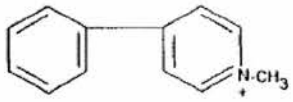

MPP$^+$

11 2-Methyl harmaline

13 2-Methyl-6-methoxy harmalan

Table 3.4.4.1. Ki values for the β-carbolines shown in Fig 3.3.1. Data is taken from (124).

β-Carboline	K_i (μM)
1	3.34
2	1.43
3	0.41
4	0.26
5	0.68
6	0.16
7	0.005
8	0.069
9	0.015
10	0.048
11	0.14
12	0.39
13	1.23

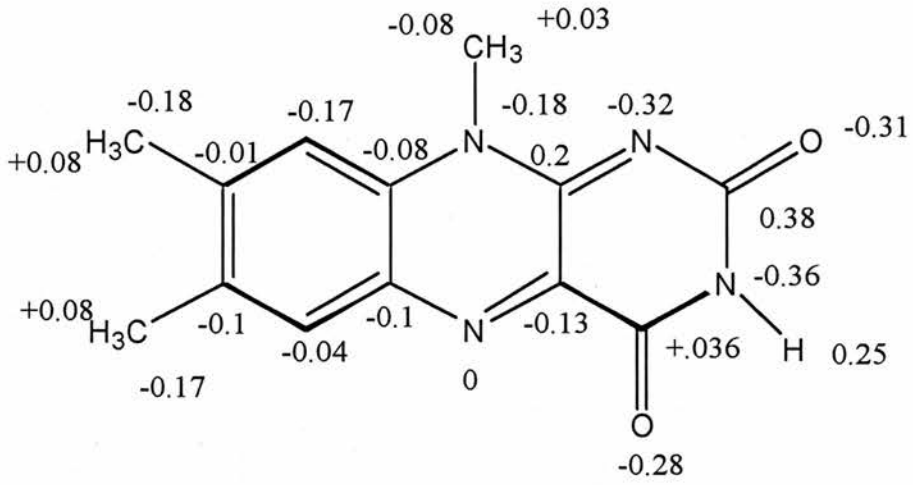

Fig. 3.4.4.2. Structure of lumiflavin with atom centered charges.

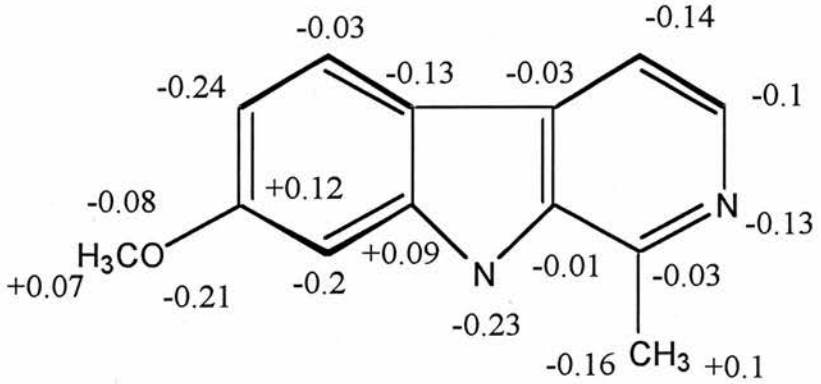

Fig. 3.4.4.3. Structure of harmine with atom-centered charges.

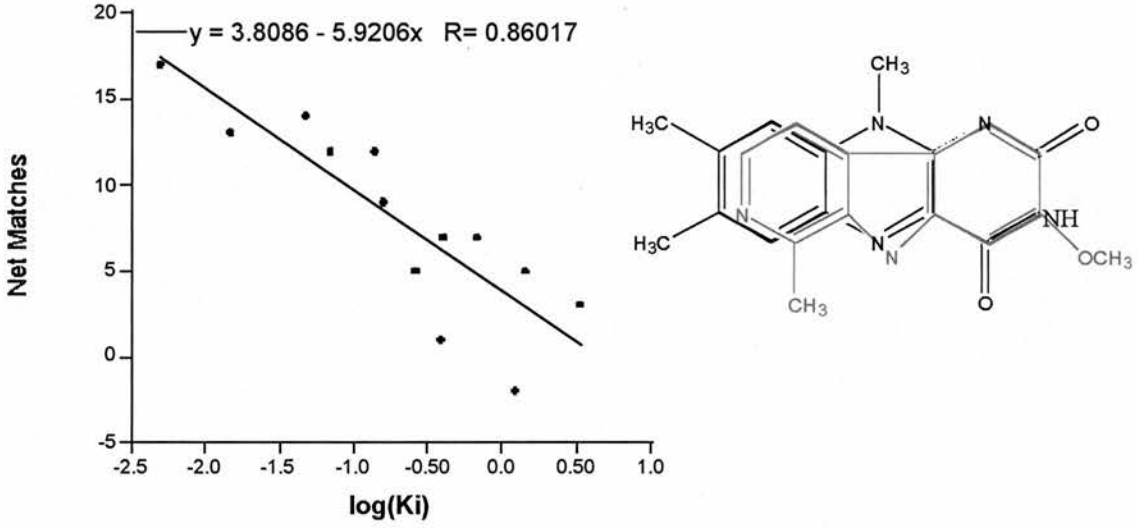

Fig. 3.4.4.4. Charge matching scores correlate with K_i values. The optimal stacking orientation for harmine on flavin, based on HOMO/LUMO patterns and molecular electrostatic potentials is shown above (right). The graph (left) shows the correlation between the net score for the electrostatic attraction between each β-carboline derivative and lumiflavin and the logarithm of the K_i values μM. The derivatives used and their K_i values are listed in Table 3.4.4.1 (124).

3.5. Circular dichroism spectroscopy

Circular dichroism spectroscopy is a form of light absorption spectroscopy that measures the difference in absorbance by a substance of right- and left-circularly polarized light (rather than the commonly used absorbance of isotropic light). Right- and left-circularly polarized light will be absorbed to different extents at some wavelengths due to differences in extinction coefficients for the two polarized rays, called circular dichroism. The phenomenon of circular dichroism is very sensitive to the secondary structure of polypeptides and proteins as well as conformational changes. The three aromatic side chains that occur in proteins (phenyl group of Phe (265-275 nm), phenolic group of Tyr (280 nm), and indole group of Trp (293 nm) have absorption bands in the ultraviolet spectrum. Absorbance in these wavelengths can be used to determine whether the environments of these residues have changed upon ligand binding.

Perturbation of the visible absorbance spectrum of the flavin cofactor of MAO A by D-amphetamine, the small substrate-analogue inhibitor, is shown in Fig. 3.2.1.10. The difference spectrum shows considerable fine structure, characterised by an increase in the absorbance at 508 nm and a decrease at 400 nm. The larger rigid molecule, pirlindole **6**, induces a different change (Fig. 3.2.1.5), with a clear decrease in absorbance at 500 nm. Such perturbations could arise from stacking interactions (116) or perturbation of the environment of the flavin (130). In earlier work reported in chapter 3.2 of this thesis, the lack of correlation between the extinction coefficient for ligand-induced decrease at 500 nm and K_i values for the inhibitors suggested that perturbation of protein was the more

likely explanation (103). The structure of MAO B (42) revealed that both the flavin and the substrate cavity were surrounded by aromatic residues, so we have used circular dichroism (CD) to probe the alterations in the environment of aromatic residues in MAO A in the absence and presence of ligands. CD allows the investigation of protein conformational change upon ligand binding and reduction of the flavin.

3.5.1. Inhibitor perturbation of the CD spectrum of MAO A is small

The CD spectrum of MAO A is shown in Fig. 3.5.1.2 (solid line). There are only relatively small, broad signals in the flavin region (350-520 nm, Fig. 3.5.1.2). In contrast, distinctive fine structured signals with at least three peaks are observed in the aromatic region (260-310 nm, Fig. 3.5.1.2 right). The classical inhibitor, D-amphetamine, and the antidepressant, pirlindole, were added to MAO A at concentrations over 100 times K_i to ensure saturation. Fig. 3.5.1.2 shows that there is relatively little difference between the CD spectra for the free enzyme and the enzyme-inhibitor complexes in the flavin region, and only minor alterations in the aromatic region, the principal spectral features being preserved. The tyrosine peak at 285 nm is somewhat decreased in the presence of D-amphetamine, but is enhanced together with the tryptophan peak at 293 nm in the presence of pirlindole. These data indicate that inhibitor binding does not greatly perturb the aromatic cage around the active site, but there may be subtle differences between the orientations of pirlindole and amphetamine bound within this active site cage.

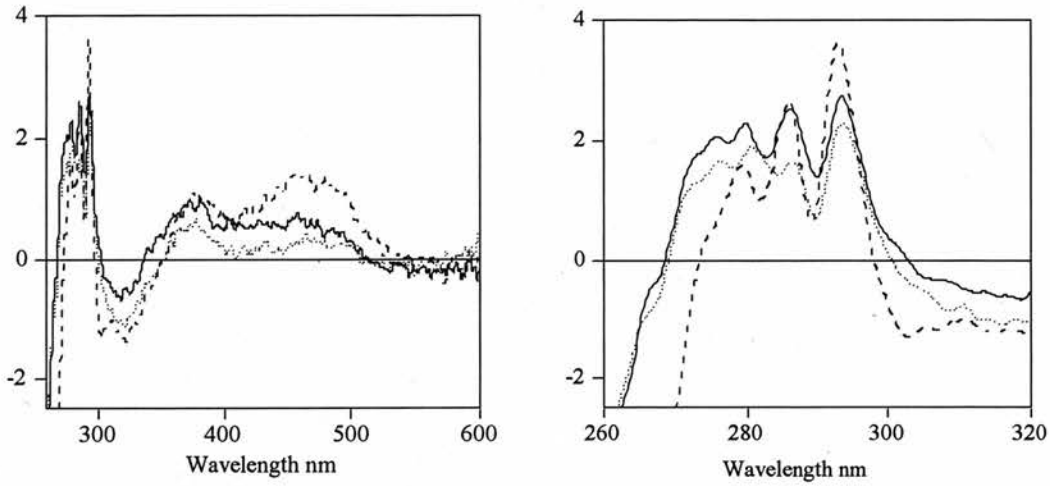

Fig. 3.5.1.2. CD spectra of MAO A. CD spectra of MAO A alone (13.2 μM, solid line), MAO A (13.2 μM) with D-amphetamine (0.5 mM (25 times K_i), dotted line), and MAO A (14.3 μM) with pirlindole (30 μM (600 times K_i), dashed line) were recorded in 0.5 cm pathlength anaerobic cells (above left). The right hand figure expands the aromatic region of the spectrum.

3.5.2. Reduction of MAO A induces large alteration in CD spectrum

Both kinetic and absorbance spectrophotometric studies showed that the presence of inhibitor in the active site also has an effect on the redox properties of the flavin. Fig. 3.5.2.1 contrasts the partial generation of semiquinone, as indicated by the small peak at 410 nm during reduction of free MAO A by dithionite (Fig. 3.5.2.1a), with the appearance of only semiquinone (large 412 nm peak) in the presence of D-amphetamine. Further reduction is not observed for the enzyme-inhibitor complex (5).

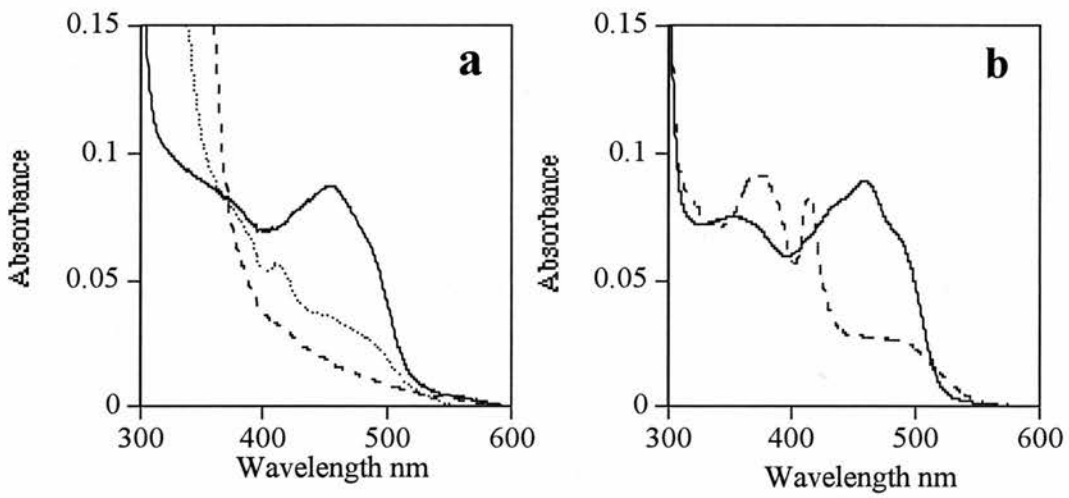

Fig. 3.5.2.1. UV-Visible absorption spectra of MAO A . (a) Oxidised MAO A (13.2 μM, solid line) was reduced by the addition of dithionite to obtain a partial yield of semiquinone (dotted line), and further reduced by more dithionite to the fully reduced form (dashed line). (b) In contrast, the mixture of oxidised MAO A (13.2 μM) and D-amphetamine (1010 μM) (solid line) is only reduced to the anionic semiquinone even with excess dithionite (dashed line).

When the MAO A-amphetamine complex is reduced to the semiquinone form, there are small reductions in the broad signals due to flavin from 350-500 nm (Fig. 3.5.2.2, dashed line). However, a dramatic change is observed in the aromatic region of the CD spectrum, such that the CD signal is more than doubled below 290 nm. The changes are seen in the signals due to tyrosine at 280 nm and phenylalanine at 265-275 nm, but not in that signal arising from tryptophan at 293 nm (Fig. 3.5.2.2, right). Fully reduced enzyme (in the absence of ligands) showed an even greater increase in the CD signal for the aromatic region, with all peaks being enhanced (Fig. 3.5.2.2 right, dotted line).

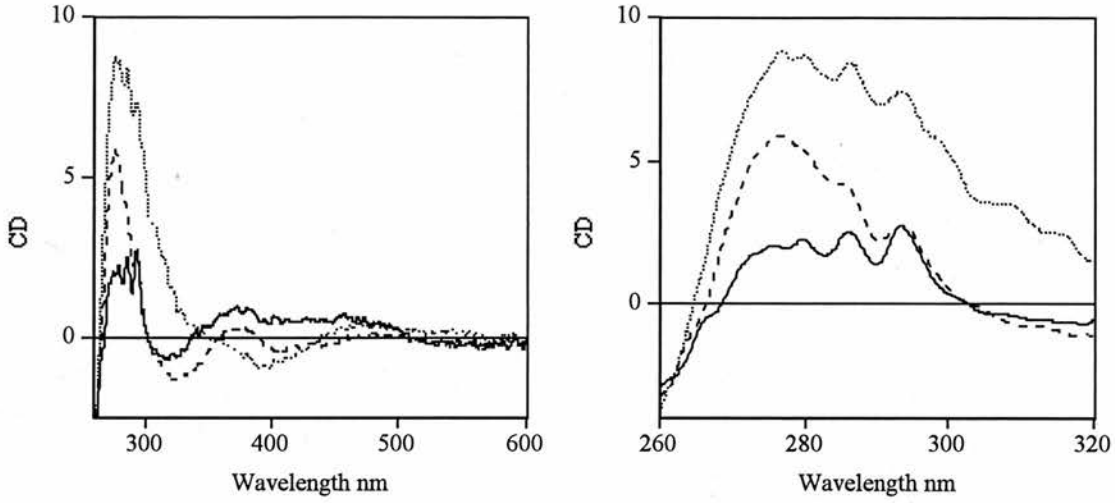

Fig. 3.5.2.3. Reduction of MAO A alters the CD spectrum. The CD spectra of MAO A (13.2 μM) in 0.5 cm pathlength cell show: oxidised MAO A (as in Fig.3.5.1.2, solid line), the MAO A –amphetamine (0.5 mM) complex reduced to semiquinone (dashed line), and fully reduced MAO A (dotted line) (above left). The graph on the right expands the aromatic region of the spectrum.

3.5.3. Substrate reduction gives a different CD alteration.

When MAO is reduced by substrate, no 412 nm peak is ever detected in the visible absorption spectrum (44,131). Fig. 3.5.3.1 shows the CD spectrum of MAO A reduced by a 300-fold excess of benzylamine (3 mM). The spectrum is similar to that for the free enzyme fully reduced by dithionite but there are small alterations in the broad negative signal in the flavin region and an enhancement in the aromatic region. In the presence of substrate, the signal is more negative than for the dithionite-reduced enzyme both in the flavin region and in the 265-285 nm region associated with phenylalanine and tyrosine residues. Reduction also accompanies the covalent modification of the flavin by the suicide inhibitor, clorgyline (10). The CD spectrum (Fig. 3.5.3.1) of the covalently modified reduced enzyme (dash and dot line) is dramatically different from either the free reduced enzyme (dashed line) or the substrate-reduced enzyme (dotted line). For the covalently modified reduced enzyme, there is no difference from oxidised enzyme in the flavin region (360-500 nm), in contrast to the other reduced forms. However, there is a large negative CD peak between 310 nm and 360 nm, and a large increase in the positive CD signal in the aromatic region, with the tryptophan (293 nm) and tyrosine (280 nm) peaks increased to a level similar to the free reduced enzyme (Fig. 3.5.3.1). The most obvious difference in this region is that the amplitude of the lowest wavelength peak in the aromatic region (phenylalanine, 265-275 nm) is more than twice that seen for free dithionite-reduced MAO A or for the enzyme reduced by and complexed with substrate. Thus, the environment of aromatic residues is affected by this covalent ligand to the flavin. The major negative region in the CD spectrum for the clorgyline-modified MAO

A at 310-360 nm may be due to constraints on the flavin as a result of the N5 modification (132).

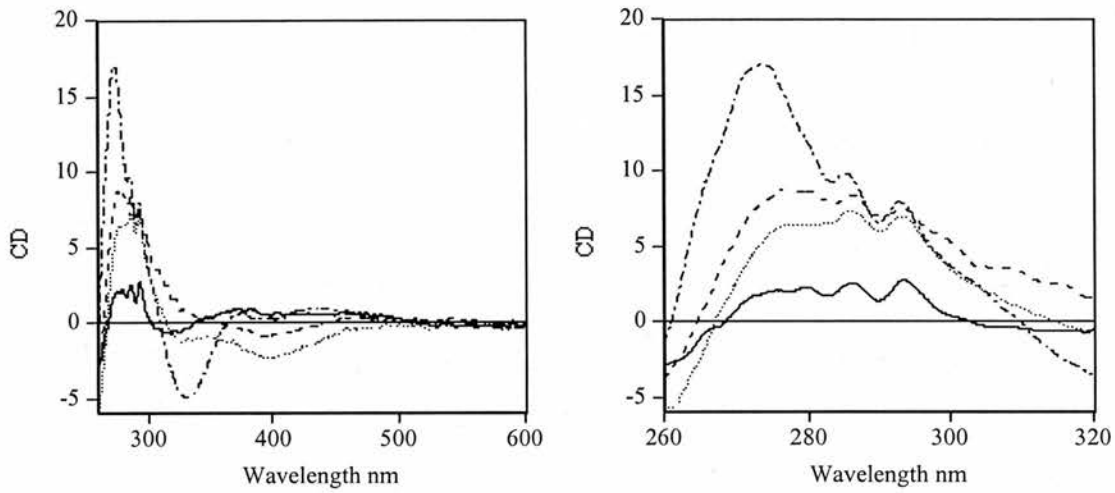

Fig. 3.5.3.1. Comparison of the CD changes induced by reduction. The CD spectra of MAO A (13.2 μM) in 0.5 cm pathlength cell show: oxidised MAO A (from Fig. 3.5.1.2 for comparison, solid line), MAO A reduced by dithionite (dashed line), MAO A reduced by 3 mM benzylamine (dotted line), and MAO A (14.3 μM) reduced and covalently modified by 30 μM clorgyline (dotted-dashed line) (above left). The graph on the right expands the aromatic region of the spectrum.

4. Discussion

4.1. Kinetics

SAR and QSAR studies have identified the size and functional determinants important for inhibitor binding to MAO (reviewed in (29)). These studies have shown that compounds need to be hydrophobic in nature, contain an aromatic ring, and contain a nitrogen, oxygen or sulphur within two bonds of the aromatic ring. In addition to this, rigid molecules should have size dimensions of less than 14 Å (length) x 7 Å (height) x 4 Å (width) and 8.5 Å (length) x 5.1 Å (height) x 1.8 Å (width) for MAO A and B respectively (101,110). The recently solved 3D crystal structure has shown that the active site of MAO B is indeed hydrophobic in nature, and a theoretical mould based on kinetic data from a group of pirlindole compounds was similar in shape to the real active site of MAO B (114).

The influence of the dimensions of pirlindole on affinity to MAO A was investigated by introducing groups of differing sizes on to C8 and also N3 of the pirlindole structure to vary the length, height and width of the molecule, to see how substituents at each end affect inhibition. Increasing the size of substituent on C8 increases inhibition up to a point. Comparing to the non-substituted inhibitor **1** with the methyl (9.87 Å total length) and cyclohexyl (13.07 Å length) C8 substituents, both improve inhibition with K_i values of 0.264 μM and 0.050 μM respectively. The compound with a C8 admantyl substituent is at the limit of size to fit the box. It is larger in height at 7.2 Å and at the very limit of width, at 4.448 Å. Although the length of the molecule is within the size limits of the box, the extra width of the molecule may position the large C8 substituent in an

orientation that is sterically hindered, and therefore the inhibitor does not bind as well as the methyl or cyclohexyl derivatives. The methyl and cyclohexyl derivatives show better inhibition than the non-substituted inhibitor. The increased size of substituent will allow greater interactions with the active site of the enzyme. Presumably the C8 substituent is orientated in a hydrophobic pocket, so that binding of these hydrophobic groups is favoured. Kinetic data on pirlindoles with various different hydrophilic C8 substituents showed that these substituents were not tolerated even though they were well within the size limits of the active site (101).

The introduction of a methyl group at C10 was studied to see if the position of the substituent on this ring was important. Inhibitor **18** with a methyl at C10 showed no improvement in inhibition compared with the unsubstituted inhibitor **1**, in contrast to inhibitor **6**, with a methyl group at C8, which showed 20-fold better inhibition than inhibitor **1**. Inhibitor **19**, with methyl groups at both C10 and C8 has a K_i of 0.0157 μM, 17-fold lower than the C8 methyl compound. Why the addition of a C8 and C10 methyl group is better than the C8 methyl alone, whereas the C10 methyl only derivative does nothing to increase inhibition is not clear. There may be increased hydrophobic interactions with two methyl groups that can only occur when both methyl groups are present and cannot occur when the C10 methyl is present by itself.

Substituents on N3 do not confer the advantage that they do on C8. N3 substituents of various sizes were introduced to inhibitors with either no substituent, a methyl or cyclohexyl substituent on C8. Preliminary IC_{50} values for the cyclohexyl series were

determined in Moscow, but were not available for further testing in St Andrews, they will still be discussed. For the series with no substituent on C8, substituents on N3 increased inhibition marginally. For the methyl and cyclohexyl series, addition of any substituent decreased inhibition, the larger the substituent the poorer the inhibitor. Although the methyl series inhibitors **6**, **7** and **8** were within the size limits of the box, inhibitor **10** (C8-methyl, N3-admantyl) was outside the limit of the box. So why were they all poor inhibitors? Two factors come into play with this set of compounds. Firstly, the interaction of N3 with the flavin. From the crystal structure of MAO B complexed with isatin, the nitrogen in isatin is orientated towards N5 of the flavin, as if it were being orientated for catalysis. This nitrogen corresponds to N3 in pirlindole; its proximity to the flavin may be assumed on the basis of spectral data discussed in more detail later. In reductive titrations of MAO A complexed with inhibitors, MAO A complexed with an inhibitor with an unsubstituted N3 such as **6**, always stabilized the semiquinone upon reduction with dithionite, and no further reduction was seen thereafter (Fig. 3.2.1.5). When MAO A is complexed with an inhibitor that is substituted on N3, then the reductive titration is similar to unliganded enzyme. The yield of semiquinone is comparable to unliganded enzyme and full reduction follows (Fig. 3.2.1.4, inhibitor **4**,Fig. 3.2.1.12, unliganded MAO A). This indicates that when N3 is unsubstituted it is free to interact with flavin, but when it is substituted it cannot interact with the flavin and a normal reductive titration is seen. This nitrogen is one key for inhibition of MAO A by pirlindole: by adding a substituent on to N3, it will not be available to interact with the N5 of the flavin, which will cause weaker binding.

The other possibility for the poorer binding of these inhibitors is the orientation of the aromatic ring relative to Tyr-404 and Tyr-444 in MAO A. The aromatic ring of isatin lies between Tyr-398 and Tyr-435 in the MAO B structure (43), if there is a substituent on N3 of the pirlindoles this would orientate the inhibitor further from the flavin and the aromatic ring of pirlindole would not be able to stack as well with the two tyrosine rings, and therefore result in poorer binding.

Why do N3 substitutions on the non-C8 substituted series increase inhibition? The increase in inhibition by these substitutions is very small. Inhibitor **1** with no substituents has a K_i of 5.16 μM and inhibitor **4** with a cyclohexyl group on N3 has a K_i of 2.92 μM, not even a 2-fold change. Inhibitor **1** with no C8 substituent has little interaction with the hydrophobic pocket that accommodates the C8 substituents. Either the N3 substituent pushes the C8 region closer to the hydrophobic region and therefore allow for more hydrophobic interaction, or, the molecule is flipped so that the N3 substituent lies in the hydrophobic pocket usually accompanied by the C8 substituent. Either way a very little increase in inhibition is seen with this series, but for the methyl or cyclohexyl series, N3 substituents are detrimental to inhibition.

Another factor affecting inhibition is the saturation at N3. Inhibitors **21**-**24** all have a double bond at N3 (Table 3.1.1.1). All 4 de-hydro compounds had lower K_i values than their saturated derivatives. Fig. 3.4.2.1 (bottom row) shows the side view of inhibitors **6** and **21**. Inhibitor **21** is flatter than **6**, this may allow a better fit between the two tyrosines and therefore greater affinity. One other possibility could be that the kinetic barrier the

enzyme needs to overcome in order to oxidise substrates, but cannot overcome with inhibitors, is smaller in the dehydro derivatives than the saturated ones. The energy barrier cannot be overcome to oxidise the inhibitor but results in a tighter binding complex. In Fig. 3.4.2.1 (middle row) we can see that the electrons in inhibitor **21** are axial to the ring rather than above the ring, as in inhibitor **6**, indicating the flavin may have easier access to the electrons of the nitrogen.

One surprise result was the low K_i value for inhibitor **26**. Previous studies on hydrophilic electron donating and withdrawing C8 subsituents showed that there was no correlation between K_i and σ, the parameter describing the degree to which a substituent donates or withdraws electron when attached to an aromatic ring. The compounds studied were all saturated at N3 The study tested the idea that electron density in this aromatic ring was crucial, but it was not. In inhibitor **26**, the electronic effect of the Br atom can have not only an effect on the aromatic ring it is attached to, but also at the N3 that is now conjugated with the rest of the molecule. If indeed this is the case, then the Br has a dramatic effect on inhibitor binding. This idea would need to be tested with a series of de-hydro derivatives with various electron donating or withdrawing substituents at C8. It seems unlikely that Br is interacting favorably in the same way other C8 substituents do. Although hydrogen bonding might improve interaction to Br in this area, it is unlikely as other similar C8 substituents were poor inhibitors.

A few inhibitors were selected to be tested for time dependence which has been reported previously for β-carbolines (109). The K_i values for inhibitors **6**, **11**, **21** and **23**

were determined after 5 minutes pre-incubation of enzyme and inhibitor. All 4 inhibitors showed lower K_i values after 5 minutes pre-incubation, and the differences between the four inhibitors remained the same. Several inhibitors were tested for their inhibition over a time course of 5 minutes. Fig. 3.1.1.2 shows an example of a plot of activity verses time for inhibitor **1**. All the inhibitors tested showed a similar profile. The reason for the time dependent inhibition in MAO A is unclear. One possibility involves the entrance cavity seen in the MAO B structure, it is not known whether MAO A has this entrance cavity. If it does, it may be possible that the time dependence seen is a result of the time it takes for the inhibitor to transverse the entrance cavity and occupy the active site. The initial K_i values may be a measure of a high distribution of inhibitor in the entrance cavity, whereas the 5 minute pre-incubated K_i values are a measure of a higher proportional occupancy of the active site. However, CD and UV-vis spectroscopy has not been able to detect any differences over the 5 minutes this phenomenon is seen. Spectral changes after inhibitor binding are immediate, both for harmine (109) and the pirlindoles studied here (103).

Fig. 3.1.1.3 shows the Lineweaver-Burk plot for an initial K_i determination for inhibitor **2** (left) and a 5-minute pre-incubated K_i for inhibitor **11** (right). The intercepts for the plot for inhibitor **2** lies slightly to the left of the *y* axis suggesting that it not strictly competitive inhibition and is showing signs of mixed inhibition. The intercept for the plot for inhibitor **11** is shifted well to the left of the y-axis and is nearly down to the *x*-axis, this is typical of mixed inhibition. There are several possibilities in the inhibition of MAO A that could explain these results. From the MAO B structure two cavities are

seen, an entrance cavity and a substrate cavity. It may be possible to bind both inhibitor and substrate in each of these two cavities forming a non-productive or less productive ESI complex depending on which cavity is occupied by substrate or inhibitor. Another possibility involves the time dependence seen after 5 minutes in this inhibition. After a 5-minute pre-incubation of enzyme and inhibitor, we see a lower K_i value. This could be due to a second type of EI complex where the inhibitor binds more tightly in an EI* complex. This complex may be so stable that it, in effect, reduces the amount of available enzyme for catalysis and reduces V_{max} as a result. This idea is more consistent with the kinetic data available.

The stopped-flow spectrometry was performed to investigate whether inhibitors bind to the reduced form of the enzyme and how this affects the redox properties of the flavin. Substrates bind to the reduced form of the enzyme and stimulate the re-oxidation by O_2 up to 120-fold depending on the substrate used (20). Previous studies have shown that amphetamine and MPP^+ bind to the reduced enzyme and completely inhibit re-oxidation (127). It was hoped that by varying the inhibitor concentration over an appropriate range, a K_D could be determined for one of the pirlindole analogues. The experiment was also repeated for kynuramine to determine the K_D for substrate binding to the reduced enzyme. After initial trials, 7 was chosen to study its binding to reduced enzyme. It did inhibit re-oxidation, however, it did not inhibit it completely as was reported for amphetamine previously. Kynuramine was shown to stimulate re-oxidation as reported before. Fig. 3.1.2.1 shows the re-oxidation traces for enzyme alone, enzyme with kynuramine, and enzyme with inhibitor 7, to demonstrate the differences in the rates of

re-oxidation. Inhibitor 7 inhibits the re-oxidation in a concentration dependent manner with maximal inhibition occurring at about 50 μM. For inhibitor 7, the rate decreases with increased inhibitor concentration and the relative amplitudes remain the same with varying inhibitor concentration. It must be noted that for the re-oxidation, the air-saturated buffer contained no ligand, either inhibitor or substrate.

Kynuramine stimulates re-oxidation in a concentration dependent manner with maximal stimulation occurring at about 5 μM, a similar concentration to the enzyme. One thing that is different about this data compared to the data reported previously are the phases of re-oxidation. Previous reports have given just one rate for the re-oxidation of MAO A, but in this study we saw biphasic re-oxidation which could not be fitted by monophasic or triphasic analysis. The relative amplitudes of the two phases changed with the concentration of substrate. For substrate the rate increases with increasing substrate concentration for the fast phase, for the slow phase the rate increases up to 6 μM and then got lower. The amplitude also changes with increased substrate concentration, the amplitude of the slow phase of re-oxidation gets smaller with increased substrate concentration. The slow phase getting slower with increased substrate is due to re-reduction by substrate. The original experiments analysed the data to account for re-reduction (63). Why the amplitude changes with increased substrate concentration is not clear, but may be due to the buffer containing no substrate so that the slow phase is a combination of the off rate of substrate and reduced enzyme and re-oxidation of unliganded enzyme, this effect will be greatest at low concentrations, whereas at high concentrations this effect is small.

Why substrates stimulate re-oxidation and inhibitors inhibit it is not clear. In the case of amphetamine, the only structural difference to its parent substrate, β-phenylethylamine, is a methyl group, which, in the D-isomer, is thought to occupy the position of the non-abstracted proton. How this has such a dramatic effect on the redox properties of the flavin is not clear. It may be possible that when substrates are bound to reduced enzyme, they are orientated with the lone pair of electrons from the amine adjacent to the N5 region of the flavin. This increased electron density causes a shift in the potential of the flavin as seen in the reductive mid-point potentials (50), and increase the rate of re-oxidation. If this is the case, inhibitors must bind and influence the flavin in a different way to influence the flavin so as to decrease the rate of re-oxidation.

4.2. Spectral studies

Previous spectral studies on MAO A have demonstrated a change in the spectrum of FAD upon inhibitor binding (101-103). Inhibitor binding also stabilizes semiquinone formation upon reduction by dithionite and no further reduction is seen. The spectral changes seen when inhibitors bind to MAO A were thought to contain characteristic charge transfer bands consistent with the theory of inhibitor stacking with the flavin in the active site. The inhibitors studied here show characteristic spectral changes upon inhibitor binding, and some, but not all, stabilize the semiquinone during reduction by dithionite. Figs. 3.2.1.1 to 3.2.1.11 show the spectral changes of inhibitor binding to MAO A and also the spectral changes associated with reduction by dithionite of the enzyme inhibitor complex. The majority of the inhibitors (**1**, **2**, **6**, **8**, **11**, **21**, **23** and MPP^+) give a similar spectral change in the difference spectrum. This is characterized by a decrease in absorbance at 465 nm and 495 nm, and in some cases a small increase in absorbance at 530 nm. The increase at 530 nm was interpreted as a charge transfer band, originally thought to be caused by stacking of inhibitor and flavin. Inhibitor **4** and amphetamine have different difference spectra from the other inhibitors studied. They are characterized by an increase in absorbance at 508 nm and decreases in absorbance at 485 nm, 450 nm, and, for amphetamine also at 395 nm. Inhibitor **2** shows a hybrid spectrum between these two types; it has the classic features of the normal spectrum with a decrease at 495 nm and 465 nm, but also shows signs of an increase at 508 nm. The two types of spectra are not strictly structure specific. The two inhibitors giving the spectrum dominated by an increase at 508 nm have a substituent on or near their amine

(amphetamine is α-methylated), but some inhibitors in the other class of spectrum also have substituted amines. It may be possible to rationalize the spectra depending on the type of group that might be interacting with the flavin. From the crystal structure of MAO B with isatin bound, the N2 amine of the isatin lies edge-on with the N5 of the flavin. If this is the same in pirlindole, then it would be expected that the inhibitors with substituents on N3 would give spectral changes different from the unsubstituted inhibitors. Some of the N3 substituted inhibitors have an oxygen in the N3 substituent; so perhaps the lone pair of electrons from this oxygen can interact with the flavin instead of N3, giving similar spectral changes. For inhibitor **4** and amphetamine, the inhibitors may be orientated with the cyclohexyl group or methyl group interacting with the flavin causing the different spectral changes. What about MPP^+? This inhibitor has a substituted nitrogen but gives a classic double minima at 495 and 465 nm. Spectral changes of this sort are very difficult to rationalise unless there are crystal structures available for comparison and a large sample of systematically substituted inhibitors.

Monomeric sarcosine oxidase has been crystalised in the presence of inhibitors stacking with the flavin in the active site. The spectral changes seen upon inhibitor binding are quite different from the ones seen in MAO A. The charge transfer bands seen at wavelengths above 600 nm are very broad and larger than the charge transfer bands seen in MAO A (133). The crystal structure of MAO B has revealed that inhibitors bind end-on to the flavin and there is not enough room for inhibitors to stack with the flavin as they would in solution. This remains to be proven in MAO A but it seems likely that inhibitors bind in the same way.

To assess the magnitude of the spectral changes and to correlate them with the structure of the inhibitors, the extinction coefficients at 500 nm were determined for the eight pirlindole inhibitors tested (Table 3.2.1.1.). For the inhibitors giving a positive change in absorbance, the wavelength measured was 508 nm, for the inhibitors giving a decrease in absorbance, the wavelength measured was 495 nm. Comparing the extinction coefficients for compounds **6**, **11**, **21** and **23**, we see an interesting trend. The coefficients for the cyclohexyl derivatives **11** and **23** are 82% higher than those for the methyl derivatives **6** and **21**, correlating with greater affinity as observed with lower K_i values for the cyclohexyl derivatives. For either cyclohexyl or methyl derivative, addition of a double bond at N3 resulted in an extinction coefficient that is only about 55% of that for the saturated derivative despite the lower K_i values (Table 3.1.1.1). Structure and extinction coefficients do not show a trend with K_i. A trend is seen between structure and extinction coefficient in this sample (**6**, **21**, **11**, **23**) but is not seen with the remaining inhibitors. As discussed before, inhibitor **4** and amphetamine give an increase at 508 nm but this cannot be rationalized with structure. For any substantial conclusions to be made from this study, a larger number of compounds need to be tested.

Unlike the spectral changes induced by inhibitor binding, dithionite reduction of the enzyme-inhibitor complex does show a structure-dependent change. Inhibitors with an unsubstituted nitrogen will stabilize the semiquinone with 100% yield, and no further reduction is seen. For inhibitors with a substituent on N3, a reductive titration similar to non-liganded enzyme (Fig. 3.2.1.12) is seen. A small amount of semiquinone is seen and

full reduction is reached. Figs. 3.2.1.3, 3.2.1.4 and 3.2.1.6 show the reductive titrations of inhibitors **2**, **4** and **8**. Inhibitors **2** and **8** have spectral interference from the inhibitor spectrum so the region where the semiquinone is seen is masked. The spectrum of the reductive titration of MAO A-inhibitor **4** shows clearly the appearance of semiquinone and subsequent full reduction. This is very similar to the reductive titration of MAO A alone in Fig. 3.2.1.12. Why would these two types of inhibitors give such different reductive titration patterns? For the inhibitors with no N3 substitutions, the nitrogen is free to interact with the N5 of the flavin, as seen in the crystal structure for the MAO B-isatin complex. This interaction still allows the first electron to be transferred to the flavin, however this complex is very stable and lowers the midpoint potential for the second electron transfer too far to be overcome by the reductive potential of dithionite. Inhibitors with a substituent on N3 do not stabilize the semiquinone upon reduction. The nitrogen does not have access to the N5 of the flavin and therefore cannot form the semiquinone-stabilizing complex. The flavin will behave as if there is nothing bound and a normal reductive titration is seen. This is clear evidence that, as seen in the MAO B structure, inhibitors in MAO A bind edge on with the flavin, and the nitrogen is close to N5 of the flavin. One anomaly to this set of data is MPP^+. This inhibitor stabilizes the semiquinone, but has a methyl group on its nitrogen. However, MPP^+ has a positive charge on its nitrogen, and as a result, might orientate itself in the active site differently so that it can stabilize the semiquinone.

Fig. 3.2.1.13 shows the plots of absorbance versus volume of dithionite added for two different reductive titrations. On the left is a titration of MAO A with nothing bound (A),

and on the right, a titration of MAO A with pirlindole bound (B). The first half of the unliganded MAO A titration shows an increase in absorbance at 377 nm and 412 nm characteristic of the production of semiquinone. At the same time, the absorbance at 456 nm is decreasing, this continues on the same slope for the rest of the titration, the absorbance at 377 nm and 412 nm lowers during the second half of the titration, all three wavelengths level off at the same end point. From this plot, it is clear that the decrease in absorbance at 456 nm occurs uniformly throughout, whereas the changes in absorbance at 377 nm and 412 nm have two distinct phases, corresponding to the first and second electrons being added to the flavin. The second plot shows the reductive titration plot for the MAO A-inhibitor **6** complex, which stops at the semiquinone. The plot seems to have two phases; the first phase comprises the majority of the spectral change, with the second phase comprising the reminder of the change. The increase at 385 nm and 412 nm mirror each other throughout the titration, with almost identical amplitudes of change. The second peak seen in the semiquinone has shifted from 377 nm to 385 nm when in the presence of the inhibitor. The decrease in absorbance at 456 nm occurs with two phases in a similar way to the increase at 385 nm and 412 nm. The mM extinction coefficient for the two semiquinone peaks at 412 nm 380 nm (377 nm for unliganded MAO A and 385 nm for MAO A-**6** complex) are comparable to the values determined in (102). For the unliganded enzyme, the extinction coefficients (mM^{-1} cm^{-1}), were, 1.80 (377 nm) and 1.63 (412 nm), lower than the literature values of 2.74 and 2.11 mM^{-1} cm^{-1}, respectively (102) presumably because the yield of semiquinone is somewhat variable. For the MAO A-**6** complex the extinction coefficients were 5.787 (385 nm) and 5.34 (412 nm), very similar to the literature values of 5.65 and 5.27 mM^{-1} cm^{-1}, respectively.

4.3. Redox potentiometry

The redox potentials of MAO A and MAO B have been determined previously using redox dyes and the xanthine-urate couple catalysed by xanthine oxidase as the source of electrons (50). This method was repeated to obtain mid-point potentials for MAO A in the presence of several inhibitors, but consistent results could not be obtained due to problems with equilibrium between the dye and the flavin. An alternative method to determine the redox potentials of flavoenzymes was attempted at the University of Edinburgh. This method involves successively lowering the potential applied to the enzyme sample to reduce the flavin and then increasing the potential stepwise to re-oxidise the enzyme. By plotting the applied potential against change in absorbance at 456 nm, the mid-point potential can be determined using the Nernst equation. The enzyme needs to be in a solution of high salt (500 mM KCl) to aid electron transfer from the electrode to the flavin. When MAO A is reduced using this system it does not yield any semiquinone, either during reductive step or the oxidative step (Fig. 3.3.1). The equilibrium problems seen with the dye method still remain. The applied potential should reach equilibrium with the solution potential within 5 minutes, but with MAO A, this was taking far longer (up to 45 minutes). The spectral changes induced by reduction were almost instantaneous, but the potential changes took longer. Looking at the redox plot in Fig. 3.3.2 the oxidative plot is shifted to the right compared to the reductive plot. This is clear evidence that the system is not at equilibrium, and therefore the values for the mid-point potentials are not valid. Interestingly, the value obtained from the reductive step is similar to the value determined from the dye method (-210 mV) (50) which also had

equilibrium problems. The lack of semiquinone in the reductive phase was either due to the high salt buffer used in this experiment, or to the method of electron delivery to the flavin.

4.4. Theoretical studies

Several reversible inhibitors have been investigated using a number of theoretical calculations to determine whether it would be favorable for them to stack with the flavin. The original idea of stacking came from a spectral study of β-carbolines and riboflavin in solution (100). This study suggested from the spectral changes induced by inhibitors on the spectrum of riboflavin in solution that these inhibitors were stacking with riboflavin. Similar spectral changes were seen when the enzyme was titrated with inhibitor (102). From this data it seemed reasonable that this could be how MAO A inhibitors interacted with the enzyme, so theoretical studies were undertaken to determine whether it was energetically favorable for stacking to occur between inhibitor and flavin, and to determine the overlay for several inhibitors with the isoalloxazine ring system of the flavin (129). Fig. 3.2.1.5 shows that pirlindole (**6**), induced spectral changes similar to those of the β-carbolines, theoretical calculations were undertaken to determine whether they too could stack with the flavin in MAO A.

The main spectral evidence for the stacking interaction was the appearance of charge transfer bands upon addition of inhibitor to riboflavin (100). Charge transfer bands are usually broad and appear at longer wavelengths than the absorbance of the two participating species. In charge transfer there is partial transfer of electron from a donor

species to an acceptor species. The isoalloxazine ring in FAD is well known to be electron deficient, so it will act as the acceptor, and the inhibitor as the donor. Partial electron transfer will occur from the highest occupied molecular orbital (HOMO) of the donor to the lowest unoccupied molecular orbital (LUMO) of the accepter. The greater the overlap of the HOMO and LUMO orbitals of the two species, the greater the association between the two molecules is favored energetically. Two pirlindoles were studied, inhibitors **6** and **21**. The complimentarity of HOMO/LUMO overlap was very good between both inhibitors and the flavin.

The second calculation was to determine the distribution of charge within the two inhibitors and lumiflavin. Lumiflavin has two areas of negative charge centered around the two carbonyls; the remainder of the molecule has a slight positive charge. Inhibitor **6** has an area of negative charge centered above N3, while inhibitor **21** has its negative charge centered around N3 in a more equatorial position. The remainder of the molecule is slightly positive with a small area of negative charge above and below the center of the aromatic ring. This allows for a very good complimentarity between both inhibitors and the flavin for both charge and HOMO/LUMO overlap. The overlay for inhibitor **6** is shown in Fig. 3.4.3.1. These calculations could not distinguish between the two inhibitors with different K_i values. Given the lack of correlation between K_i and the differences in the extinction coefficients and the spectral data from reductive titrations in the presence of inhibitors, this thermodynamic analysis supports the view that stacking does not contribute to binding in the active site of MAO A. This conclusion was vindicated when

the structure of MAO B was published in 2003 showing that isatin binds perpendicular to the flavin and lies between two tyrosine residues.

An attempt was made to crystallise some of the inhibitors used in this study so as to verify the theoretical structures used in the theoretical calculations. Inhibitor **10** crystallised and the structure was solved. Although this inhibitor has a large admantyl group attached to N3, the main four-ringed system looks very similar to the theoretical structure seen for inhibitor **6**, which is the same as **10** without the admantyl group. This is very reassuring, as whenever using theoretical calculations there is always some doubt as to how close to the true structure the theoretical structure is.

Another attempt to try to quantify the link between structure and K_i was to look at charge matching between a group of β-carbolines and lumiflavin. This series of inhibitors have similar sizes, with small alterations in aromaticity and additions of either methyl or methoxy substituents. This series of inhibitors was chosen for the study because the compounds were of similar size and the only structural changes would have an effect on the electronic properties of the molecules. A study of the complexation of tetrakis(phenylethynyl)ethane and 2,4,7-trinitrofluoren-9-one (134) showed that charge matching was the main factor in determining the stability of the complex, and that HOMO/LUMO overlap was random throughout a series of complexes. The β-carbolines were overlaid with lumiflavin in the predetermined overlay (129) and net score for charge matching was totaled. The scores were plotted against log K_i, shown in Fig. 3.4.4.4. A good trend is seen between K_i and charge matching. The only problem is that this

stacking interaction between inhibitor and flavin does not occur in MAO A, so how can we explain these results? The structure of MAO B complexed with isatin has isatin stacking between two tryosines, and perhaps these tyrosines could have a charge distribution similar to the flavin. A study of charge matching between these inhibitors and the two tyrosines may determine whether this is true, the main problem is that there are two tyrosines which will not be perfectly aligned with the inhibitor and makes this study complicated.

4.5. Circular dichroism spectroscopy

Apart from kinetics, the techniques used in this study of MAO A have all offered a rather static picture of the enzyme. Circular dichroism offers the opportunity to study MAO A in a dynamic way. Ligand binding and reduction of the flavin co-factor by dithionite, substrate and irreversible inhibitor have all been studied here by circular dichroism spectroscopy.

Spectral studies have shown that the spectrum of the flavin in MAO A is perturbed by inhibitors upon binding. In addition, some classes of inhibitors can stabilize the semiquinone form of the flavin during reduction. This indicates a close association between the inhibitor and the flavin and, from reductive titrations, it is clear that inhibitors alter the redox properties of the flavin. The active site of MAO B has been shown to be hydrophobic in nature, and lined with many aromatic residues. The structure of MAO B-isatin complex shows isatin bound edge on to the flavin between two tyrosine residues. Amphetamine and pirlindole were investigated using CD to determine whether

they affect the CD spectrum of the flavin as seen in the UV-vis spectrum, and also whether their binding altered the environment of the aromatic residues in the active site. Amphetamine induces quite small changes in the CD spectrum. It gives a small alteration at 282 nm, the region associated with tyrosine, but no other perturbation to aromatic residues. This pattern is consistent with amphetamine binding between the two tyrosines and orientated edge-on to the flavin in the same manner as isatin in MAO B. Pirlindole, in contrast, induces increases in the CD spectrum across the aromatic region, with the greatest effects seen on the tyrosine peak at 282 nm, and the tryptophan peak at 293 nm. The larger size of the pirlindole molecule will allow it to make contact with many more aromatic residues in the substrate-binding cavity than the smaller amphetamine molecule.

The UV-vis spectrum of MAO A changes considerably during reduction of the flavin in the active site. Surprisingly, this region changes very little in the CD spectrum when the enzyme is reduced. There is a small reduction in intensity from 350 nm to 450 nm, but the main area of change is in the aromatic region. The oxidised flavin in most flavoenzymes is planar, but upon reduction the flavin adopts a bent conformation. This should give rise to considerable changes in the CD spectrum. However, in the structures of MAO B (42,43) the flavin in both the oxidized and reduced forms is bent, which would explain the lack of significant change in the CD signal in the flavin region during reduction. However, the aromatic region shows considerable change upon reduction. To produce a full yield of semiquinone, MAO A was complexed with amphetamine and reduced to give 100% semiquinone. In the semiquinone form, the phenylalanine (265-275 nm) and the tryptophan (293 nm) regions are altered the most, with the tyrosine region

remaining unchanged. For the fully reduced enzyme, all three peaks (tyrosine, tryptophan and tyrosine) are enhanced greatly. It is clear that reduction of the flavin perturbs the aromatic residues in MAO A. For the MAO A-amphetamine complex reduced to the semiquinone, the two tyrosines that amphetamine binds between will already be constrained and therefore show little change in their CD signal.

In addition to dithionite reduction, the flavin can also be reduced by substrate, or by an irreversible (suicide) inhibitor. Fig. 3.5.3.1 shows the CD spectra after reduction of MAO A by dithionite, benzylamine, or clorgyline. Both dithionite and benzylamine increase the CD signal in the aromatic region to the same extent, all three aromatic peaks are enhanced. The main difference between the two forms of reduction is the flavin region. The dithionite reduced sample shows a small reduction in CD signal in the flavin, whereas the substrate reduced sample shows a greater reduction in CD signal in the flavin region. If both dithionite and benzylamine dissociate quickly from the enzyme after reduction then it would be hard to explain the differences seen here. However, substrate binds to reduced enzyme and alters the redox properties of the flavin, the rate of re-oxidation in the presence of benzylamine is 25-fold higher than non-liganded enzyme. This would suggest that benzylamine bound to the reduced enzyme is interacting with the flavin, explaining the changes in CD signal seen in the flavin region. When clorgyline reduces the flavin there is a very large difference in the 265-275 nm region associated with phenylalanine. This may be due to a phenylalanine close to the flavin (Phe-343 in MAO B), which could have an altered interaction with the flavin when clorgyline is covalently bound. This could also result from interaction of clorgyline with Phe in the

aromatic cage. If this were true, it would have to be a specific interaction as the Tyr and Trp signals are not enhanced to the same degree as the Phe signal. The other large difference that depends on the reduction method used is seen at 330 nm for the clorgyline-reduced MAO A. This may be due to the N5 modification of the flavin by clorgyline because it is not seen in the other samples. This CD study shows the subtle changes seen in the aromatic amino acid side chains in the active site of MAO A during ligand binding and during redox changes of the flavin. When looking at this data in conjunction with spectroscopic data it provides a more dynamic picture of the processes involved in ligand binding.

4.6 Summary of results

The picture we see for the binding of pirlindole in the active site of MAO A is that of the molecule lying edge-on to the flavin with its N3 nitrogen facing N5 of the flavin. The inhibitor lies between the two tyrosines that orientate substrates and inhibitors towards the flavin. Despite theoretical calculations suggesting that stacking of inhibitor and flavin is possible, it is more likely that inhibitors lie in between the two tyrosines. CD results suggest that amphetamine sits between the two tyrosines, as tyrosine is the only aromatic residue type perturbed by its binding. Pirlindole, along with its effects on tyrosine, also perturbs tryptophan and phenylalanine, adding to its interaction with the flavin and explaining its lower K_i value. The C8 substituents lie away from the flavin in a hydrophobic pocket. The optimal size of C8 substituent is cyclohexyl, larger substituents only being tolerated if they are flexible. Substituents on N3 are not tolerated, due to their interference with the interaction between N3 of pirlindole and N5 of the flavin. This

interaction helps to stabilize the semiquinone form of the flavin when enzyme-inhibitor complex is reduced. When pirlindole is substituted at N3, no stabilization of the semiquinone is seen during reduction, as the substituent has blocked the pirlindole-N3-N5 flavin interaction. Saturation at N3 of the pirlindole is important, the de-hydro derivatives always give lower K_i values. Comparing the theoretical view of the electrostatic potential of the saturated and de-hydro derivatives of pirlindole, it is clear to see there is an increased electron density around the dehydro derivative in the position where the N3-N5 interaction would occur. The view of the saturated inhibitor shows instead the electrons above the nitrogen, so presumably the increased electron density around the nitrogen in the dehydro derivative allows for a stronger interaction between the inhibitor and flavin. Also with a flatter structure it can fit between the tyrosines better.

5. References

1. Massey, V. (1995) *Faseb J* **9**, 473-475
2. Clark, W.M., and Lowe, H.J. (1956) *J Biol Chem* **221**, 983-992
3. Fraaije, M.W., and Mattevi, A. (2000) *Trends Biochem Sci* **25**, 126-132
4. Bjornberg, O., Rowland, P., Larsen, S., and Jensen, K.F. (1997) *Biochemistry* **36**, 16197-16205
5. Mewies, M., Packman, L.C., Mathews, F.S., and Scrutton, N.S. (1996) *Biochem J* **317 (Pt 1)**, 267-272
6. Fraaije, M.W., van den Heuvel, R.H., van Berkel, W.J., and Mattevi, A. (1999) *J Biol Chem* **274**, 35514-35520
7. Pace, C., and Stankovich, M. (1986) *Biochemistry* **25**, 2516-2522
8. Suzuki, H., Katsumata, Y., and Oya, M. (1979) in *Monoamine Oxidase: Structure, Functions and Altered Functions* (Murphy, D. L., ed), Academic Press, New York
9. Nicklas, W.J., Vyas, I., and Heikkila, R.E. (1985) *Life Sci* **36**, 2503-2508
10. Johnston, J.P. (1968) *Biochem Pharm* **17**, 1285-1297
11. Knoll, J., and Magyar, K. (1972) *Adv Biochem Psycopharm* **5**, 393-408
12. Nicholls, D.G. (1994) *Proteins, Transmitters and Synapses*, Blackwell Scientific Publications
13. Hsu, Y.P., Weyler, W., Chen, S., Sims, K.B., Rinehart, W.B., Utterback, M.C., Powell, J.F., and Breakefield, X.O. (1988) *J. Neurochem.* **51**, 1321-1324
14. Weyler, W. (1989) *Biochem. J.* **260**, 725-729
15. Donnelly, C.H., and Murphy, D.L. (1977) *Pharmacology* **26**, 853-858

16. Minamiura, N., and Yasunobu, K.T. (1978) *Arch Biochem Biophys* **189**, 481-489

17. Kearney, E.B., Salach, J.I., Walker, W.H., Seng, R.L., Kenney, W., Zeszotek, E., and Singer, T.P. (1971) *Eur. J. Biochem.* **24**, 321-327

18. Walker, W.H., Kearney, E.B., Seng, R.L., and Singer, T.P. (1971) *Eur. J. Biochem.* **24**, 328-331

19. Nandigama, R.K., and Edmondson, D.E. (2000) *Journal of Biological Chemistry* **275**, 20527-20532

20. Tan, A.K., and Ramsay, R.R. (1993) *Biochemistry* **32**, 2137-2143

21. Weyler, W., Hsu, H.P., and Breakefield, X.O. (1990) *Pharmac. Ther.* **47**, 391-417

22. Yu, P.H., and Davis, A.B. (1988) *Int. J. Biochem.* **20**, 1197-1201

23. Benedetti, M.S., and Dostert, P. (1985) *TIPS*, 246-251

24. Chiba, K., Trevor, A., and Castagnoli, N. (1984) *Biochemical and Biophysical Research Communications* **120**, 574-578

25. Sablin, S.O., Krueger, M.J., Singer, T.P., Bachurin, S.O., Khare, A.B., Efange, S.M.N., and Tkachenko, S.E. (1994) *Journal of Medicinal Chemistry* **37**, 151-157

26. Singer, T.P. (1991) in *Chemistry and Biochemistry of Flavoenzymes* (Muller, F., ed) Vol. II, pp. 437-470, CRC Press, Boca Raton, FL

27. Dostert, P.L., Strolin Benedetti, M., and Tipton, K.F. (1989) *Med Res Rev* **9**, 45-89

28. Efange, S.M.N., Michelson, R.H., Tan, A.K., Krueger, M.J., and Singer, T.P. (1993) *Journal of Medicinal Chemistry* **36**, 1278-1283

29. Wouters, J. (1998) *Curr Med Chem* **5**, 137-162

30. Wouters, J., and Baudoux, G. (1998) *Proteins* **32**, 97-110

31. Lan, N.C., Heinzmann, C., Gal, A., Klisak, I., Lai, E., Grimsby, J., and Sparkes, R.S.

32. Singer, T.P., and Baron, E.S.G. (1945) *J. Biol. Chem.* **157**, 241-253

33. Miller, J.R., and Edmondson, D.E. (1999) *J Biol Chem* **274**, 23515-23525

34. Vintem, A.-P.B. (2003) in *biology*, University of St Andrews, St Andrews

35. Kwan, S.W., Lewis, D.A., Zhou, B.P., and Abell, C.W. (1995) *Arch Biochem Biophys* **316**, 385-391

36. Kwan, S.-W.A., C. (1991) *Comp. Biochem. Physiol.* **102B**

37. Kirksey, T.J., Kwan, S.W., and Abell, C.W. (1998) *Biochemistry* **37**, 12360-12366

38. Nandigama, R.K., Miller, J.R., and Edmondson, D.E. (2001) *Biochemistry* **40**, 14839-14846

39. Binda, C., Coda, A., Angelini, R., Federico, R., Ascenzi, P., and Mattevi, A. (1999) *Structure Fold Des* **7**, 265-276

40. Trickey, P., Basran, J., Lian, L.Y., Chen, Z., Barton, J.D., Sutcliffe, M.J., Scrutton, N.S., and Mathews, F.S. (2000) *Biochemistry* **39**, 7678-7688

41. Wouters, J., Ramsay, R., Goormaghtigh, E., Ruysschaert, J.M., Brasseur, R., and Durant, F. (1995) *Biochem Biophys Res Commun* **208**, 773-778

42. Binda, C., Newton-Vinson, P., Hubalek, F., Edmondson, D.E., and Mattevi, A. (2002) *Nature Structural Biology* **9**, 22-26

43. Binda, C., Li, M., Hubalek, F., Restelli, N., Edmondson, D.E., and Mattevi, A. (2003) *Proc. Natl. Acad. Sci. U.S.A.* **100**, 9750-9755

44. Weyler, W., and Salach, J.I. (1985) *Journal of Biological Chemistry* **260**, 3199-3207

45. Binda, C., Newton-Vinson, P., Hubalek, F., Edmondson, D.E., and Mattevi, A. (2001) *Nat Struct Biol*

46. Geha, R.M., Rebrin, I., Chen, K., and Shih, J.C. (2001) *J Biol Chem* **276**, 9877-9882

47. Weyler, W. (1987) *Archives of Biochemistry and Biophysics* **255**, 400-408

48. McEwen, C.M., Jr., Sasaki, G., and Jones, D.C. (1969) *Biochemistry* **8**, 3952-3962

49. Binda, C., Mattevi, A., and Edmondson, D.E. (2002) *J Biol Chem* **277**, 23973-23976

50. Sablin, S.O., and Ramsay, R.R. (2001) *Antioxidants & Redox Signaling* **3**, 723-729

51. Ramsay, R.R., and Gravestock, M.B. (2003) *Mini Rev Med Chem* **3**, 129-136

52. Knoll, J. (2000) *Neurobiology (Bp)* **8**, 179-199

53. Irwin, I., and Langston, J.W. (1985) *Life Sci* **36**, 207-212

54. Group, P.S. (1989) *N Engl J Med* **321**, 1364-1371

55. Riederer, P., Danielczyk, W., and Grunblatt, E. (2004) *Neurotoxicology* **25**, 271-277

56. Holschneider, D.P., Scremin, O.U., Chen, K., and Shih, J.C. (1999) *Life Sci* **65**, 1757-1763

57. Xu, L., Ma, J., Seigel, G.M., and Ma, J.X. (1999) *Biochem Pharmacol* **58**, 1183-1190

58. Weinstock, M., Gorodetsky, E., Poltyrev, T., Gross, A., Sagi, Y., and Youdim, M. (2003) *Prog Neuropsychopharmacol Biol Psychiatry* **27**, 555-561

59. Honig, L.S. (1999) *Neurology* **53**, 1158

60. Ilett, K.F., George, C.F., and Davies, D.S. (1980) *Biochem Pharmacol* **29**, 2551-2556

61. Benedetti, M.S., Boucher, T., Carlsson, A., and Fowler, C.J. (1983) *Biochem Pharmacol* **32**, 47-52

62. Pearce, L.B., and Roth, J.A. (1985) *Biochemistry* **24**, 1821-1826

63. Ramsay, R.R., Koerber, S.C., and Singer, T.P. (1987) *Biochemistry* **26**, 3045-3050

64. Ramsay, R.R. (1991) *Biochemistry* **30**, 4624-4629

65. Tan, A.K., and Ramsay, R.R. (1993) *Biochemistry* **32**, 5490-5490

66. Singer, T.P., and Ramsay, R.R. (1995) *Faseb Journal* **9**, 605-610

67. Tan, A.K., and Ramsay, R.R. (1993) *Biochemistry* **32**, 2137-2143

68. Husain, M., Edmondson, D.E., and Singer, T.P. (1982) *Biochemistry* **21**, 595-600

69. Houslay, M.D., and Tipton, K.F. (1975) *Biochem J* **145**, 311-321

70. Edmondson, D.E., Bhattacharyya, A.K., and Walker, M.C. (1993) *Biochemistry* **32**, 5196-5202

71. Cram. (1965) *Fundamentals of Carbanion Chemistry* (Academic Press, N. Y., Ed.)

72. Stubbe, J., Fish, S., and Abeles, R.H. (1980) *J Biol Chem* **255**, 236-242

73. Tober, C.L., Nicholls, P., and Brodie, J.D. (1970) *Arch Biochem Biophys* **138**, 506-514

74. Walsh, C.T., Schonbrunn, A., and Abeles, R.H. (1971) *J Biol Chem* **246**, 6855-6866

75. Fendrich, G., and Abeles, R.H. (1982) *Biochemistry* **21**, 6685-6695

76. Smith, T.E., Weissbach, H., and Udenfriend, S. (1962) *Biochemistry* **1**, 137-143

77. Silverman, R.B., and Hoffman, S.J. (1981) *Biochem Biophys Res Commun* **101**, 1396-1401

78. Silverman, R.B., and Zieske, P.A. (1986) *Biochemistry* **25**, 341-346

79. Hamilton, G.A. (1971) in *Progress in Bioorganic Chemistry* (Kedzy, F. J., ed), pp. 83-157, Wiley-Interscience, New York

80. Yue, K.T., Bhattacharyya, A.K., Zhelyaskov, V.R., and Edmondson, D.E. (1993) *Arch Biochem Biophys* **300**, 178-185

81. Newton-Vinson, P., Hubalek, F., and Edmondson, D.E. (2000) *Protein Expr Purif* **20**, 334-345

82. Weyler, W., Titlow, C.C., and Salach, J.I. (1990) *Biochemical and Biophysical Research Communications* **173**, 1205-1211

83. Miller, J.R., and Edmondson, D.E. (1999) *Biochemistry* **38**, 13670-13683

84. Eberson, L.E., and Persson, K. (1962) *J Med Pharm Chem* **91**, 738-752

85. Bruice, T.C. (1980) *Advances in chemistry seies 191: Biometric Chemistry*, American chemical society: Washington, DC.

86. Massey, V.G., S. (1983) in *34 Mosbach Colloquium* (Sund, H. U., V., Ed. Springer, Berlin., ed)

87. Silverman, R.B. (1992) *Adv. in Elect. Trans. Chem.* **2**, 177-213

88. Belleau, B., and Moran, J. (1963) *Ann N Y Acad Sci* **107**, 822-839

89. Tomilov, A.P., Maironovskii, S.G., Fioshin, M.Y., and Smirnov, V.A. (1972) *Electrochemistry of Organic Compounds*, Haldsted Press, New York

90. Tan, A., Glantz, M.D., Piette, L.H., and Yasunobu, K.T. (1983) *Biochem Biophys Res Commun* **117**, 517-523

91. Barsky, J., Pacha, W.L., Sarkar, S., and Zeller, E.A. (1959) *J Biol Chem* **234**, 389-391

92. Egashira, T., and Yamanaka, Y. (1981) *Jpn J Pharmacol* **31**, 763-770

93. Murphy, D.L. (1976) in *Monoamine Oxidase and Its Inhibition* (Knight, J., ed), pp. 341-351, Elsevier, Amsterdam

94. Silverman, R.B. (1983) *J Biol Chem* **258**, 14766-14769

95. Paech, C., Salach, J.I., and Singer, T.P. (1980) *J. Biol. Chem.* **255**, 2700-2704

96. Silverman, R.B., and Zieske, P.A. (1985) *Biochemistry* **24**, 2128-2138

97. Mitchell, D.J., Nikolic, D., van Breemen, R.B., and Silverman, R.B. (2001) *Bioorg Med Chem Lett* **11**, 1757-1760

98. Silverman, R.B. (1984) *Biochemistry* **23**, 5206-5213

99. Zhong, B., and Silverman, R.B. (1997) *J. Am. Chem. Soc.* **119**, 6690-6691

100. Codoner, A., Monzo, I.S., Ortiz, C., and Olba, A. (1989) *Journal of the Chemical Society-Perkin Transactions 2*, 107-111

101. Medvedev, A.E., Ramsay, R.R., Ivanov, A.S., Veselovsky, A.V., Shvedov, V.I., Tikhonova, O.V., Vintem, A.-P.B., Davidson, C.K., Moskvitina, T.A., Fedotova, O.A., and Axenova, L.N. (1999) *Neurobiology* **7**, 151-158

102. Ramsay, R.R., and Hunter, D.J.B. (2002) *Biochimica Et Biophysica Acta-Proteins and Proteomics* **1601**, 178-184

103. Hynson, R.M.G., Wouters, J., and Ramsay, R.R. (2003) *Biochemical Pharmacology* **65**, 1867-1874

104. Rendenbach-Muller, B., Schlecker, R., Traut, M., and Weifenbach, H. (1994) *Bioorg Med Chem Lett 4*, 1195-1198

105. Mazouz, F., Gueddari, S., Burstein, C., Mansuy, D., and Milcent, R. (1993) *J Med Chem* **36**, 1157-1167

106. Medvedev, A.E., Ivanov, A.S., Kamyshanskaya, N.S., Kirkel, A.Z., Moskvitina, T.A., Gorkin, V.Z., Li, N.Y., and Marshakov, V. (1995) *Biochem Mol Biol Int* **36**, 113-122

107. Medvedev, A.E., Ivanov, A.S., Veselovsky, A.V., Skvortsov, V.S., and Archakov, A.I. (1996) *J Chem Inf Comput Sci* **36**, 664-671

108. Singer, T.P., Salach, J.I., and Crabtree, D. (1985) *Biochem Biophys Res Commun* **127**, 707-712

109. Kim, H., Sablin, S.O., and Ramsay, R.R. (1997) *Archives of Biochemistry and Biophysics* **337**, 137-142

110. Medvedev, A.E., Ivanov, A.S., Kamyshanskaya, N.S., Kirkel, A.Z., Moskvitina, T.A., Gorkin, V.Z., Li, N.Y., and Marshakov, V.Y. (1995) *Biochemistry and Molecular Biology International* **36**, 113-122

111. Gorkin, V.Z. (1983), Oxford, Pregamon press

112. Medvedev, A.E., Veselovsky, A.V., Shvedov, V.I., Tikhonova, O.V., Moskvitina, T.A., Fedotova, O.A., Axenova, L.N., Kamyshanskaya, N.S., Kirkel, A.Z., and Ivanov, A.S. (1998) *Journal of Chemical Information and Computer Sciences* **38**, 1137-1144

113. Veselovsky, A.V., Ivanov, A.S., and Medvedev, A.E. (1998) *Biochemistry-Moscow* **63**, 1441-1446

114. Veselovsky, A.V., Ivanov, A.S., and Medvedev, A.E. (2004) *Neurotoxicology* **25**, 37-46

115. Veselovsky, A.V., Tikhonova, O.V., Skvortsov, V.S., Medvedev, A.E., and Ivanov, A.S. (2001) *Sar and Qsar in Environmental Research* **12**, 345-358

116. Moureau, F., Wouters, J., Depas, M., Vercauteren, D.P., Durant, F., Ducrey, F., Koenig, J.J., and Jarreau, F.X. (1995) *European Journal of Medicinal Chemistry* **30**, 823-838

117. Harfenist, M., Joseph, D.M., Spence, S.C., McGee, D.P., Reeves, M.D., and White, H.L. (1997) *J Med Chem* **40**, 2466-2473

118. Gnerre, C., Catto, M., Leonetti, F., Weber, P., Carrupt, P.A., Altomare, C., Carotti, A., and Testa, B. (2000) *J Med Chem* **43**, 4747-4758

119. Weyler, W., Titlow, C.C., and Salach, J.I. (1990) *Biochem Biophys Res Commun* **173**

120. Weyler, W., and Salach, J.I. (1985) *J. Biol. Chem.* **260**, 13199-13207

121. Li, M., Hubalek, F., Newton-Vinson, P., and Edmondson, D.E. (2002) *Protein Expr Purif* **24**, 152-162

122. Weissbach, H., Smith, T.E., Daly, J.W., Witkop, B., and Udenfriend, S. (1960) *J Biol Chem* **235**, 1160-1163

123. Laaksone, L. (1999), 10:33 Ed., J Mol Graph

124. Kim, H., Sablin, S.O., and Ramsay, R.R. (1997) *Arch Biochem Biophys* **337**, 137-142

125. Fujita, T., Iwasa, J., and Hansch, C. (1964) *Journal of American Chemical Society* **86**, 5176

126. (2003) https://www.hit2lead.com

127. Ramsay, R.R. (1991) *Biochemistry* **30**, 4624-4629

128. Sablin, S.O., and Ramsay, R.R. (2001) *Antioxid Redox Signal* **3**, 723-729

129. Moureau, F., Wouters, J., Depas, M., Vercauteren, D.P., Durant, F., Ducrey, F., Koenig, J.J., and Jarreau, F.X. (1995) *Eur. J. Biochem.* **30**, 823-838

130. Gadda, G., Wels, G., Pollegioni, L., Zucchelli, S., Ambrosius, D., Pilone, M.S., and Ghisla, S. (1997) *Eur J Biochem* **250**, 369-376

131. Ramsay, R.R., Sablin, S.O., and Singer, T.P. (1995) *Progress in Brain Research* **106**, 33-39

132. Edmondson, D.E. (2004) *Journal of Biological Chemistry* **in press**

133. Wagner, M.A., Trickey, P., Chen, Z.W., Mathews, F.S., and Jorns, M.S. (2000) *Biochemistry* **39**, 8813-8824

134. Philp, D., . Gramlich. V,. Seiler. P,. Diederich. F. (1995) *J. CHEM. SOC. PERKIN TRANS.* **2**, 875-886